Author:
De Oliveira Emawodia, Joy

Title:
The Development and Use of Bioinks for Tissue Engineering to treat Congenital Heart Disease

Author:
De Oliveira Emawodia, Joy

Title:
The Development and Use of Bioinks for Tissue Engineering to treat Congenital Heart Disease

The Development and Use of Bioinks for Tissue Engineering to treat Congenital Heart Disease

Joy de Oliveira Emawodia

A dissertation submitted to the University of Bristol in accordance with the requirements for award of the degree of Master of Research in Cardiology in the Faculty of Health Sciences, Medical School.

Date of submission: 31st July 2019

Word count: 25,322

ABSTRACT

Congenital heart disease (CHD) are the most common anomaly among new-borns, it affects 1% of live births worldwide and approximately 4,600 new-borns in the UK. Tissue engineering creates functional living replacements for tissues or organs with the vision to meet the demand for organs worldwide which in turn can help treat CHD.

This study explored 3D bioprinting for gelatine methacrylol (GelMA), polyethylene glycol diacrylate (PEG-DA)-Alginate and alginate- nanocellulose (AL/N) hydrogels. Also, investigated cell viability and biomechanical properties for these biomaterials.

AL/N constructs demonstrated high biocompatibility with over 80% cell viability through 21 days. The cells in AL/N detached from constructs from day 7 and by day 21 all cells were found attached to the well-plate. GelMA-based constructs presented live-cells in all concentrations by day 21, except 20% GelMA which presented abundant cell death from day 1. The addition of hyaluronic acid to the 5% concentration improved biomaterial viscosity enabling the formation of grid-pattern constructs, reduced the overall bioprinting process time and presented live-cells in constructs for 21 days. PEG-DA Alginate when directly printed with cells presented abundant cell death from day 1. When PBS-rinsed prior to cell seeding, it demonstrated live cells in constructs but from day 14 most cells were dead.

For biomechanical properties, AL/N and PEG-DA Alginate presented comparable results to native heart structures when cell-free. AL/N demonstrated significantly higher tensile strength and elastic potential compared to other biomaterials. The addition of cells to constructs reduced tensile strength and elastic potential overall.

The change in biomechanical properties with the presence of cells suggests that the constructs investigated in this study are more suitable as delivery vehicles to treat damaged tissue rather than tissue fabrication.

ACKNOWLEDGMENTS

I would like to say thanks to my parents and sisters who have made huge sacrifices to enable me to have the opportunity to be part of this degree and fulfil my dream to start my research career.

I am immensily grateful to my supervisor Dr. Mohammed Ghorbel who has supported me in the journey of completing this dissertation. During my research, he has motivated me to strive for more and helped me to improve critical thinking. Most importantly, he taught me to not see negative results as failure but as valuable information for the research community.

I would like to also say thank you to Dr. Ambra Albertario and Dr. Dominga Iocabazzi who provided guidance and taught me various lab techniques. Most importantly, I say thanks to them for letting me be involved in their own research whenever I wanted to enhance knowledge on the various research happening in the group.

I thanks Sahirah Aslam who I mentored but who in the process extended my knowledge and inspired me everyday through hard work and positive attitude.

I declare that the work in this dissertation was carried out in accordance with the requirements of the University's Regulations and Code of Practice for Research Degree Programmes and that it has not been submitted for any other academic award. Except where indicated by specific reference in the text, the work is the candidate's own work. Work done in collaboration with, or with the assistance of, others, is indicated as such. Any views expressed in the dissertation are those of the author.

SIGNED: [redacted] DATE: 31/07/2019

DATE 31/01/2020
(corrections)

CONTENTS

1.1 Heart Development and structure

Heart development is initiated with a two-layered ovoid embryonic plate, these layers stretch and exchange cells within themselves leading to the formation of an additional layer in between, the mesoderm. The cells that form the heart are derived from the mesodermal layer while ectoderm and endoderm are responsible for the development of the neural cavity and lining of organs, respectively (Moorman et al., 2003). Further growth of the embryonic plate creates distinctive regions of development, keeping neural tube development to an apical side and heart development located in the centre (Anderson et al., 2003). Folding and further stretching of the plate results in the formation of the known four chamber heart structure: the left and right atria (LA & RA), the upper chambers; and the right and left ventricles (RV & LV), the lower chambers (Zaidi and Brueckner, 2017, Courtney et al., 2018).

In a normal new-born heart, the right atrium receives deoxygenated blood from systemic circulation, through the tricuspid valve (Figure 1.1). The blood is directed to the right ventricle which contracts and directs blood to the pulmonary circulation through the pulmonary valve and artery (Klabunde, 2012). The pulmonary system is responsible for gas exchange, the fileted oxygenated blood is directed to the left atrium. Through the bicuspid valve, blood is delivered to the left ventricle contracting and sending oxygenated blood back to systemic circulation through the aorta (Levick, 2010).

In the foetal heart, the placenta is the organ responsible for gas exchange. At this stage, lung function is not in use (Friedman and Fahey, 1993). Instead, most of the blood is carried away from the lungs through two connections: fossa ovalis (FO) and ductus arteriosus (DA, Figure 1.2). FO is the connection between right and left atria while DA connects the aorta and pulmonary artery. In the foetal heart, blood is received in the RA and can either travel directly to the LA or directed to RV which then flows to the pulmonary artery. After birth the pressure in the left side of the heart increases causing DA and FO to close, these modifications are permanent and lead blood-flow into lungs (Webster and De Wreede, 2016).

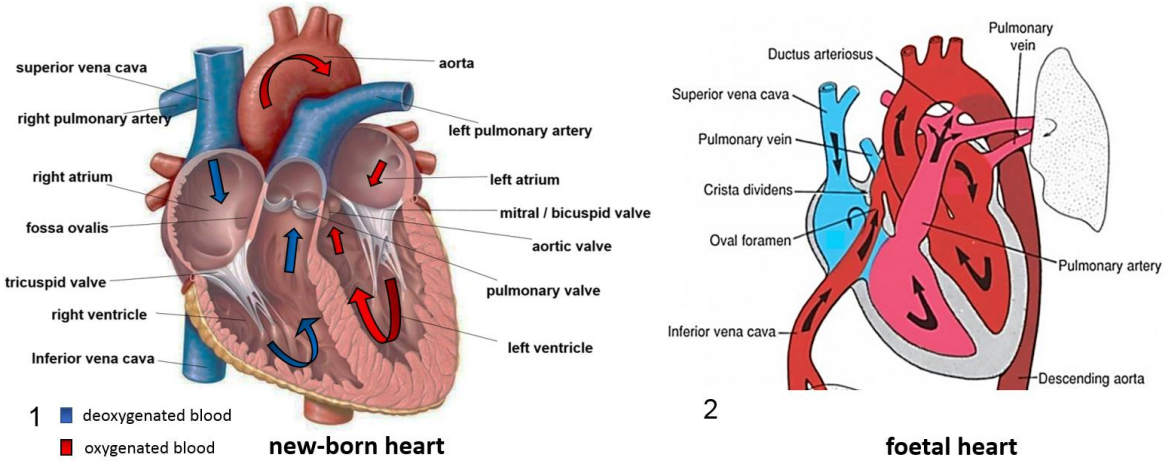

Figure 1. New-born heart depicts the four-chambered heart structure, valves and blood flow direction.1.2 Foetal heart demonstrates the direction of blood flow and difference in structure from a new-born by the presence and use of FO and DA in blood circulation. Edited images (Sporcle, 2016, Brown, 2019).

1.2 Congenital Heart Disease

Congenital heart disease (CHD) are the most common anomaly among new-borns, it affects 1% of live births worldwide and approximately 4,600 new-borns in the UK (Avolio et al., 2015). CHD refers to multiple conditions in which there is a malformation of vessels or, and heart structure. These anomalies directly influence the severity of the condition and determine if surgery will be required from an early stage in life (Zaidi and Brueckner, 2017).

Septal defect is a term used for anomalies occurring within the wall that separates chambers in the heart. In atrial septal defects (Figure 2.1), an opening is located on the septum, in between atria chambers, causing oxygen-rich blood to mix with oxygen-poor blood. In most cases, this opening is due to the absence or incomplete closure of FO (Oreto et al., 2018). If the opening is small, heart repair occurs through a catheter procedure and if the opening is large, open heart-surgery is required (Vasquez and Lasala, 2013, Akagi, 2015). In ventricular septal defects (Figure 2.2.), the opening is located in between ventricles. In this scenario, the blood from LV travels to RV leading excess blood into the lungs causing the heart and lungs to work harder (Mostefa-Kara et al., 2015, Penny and Vick, 2011). If the opening is small, it does not affect the child and the hole will usually close over time. Large openings might cause murmur, and harder breathing after non-strenuous activities. In such cases, the opening is repaired by using pericardium or a patch to close the opening (Zhao et al., 2018, Perez-Negueruela et al., 2017).

Single ventricle defects are anomalies that solely affect a single ventricle in the heart, depending on the degree of the anomaly heart function can be severely affected. In Pulmonary atresia, the pulmonary valve is absent or damaged, therefore the only route for blood to reach the lungs is through DA which closes after birth (Presnell et al., 2015). Medication to keep DA open is used as a form of treatment, eventually surgery is required to replace the pulmonary valve (Grant and Berger, 2016). In Tricuspid atresia, the tricuspid valve is absent so there is a reduced amount of blood that enter the heart from the circulatory system; consequently, the amount of oxygenated blood in the body is also reduced. Treatment for this condition involve multiple surgeries to maximise paths for blood oxygenation (Allen et al., 2016). Another heart anomaly under this category is Hypoplastic Left Heart Syndrome which is characterised by the under-development of the left side of the heart. In this condition the aorta and LV cavity are reduced in size, mitral valve is closed and the blood from RV instead is taken to the circulatory system via DA. Overall, HLHS is not correctable. DA can remain open using medication, and further operations can be done in patients. In some cases, heart transplant is the only treatment available (Ohye et al., 2016, Sian Pincott and Burch, 2011).

A complex example of CHD is Tetralogy of Fallot (ToF). This defect is a combination of an overriding aorta (the aorta is not located at the usual position), right ventricular hypertrophy, pulmonary valve stenosis (narrowing of the valve) and ventricular septal defect. In this condition, oxygenated and deoxygenated blood mix and the amount of blood pumped to lung is reduced. This condition requires shunt and patch placements, and a complete repair occurs later as the individual matures (Apitz et al., 2009).

The current treatments available for CHD revolve around surgery which is crucial for the patient's wellbeing. Unfortunately, there are various constraints with the treatments currently available. In cases such as ToF, multiple surgeries are required throughout an individual's life some starting soon after birth (Brickner et al., 2000). Grafts used for treatment also have durability restrictions and often require replacement to follow suit with the development of the patient. In other cases, organ transplant is the only treatment available. Organ availability is scarce for demand and if a transplant occurs the patient might still face organ rejection due to immune incompatibility (Nerem, 2010). These limitations demonstrate that superior therapeutic strategies are urgently required to improve and prolong an individual's quality of life.

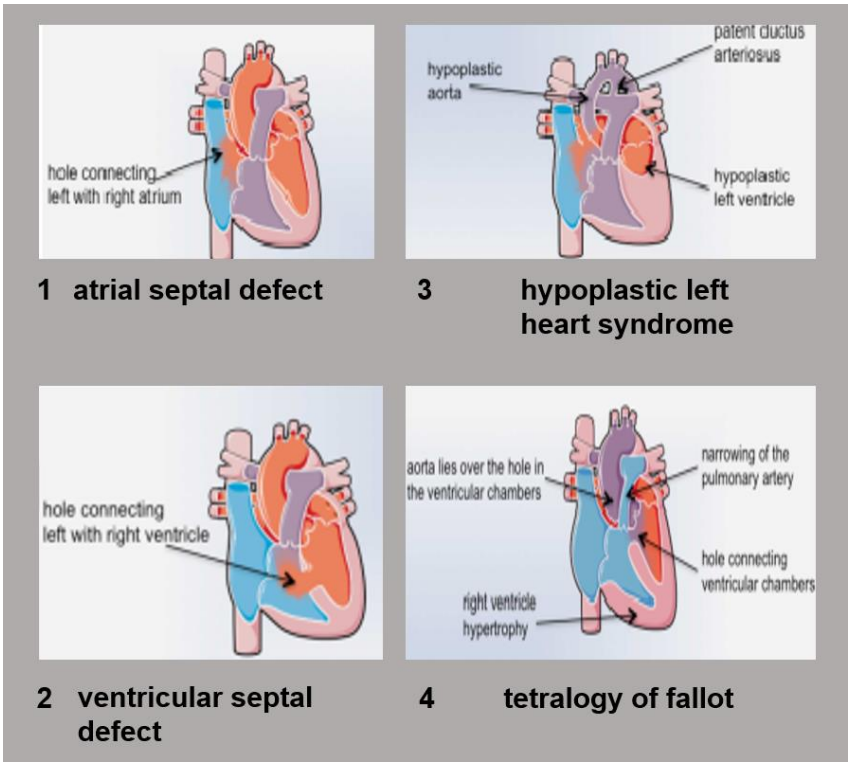

Figure 2. Congenital Heart Disease- 2.1 Atrial septal defect, the anomaly allows blood from LA to RA. 2.2 Ventricular septal defect, anomaly allows blood from LV to RV. 2.3 Hypoplastic Left Heart syndrome, underdeveloped left side of heart. 2.4 Tetralogy Fallot, misplaced aorta, narrowing of pulmonary artery, atrial defect and RV hypertrophy. Edited picture from (Avolio et al., 2015)

1.3 Tissue Engineering for Cardiovascular Research

The aim of tissue engineering (TE) is to create functional living replacements for tissues or organs (Berthiaume et al., 2011). The vision is to create organs fit for patient transplant, meeting the demand for organs worldwide. There are different approaches to tissue engineering: grafts, decellularisation of tissues for repopulation, 3-dimensional (3D) bioprinting and others (Griffith and Naughton, 2002). This project is focused on 3D bioprinting. In order to create a successful tissue model through 3D bioprinting, the following stages should be considered: imaging, design approach, biomaterial selection, bioprinting techniques, cell selection and application; Figure 3 (Bakhshandeh et al., 2017, Murphy and Atala, 2014).

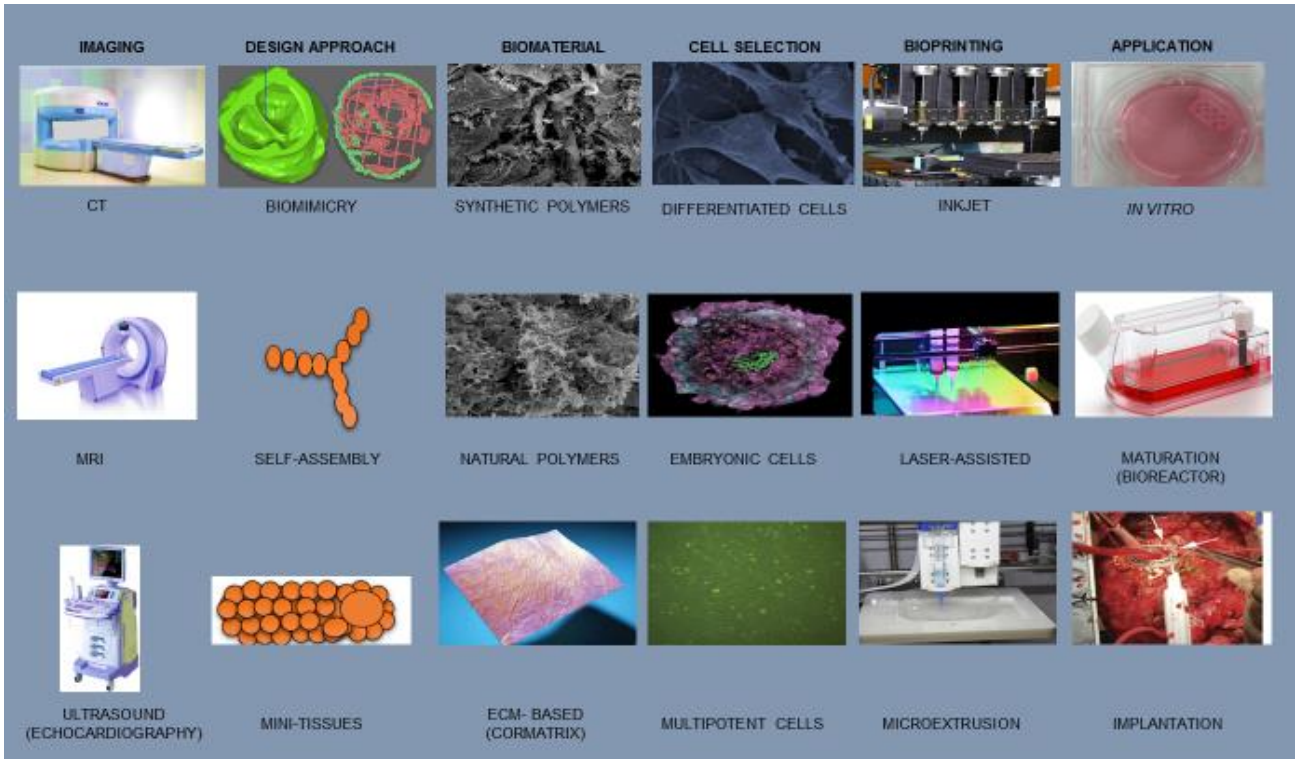

Figure 3- Considerations for 3D model creation – Imaging: CT, MRI, Echocardiography. Design approach: Biomimicry, self-assembly and mini-tissues. Biomaterial selection: synthetic polymers, natural polymers and ECM-based and CorMatrix. Cell selection: Differentiated cells, Embryonic cells and multipotent cells. Bioprinting technologies: Inkjet, Laser-assisted, and Micro-extrusion. Application: in vitro, maturation, implantation.

1.3.1 Imaging

The use of imaging machinery helps to obtain accurate anatomical information of an organ or tissue (Zhang et al., 2015b). Imaging technologies such as computerised tomography (CT), ultrasound and Magnetic Resonance Imaging (MRI) can be used to capture the overall and isolated heart structure. The captured image can be coupled with 3D printing techniques aiming to provide a similar structure and function of tissue (Garcia et al., 2018). CT provides a more detailed image than a normal x-ray and the same is true for MRI, except that it does not make use of damaging radiation (Story and Rutherford, 2015). Ultrasounds make use of sound waves to obtain images. The resolution this technology provides compared to the others is lower, however, it is apt for printing larger structures, including heart malformation models through echocardiography (Picazo-Angelin et al., 2018).

1.3.2 Design approach

Biomimicry is the imitation of life or nature. This approach requires knowledge on the tissue and organs being duplicated but also knowledge on the environment in which the structure is located. As complex as it is, biomimicry can be approached at different levels by mimicking: function, natural processes and natural systems (Zhang, 2012).

Mimicking function is the most common form of biomimetic. If one wants to mimic muscle function, a common approach is to firstly do an image analysis of the tissue. This provides information on the tissue structure (e.g. sarcomere) allowing angle and distance in between filaments measurement. Next, force analysis to calculate stress between filaments and surrounding structures. Followed by optical mapping and measuring transition of nutrients across membrane. All the information gathered can then be applied into a model being constructed with nanotechnology (Feinberg et al., 2012).

Mimicking natural processes and systems is more complex. It combines not only tissue or organ function, but these also attempt to mimic the environment in which the structures are naturally located. These approaches might use bioreactors to help control the tissue environment. Overall, biomimetic approaches combine biophysics, cell biology, biomaterials and engineering in order to create successful models (Chen and Liu, 2016).

Self-assembly uses as guidance the development of organs and tissues at embryonic level. Early stages of development for tissues naturally produce appropriate cell signalling and ECM. Therefore, if the basic embryologic anatomy is reproduced (self-assembly of cells, signalling patterns), development will naturally follow (Bishop et al., 2017). This approach does not make use of scaffolds; therefore, scaffold biocompatibility and degradation are not drawbacks (Peck et al., 2011). Moreover, cell attachment, interaction and ECM formation are facilitated as tissue development is independent on being part of a hydrogel or scaffold (Yu et al., 2016).

Mini-tissues use as basis the smallest structure of a tissue that can be reproduced. It can make use of both approaches mentioned above to enlarge the construct. Mini-tissue formation involves self-assembly of cell spheres making use of a biologically accurate design. After the high-resolution design is formed, these can self-assemble into macro-tissues (Murphy and Atala, 2014).

1.3.3 Biomaterial selection

Biomaterials can be divided according to their nature; synthetic or natural. Synthetic materials allow more control over weight distribution and molecular weight within the construct. These permit easier control of crosslinking density, consequently providing more control over mechanical properties (elasticity) in a construct (Bhatia, 2016).

Polyethylene glycol (PEG) based materials is a common example of synthetic polymer. It is commonly used in research as it is FDA-approved. PEG can be chemically modified into polyethylene glycol diacrylate (PEG-DA) and in this form cells can be encapsulated quickly within the material. Construct stability is achieved by mixing PEG with a crosslinker (eg. Irgacure) and exposing the material to UV light. The easy chemical and mechanical manipulation of the material inherently leads to lack of natural proteins for cell attachment, the material needs to be programmed to contain attachment sites. Therefore, pairing this compound with natural occurring polymers such as collagen and alginate provides cell proliferation properties (Mazzoccoli et al., 2010).

Pluronics also an FDA- approved synthetic biomaterial. It is non-toxic, available with a range of molecular weight and with different hydrophobic and hydrophilic ratios. This material presents thermosensitive properties, allows encapsulated cell-print and can be used as a scaffold material as it can be washed away easily if needed. Being an inert material, encapsulated cells tend to create cell-cell interaction in clusters rather than matrix-cell interactions in this polymer (Muller et al., 2015).

Natural polymers include materials that can be found on the extracellular matrix (collagen, gelatine, hyaluronic acid) but also in non-mammalian sources (alginate, chitosan, agarose). These materials contain high biocompatibility which facilitates the degradation process of constructs by enzymes. ECM- derived polymers, contain natural attachment sites for cells inherently promoting cell growth and proliferation eliminating the need for further modifications. (Mano et al., 2007). Most naturally derived bioinks present low viscosity which might lead to a soft construct, with low resolution and poor shape stability. Introducing functional groups to the material (eg. methacrylic acid) and making use of crosslinking improves these limitations (Boland et al., 2007).

Collagen is the most abundant component in the extracellular matrix, therefore is widely used for coating and as a bioink as it provides good cell attachment and growth factors. Collagen is a protein mainly located in connective tissues: bones, cartilage, tendons (Antoine et al., 2014). There are 16 different types of collagen in the body, 1-3 are the most abundant types. Type I is mostly used in TE as the extraction process is easy and it shows adaptability to different applications. The main sources of collagen used for bioink production are rat tail tendon, porcine and bovine as the structure of these are similar to humans (Avila Rodríguez et al., 2018)

Gelatine is derived from collagen. It is highly biocompatible, has fast degradation rate and non-immunogenicity. There are different types of gelatine, these vary according to the process used to obtain collagen prior to its isolation and the type of collagen in use. In regenerative

medicine, Type A and B of bovine and porcine-origins are commonly used as they present common structure to the ones found in humans (Echave et al., 2017).

Naturally, gelatine presents gelation characteristics at low temperatures but melts at temperatures higher than 35ºC. The fabrication of Gelatine- Methacrylol (Gel-MA) allows the overall material to withstand incubation. This compound mixture makes use of the natural ability of cell attachment from gelatine and uses methacrylol as a substance that allows material stability through the combination of a photo-initiator and UV exposure without compromising the overall ability of the material to adhere to cells and impact on degradation rate (Klotz et al., 2016, Schuurman et al., 2013).

Hyaluronic acid (HA) can be found in lower organisms (bacteria) to complex eukaryotes. In the human body, HA is present in most tissue in small amounts, however on the extracellular matrix of soft connective tissues, synovial fluid and umbilical cord, the polymer can be found in greater quantities (Camci-Unal et al., 2013). This compound can enhance cell proliferation, differentiation and repair of tissues. It creates a porous bioink which enables easy cell permeability and enables growth. It also presents viscoelastic properties in tissues, good biocompatibility and non-toxic degradation making it a unique material for TE (Zhu, 2017).

Alginate also presents high biocompatibility and low toxicity in biomedical applications. This material is obtained from brown seaweed and under mild conditions alginate can be made into hydrogel. It is a soluble material that supports cell growth. Alginate is uniquely composed of guluronic and mannuronic acid, these provide gel formation properties and increased flexibility of materials. This material has been used for wound healing methods and delivery of drug molecules extensively specifically for its ability to release reagents in a controlled manner. Alginate present fast gelling properties through multivalent cations (Ca^{2+}) application (Lin et al., 2005). The method in which the crosslinking of alginate occurs is not fully understood, Typically in TE, alginate is used on the expectance of cell delivery to an injury site with the expectation that these will create recovery of damaged tissue (Axpe and Oyen, 2016).

Extracellular Matrix (ECM) is present in all organs and tissues, it is highly important for cellular attachment and it is involved on biochemical processes such as differentiation, homeostasis and morphogenesis (Frantz et al., 2010). Each tissue can vary its ECM composition consequently changing the biomechanical properties of the compound. CorMatrix is a decellularised scaffold ECM-based that promotes cell proliferation and tissue regeneration. This material has been increasingly used for CHD research, specifically for reconstruction of greater vessels (Nelson et al., 2016) and as a patch for septal defects (Padalino et al., 2015). Oher materials used for cardiac reconstruction have shown poor tensile strength and

presented tissue calcification. CorMatrix is able to withstand pressure over 1200mmHg, presents no sign of calcification or immune response (Brinster and Patel, 2014).

A biomaterial can be further classified into chemical or physical depending on the crosslink method of use. Chemical crosslinking is maintained through covalent bonds increasing shape fidelity of a model. 2-hydroxy-1-[4-(2-hydroxyethoxy) phenyl]-2-methyl-1-propanone (Irgacure 2959) and lithium acylphosphinate salt (LAP) are commonly used substances that will capture UV light enabling the crosslinking. These are both water-soluble and not harmful to cells. The crosslinking process can occur under neutral pH, aqueous environment and room temperature. Physical crosslinking is maintained through hydrogen bonds, these are weaker interactions and possibly will not form junctions permanently. However, these are sufficient to keep construct from dissolving in media (Zhu and Marchant, 2011). An example of physical crosslinking is the gelling property of alginate using calcium mentioned previously. Natural polymers are typically crosslinked through physical properties (divalent cations or temperature change) while synthetic polymers can either be crosslinked through physical or chemical properties (Lin et al., 2005, Berger et al., 2004).

1.3.4 Bioprinting

There are three main types of bioprinter technologies: inkjet, laser-assisted and extrusion based bioprinting.

Inkjet printers were initially modified from standard 2D desktop printers by replacing the ink cartridges with a bioink (Burke et al., 2017). This was the first technology to use specific position of droplet dispersion in a controlled and repeated sequence (Figure 4.1). There are two main methods of drop on demand inkjet printing: Thermal and Piezoelectric (Majumder et al., 2016).

Thermal bioprinting uses heat to extrude the bioink material into droplets. This method creates a high speed of dispersion (1-10000 drops/sec) at low cost. It can use temperatures as high as 300°C to commence the droplet extrusion. There were concerns regarding the effect of such high temperatures in the material and the impact of this in cell viability, however, it has been shown that the increase in temperature does not affect DNA viability or stability of cells in the bioink being used. More interestingly the high temperature exposure only occurs for approximately 2us causing a 4-10°C increase in temperature of the printer head (Sundaramurthi et al., 2016). Thermal printing has been previously used to create a cardiovascular microvasculature model using endothelial cells on a fibrin-thrombin bioink. The model promoted cell proliferation and successful formation of a tubular structure (Gao et al., 2018).

Piezoelectric bioprinting makes use of acoustic waves to eject droplets. By adjusting wave duration, amplitude and pulse, the speed and size of the droplets can be manipulated. This method is slightly more advanced than thermal as it does not make use of heat and provides uniform size and speed of droplet extrusion. Additionally, piezoelectric printing overcomes cell death over shear-stress using an open pool nozzle-less ejection. Consequently, the clogging of nozzles is eliminated. There is however cell damage and lysis concerns linked with the frequency of 15-25 Hz which is used in this method (Kim et al., 2016).

The main limitations for inkjet-based bioprinting are the difficulty to use biologically relevant cell density, ≤10 million cells per ml. If higher densities are used, nozzle clogging occurs and speed of printing decreases drastically. The viscosity of the bioink used must be lower than 10mPas providing a limited 3D printing capacity and poor structure stability (Derakhshanfar et al., 2018).

Laser-assisted bioprinting (LAB) is based on laser-induced forward transfer which was built to transfer metals. This technology was improved to overcome some limitations that inkjet technology presented. A standard LAB device has a laser beam aimed at a ribbon (glass), the ribbon is covered in metallic (gold or titanium) absorbing layer film and a bioink (with or without cells) sits below this film layer (Figure 4.2). As the laser pulses on the ribbon, it causes the metallic film to evaporate and a high-pressure bubble is formed expelling the bioink into a collector plate in a droplet manner. This technology can also print ceramics and proteins (Guillemot et al., 2011).

LAB is a nozzle-free process, being such, it overcomes the drawbacks of nozzle clogging presented on inkjet and it allows higher cell density concentration, 10^8 cells/ml. Additionally, the biomaterial in use can be in a solid or liquid phase, this system allows bioinks with viscosity from 1-300 mPa/s to be printed from a pico- to micro- resolution. To achieve good resolution with LAB, there are three main factors that need to be considered: 1. the distance between the ribbon and collector plate: if the ribbon sits too high, the droplet ejection will be less accurate 2. the viscosity and thickness of the biomaterial: LAB can print a range of viscosities. However, working with higher viscosity materials will make the resolution of the final construct more accurate 3. laser fluence: laser energy delivered per unit in the ribbon area (Murphy and Atala, 2014).

Despite LAB providing great resolution and biologically relevant cell density for models, it is an expensive technology. The film coating material needs to be prepared depending on the cell type and biomaterial in use (bioink, proteins, ceramics). If multiple cell types are used, the process becomes even more costly and time consuming. Also, the vaporisation of the metallic film causes segments of metal to be found in the final product (Derakhshanfar et al., 2018).

Nonetheless, LAB has aided cardiovascular research by delivering mesenchymal stem cells on a printed grid pattern to immunodeficient rats, the technique was proven to cause functional improvement and induce regeneration of surrounding heart tissue (Gaebel et al., 2011).

Extrusion-based bioprinting (EBB) is a method that uses a robotic system with x,y and z coordinates to produce a structure. It uses STL files to guide print also controls extrusion through this code system. CT files can be directly uploaded into the system and a printing pattern will appear instantly with this technology making it the most convenient bioprinting technology (Dababneh, 2014). Unlike inkjet and LAB, this method extrudes bioinks in a continuous form. Pressure is exerted on the piston or syringe pump controlling the printing speed (Figure 4.3). After or during printing process bioinks can be subjected to a form of crosslinking to stabilise the structure (Gao et al).

An advantage of this method is that materials can be printed at room temperature with or without cells, providing a homogenous distribution throughout the construct. This method allows high cell density including the ability of materials to encapsulate cells spheroid for printing. A selection of different materials is available to use with this technology as it has a good range of viscosity. EBB is medium cost and simple to use making it the preferred choice for most labs doing small to large scale research (Bishop et al., 2017).

The cell viability for EBB can vary from 40-80%, making it lower than inkjet and LAB. The viability of the encapsulated cells is also dependent on the viscosity of the material, nozzle diameter and pressure used in the process (Nair et al., 2009). The pressure exerted on high viscosity bioink with a small nozzle diameter is higher than a low viscosity bioink with a larger nozzle diameter. High pressure creates shear-stress causing cell death. Moreover, clogging often happens when the nozzle diameter is smaller than 150 µm, using a larger nozzle makes clogging less frequent, however it compromises the resolution of the printed structure. The resolution that can be achieved with this printing method is 200µm, which is considerably low compared to inkjet and LAB.

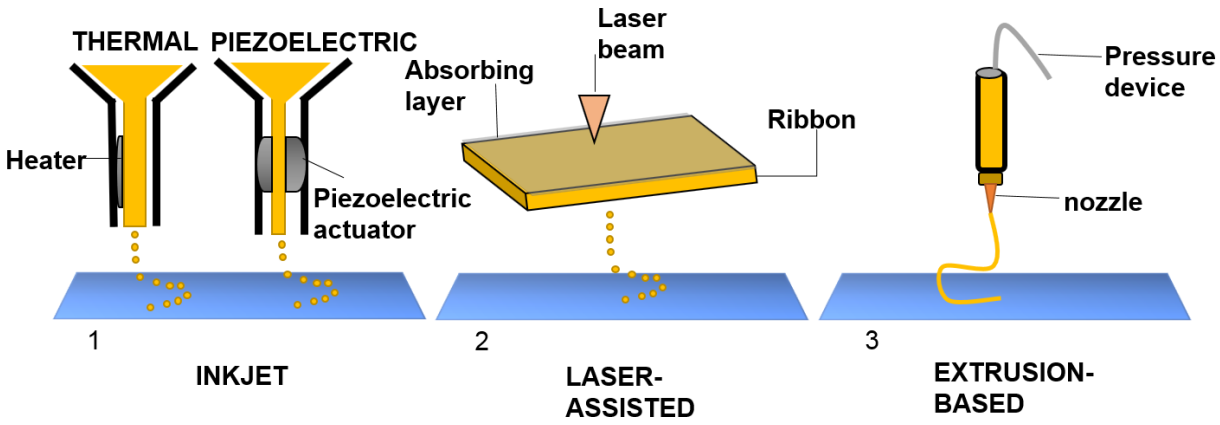

Figure 4- Bioprinter technologies. 1. Inkjet (thermal and piezoelectric) providing constructs with a droplet dispersion. 2. Laser assisted bioprinting components and droplet dispersion. 3. Extrusion based, pressure device which ejects bioink and nozzle providing a continuous dispersion of material.

1.3.5 Cell selection

Cell selection is a crucial step in tissue engineering. Once the biomaterial has been established, the cells used on the engineered model have the potential to maximise resemblance to the native tissue. Initially, the use of autologous cells in combination with engineered models were used for reimplantation and showed great success, however the process is costly, invasive and can potentially collect cells which are already damaged (Howard et al., 2008). Stem cells have been the focus of tissue engineering because unlike other cells, these are unspecialised cells that are capable of indefinite self-renewal and under specific physiological conditions, these can be induced to differentiate into tissue-specific cells with unique functions (Bianco and Robey, 2001).

Embryonic stem (ES) cells contain a pluripotent nature. ES are derived from early stage embryo development and are capable of proliferating indefinitely without senesce under specific in vitro conditions. These can uniquely differentiate into all cell types in a fully formed body, with the exception of placental and umbilical cord cells (Akutsu et al., 2006, Guillot, 2010). Adult stem cells (ASC) have a multipotent nature, these can differentiate into more than one cell type but are more limited than ES. ASC are tissue-specific, these generate all cell types of the organ from which they originated. There are various types of ASC (eg. endothelial, mammary, msesenchymal, neural, etc.), this review briefly focused on mesenchymal stem cells (Sobhani et al., 2017).

Mesenchymal stem cells (MSCs) are spindle-like shaped when adhered to plastic and present a multipotent differentiation potential being able to expand over 50 doubled proliferation without senesce signs. These cells are mainly programmed to differentiate into three lineages (chondroblast, adipocytes and osteoblasts) and present a unique cell-antigen expression. MSCs can be obtained from a variety of tissues, these include: bone marrow, umbilical cord, thymus and others (Covas et al., 2008).

Bone marrow- derived stem cells (BM-MSCs) were the first MSCs to be identified, these are usually extracted with a needle aspiration on the rear pelvic bone (El Omar et al., 2014). BM-MSCs are mainly used for bone and cartilage repair as they can differentiate into osteogenic lineages. Being the most commonly used and characterised, BM-MSCs present therapeutic potential in other areas including cardiovascular research. These cells have shown the potential to differentiate into cardiomyocytes by targeting overexpression of micro-RNAs responsible for cardiac fate and reprogramming (Fukuda, 2001, Guo et al., 2018). Unfortunately, BM-MSCs extraction is an invasive-painful procedure (Friedman et al., 2007) and the availability of these cells decrease with age (Lin et al., 2015). Due to these constraints, other MSCs need to be explored.

Wharton's Jelly (WJ) MSCs can be easily obtained through extra-embryonic tissue, the umbilical cord. The umbilical cord is obtained without health risks or harm. The interior structure has a jelly-like consistency which MSCs can be easily extracted through enzymatic digestion and tissue explant (Davies et al., 2017). WJ-MSCs present a fast proliferation rate, compared to BM-MSCs, the early passages of WJ is twice shorter for doubling cells (El Omar et al., 2014). Like BM-MSCs, WJ cells can differentiate into adipocytes, myocardial tissues, chondrocytes and others, however, the adipocyte differentiation is at a slower rate. Also, WJ cells have the potential to differentiate into cardiomyocytes and endothelial cells to repair myocardial infarction (Zhang et al., 2013).

Thymus-derived MSCs (T-MSCs) are obtained from the thymus which is located above the heart and is mainly responsible for maturation of T-cells. A year from birth, the thymus reaches its maximum size and undergoes involution. A process that causes fibrotic changes, thymocyte reduction and the emergence of adipocytes (Boehm and Swann, 2013). The involution process finalises when an individual reaches the age of fifty, at this stage the thymus is composed mainly of adipose tissue. Heart repair in patients with CHD involve a thymectomy which allows easier access to the heart, the discarded thymus can be used for MSCs extraction and further research (Iacobazzi et al., 2018). T-MSCs have increasingly been used for tissue engineering purposes in grafts as they not only provide the usual benefits of stem cells, T-MSCs also provide immune response regulation (Krampera et al., 2007). Due to its

unique features and easy accessibility, T-MSCs is a powerful therapeutic tool for tissue engineering research.

1.3.6 Application

Lastly, envisaging the application of model created is crucial, the three main applications for the printed constructs are: in vitro, implantation and maturation. In vitro testing refers to constructs which are solely designed to remain on the lab aiming to get viability data, biomechanical tests and structural analysis. Constructs with purpose of implantation require a higher standard of care than the ones in vitro as these will be transplanted into living organisms. The aim of implantation generally is to observe how the constructed model interacts in vivo and if the construct in place causes undesired immunological response. Some constructs require a period of maturation before implantation. This process may utilise a bioreactor which has the potential to mimic the body's natural environment and this process is particularly beneficial for constructs which have used differentiated cells in the process (Murphy and Atala, 2014).

1.4 Biomechanical properties

After a 3D model has been created, the biomechanical properties of model can provide valuable information. Tensile testing is a method to assess mechanical properties of biomaterials. This is particularly important as it indicates if the properties of the material are appropriate for its intended application. Tensile machines can determine the strength of the material through elongation or compression, these provide a variety of results which can be assessed and compared with the specified target tissue (Griffin et al., 2016). Maximum load and Young's modulus are crucial measurements from elongation analysis. Maximum load (N) indicates the force the material can withstand before its breaking point. While Young's modulus (MPa) is a measurement of the rigidity of the biomaterial by assessing the relation between stress and strain (Zhang et al., 2012).

The process of testing bioinks is slightly different than tissues or vessels. In comparison, bioinks require considerably less force than living tissues. Most bioinks will reach failure below 10N, therefore the appropriate machinery to test biomaterials is required to have sensitive sensors to present accurate analysis (Lee et al., 2018). Universal testing systems have a variety of components that will provide accurate measurement of samples, among all components the load cell and grips are the most important features. The load cell is an adjustable piece which should be changed dependant on the strength of the biomaterial in use. The same applies for the grips, low force grips are important for bioink testing and by placing sandpaper in between these helps hold the printed constructs in place avoiding slippage.

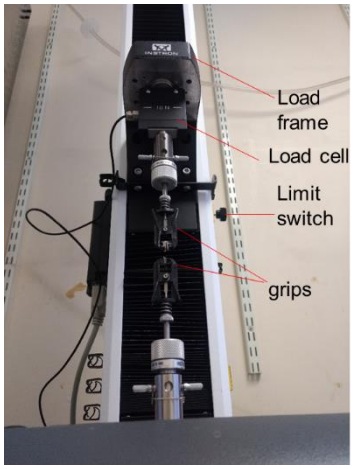

Figure 5 Tensile machine components: load frame, load cell, limit switch and grips.

TE constructs are expected to gradually mimic the mechanical and structural properties of native tissue. Acquiring biomechanical data on native cardiac human tissues is more challenging than animal models due to its limited availability. However, over the last few years with the emergence of TE more data has been gathered particularly for aortic and pulmonary valves. It is also important to compare findings of human samples with other organisms, most of research is carried out with animal models subsequently translated to humans (Kobayashi et al., 2012). Pigs are considered the most suited xenogeneic model for humans, they present anatomical similarities, including heart structure (Rodrigues, 2005, Crick et al., 1998) and physiological systems (Kalscheuer et al., 2014).

		Human	Porcine
Pressure (mmHg)	Systolic	120	130
	Diastolic	80	60
Aortic Valve	Maximum Load (kPa)	1740 ± 0.29	4000 ± 2.6
	Young's Modulus (kPa)	15340 ± 3.84	1680 ± 6.5
	Thickness (mm)	1.1 ± 0.3	0.7 ± 0.4
Pulmonary valve	Maximum Load (kPa)	2780 ± 1.05	2740 ± 1.97
	Young's Modulus (kpa)	16050 ± 2.02	15670 ± 8.63
	Thickness (mm)	0.397 ± 0.114	0.605 ± 0.196

Table 1. Biomechanical properties of Human vs Porcine (Arbeiter et al., 2012, Martin and Sun, 2012, Stradins et al., 2004, Li et al., 2008, Hasan et al., 2014, Lelovas et al., 2014)

1.5 Vascularisation of engineered tissues

The vascularisation of native tissue is obtained through vessel branches, capillaries, which redistribute blood and nutrients. This branching system allows the exchange of metabolites to be more efficient consequently maintaining the tissue live (Rouwkema et al., 2008).

A major limitation of tissue engineered constructs is the lack of an inherent vascularisation system. If engineered tissues surpass 100-200 µm thickness, the limit of oxygen diffusion, nutrient exchange will not occur limiting the ability of the construct to connect to the host tissue (Kannan et al., 2005). Simply transferring constructs from in vivo to in vitro scenario is a problematic approach as blood vessel formation is a gradual process and in the meantime that leaves cells within the constructs susceptible to death due to lack of nutrients (Jain et al., 2005).

A variety of growth factors have shown to promote blood vessel formation, these factors promote digestion of basal membrane of a capillary which allows migration, proliferation and formation of new branches of vessels (Sheridan et al., 2000). The combination of these growth factors within a scaffold allows vessels from nearby tissues to infiltrate the construct. This method also presents the time-formation limitation as the vascularisation network requires time to migrate. Another promising approach is the creation of arteriovenous loop enclosed by a polycarbonate chamber. This is a pre-vascularisation method that eradicates the need for growth factors while also promoting new tissue growth and providing an enclosed nutrient supply system within the scaffold (Lokmic et al., 2007, Laschke and Menger, 2016).

3D bioprinting presents a great opportunity to assist on the vascularisation methods mentioned above. Imaging provides an accurate picture of a tissue which can be further optimised to provide spaces for nutrient exchange without compromising shape fidelity. Moreover, the use of a porous biomaterial will facilitate cell distribution, provide space for cell adhesion and nutrient diffusion (Ko et al., 2007).

1.6 Study objectives

This project aimed to explore the construction of 3D models using extrusion based bioprinting to produce viable scaffolds using pig derived mesenchymal stem cells implemented on different biomaterials. The materials used in this project were Alginate-nanocellulose, GelMA and PEG-DA as these have previously shown biocompatibility and desired 3D properties in literature.

These following steps ensured the aims of this project were met.

1. Generation of codes to instruct bioprinter the dimension of desired constructs.
2. Code refinement to ensure shape fidelity was maintained when using different biomaterials and observation on the ability of constructs to withstand incubation.
3. Implementation of cells to biomaterials and bioprinting hydrogels for cell viability and biomechanical assessments.

2 MATERIALS AND METHODS

2.1 The design of a grid pattern

Slic3r (version 1.30-dev) was used to create a 45º grid pattern, the software provided an embedded 3D block model. The block was adjusted to 7.5(x), 15(y) and 2(x) mm per layer, the largest size prints a 12-well sized plate allows. Further adjustments were performed in the block design (Table 2) and the file was saved in G-code format.

Tissue Model Settings	
Infill density	30%
Infill pattern	Grid
Angle	45º
Skirt loops	1
Distance from object	0mm

Table 2. Design settings in Slic3r. This is a summary of the settings applied to the design used in all experiments in this project. These settings are found under 'Tissue Model settings' in the software.

2.2 The design of a four-layered construct

Following the grid patterned obtained in Slic3r, the design of multiple layers was carried on Repetir Host (version 2.01). The G-code file was loaded and code refinement aimed to provide: **(I) four-layered model, (II) good shape fidelity in bioprint, (III) UV light presence when required and (IV) relatively fast printing**. To enable g-code translation into bioprint, a series of commands were used to refine the code provided from Slic3r (Table 3).

G-commands for calibration	Translation

G21	Set units to millimetres
G90	Use absolute coordinates
G92	Use relative coordinates
M83	Use relative distances for extrusion
M84	Disable motors
G-commands for movement	
G0	Rapid positioning in axis coordinates (x/y/z)
G1	Controlled movement to the position in axis coordinates (x/y/z)
M760	Open the valve of print-head 1
M761	Close the valve of print-head 1
M764	Turn on UV
M765	Turn off UV
G0 Z50	Moves printhead upwards
Z	Height of each layer in relation to plate or previous layer (mm)
Others	
G4	Dwell time

Table 3. G- code commands used in the design. These commands were used in Repetir Host.

2.2.1 Designing construct and deletion of incompatible commands

Automatically upon loading the G-code an eight-layered grid construct is provided and the editor tab presents the full code for the construct. All layers but the first were deleted to enable an easier refinement process.

The code inherently presented incompatible commands with the bioprinter in use, Inkredible. Therefore, the following lines of code were deleted: T0 & T1 extruder, unretract & retract, all lines before G21 and all lines after M84.

2.2.2 Improving shape fidelity and speed of print

Aiming to meet the requirements for shape fidelity, the height (z) for the first layer was set to 0.2mm [G1 Z0.200 F700], each layer after that had a 0.3mm increase in height. Further refinement was performed to help prevent grid filaments from merging and repeated bioink dispersion in the same location. To achieve this, specific points that could potentially result in repeated dispersion were deleted. If certain lines within the image from the code appeared to

be in close proximity with others, it was assumed that in print this resulted in an overlap and therefore deletion was required. For deletion, the numbers following E (extrusion) presented in the code were erased (Figure 6).

To provide relatively fast printing for constructs, the speed of print (F) was set 700mm/min. To implement the change, the innate number the code provided (F2400) was substituted for F700.

2.2.3 Finalising construct

Once the first layer was fully edited with the refinements mentioned above, the parameters of the code were copied over three times changing only the height (z) settings. This settings for constructs were used with all bioinks unless specified.

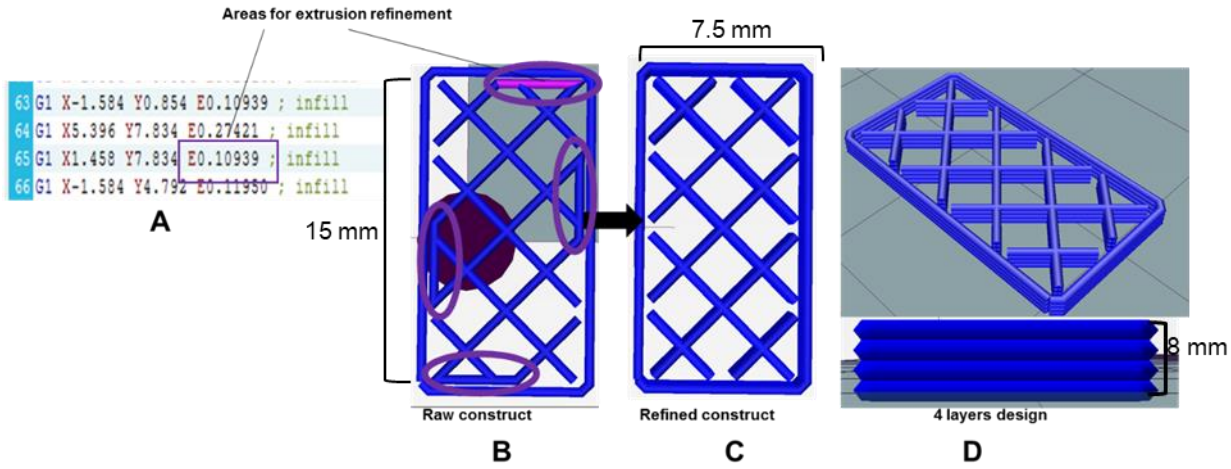

Figure 6. Design refinement. (a) shows the code provided by Repetir Host, the highlighted line is equivalent to the purple top highlighted structure in the design (b). (c) shows the final design of a layer after the refinement/deletion occurred. (d) represents the final 4 layer design which was created after (c).

2.2.4 UV light input

Depending on the bioink of use, UV light was necessary to increase shape fidelity of the construct. In such cases after bioprinting each layer, the UV was turned on and off [M764 and M765]. Moreover, the exposure time (P, milliseconds) was added to the code (Figure 7). The exposure time changed dependant on the shape fidelity obtained for each bioink.

Figure 7. Inclusion of UV light within the code. P20000 (ms) refers to the time the UV light was on. Time was changed by altering this number. M764 and M765 are input to command the turning on and off of this feature.

```
M764; Turn on the UV LED
G4 P20000; Wait for 20 seconds
M765; Turn off the UV LED
```

2.3 10-layered intercalated construct design

This construct was composed of a solid infill layer in the bottom and nine intercalated-grid 45 layers. The intercalated layers were designed as an overlap from the designed model for the four-layered constructs (Figure 8). The overlapping was obtained through trial and error from the original grid 45 code. Most changes were performed on Y coordinates but few on X. The numbers for Y were modified until the section seemed to be in the middle of the gap from the original model, this method was used throughout the entire design of a layer.

Once all parts of the construct seemed intercalated, the layers were replicated and the upper most layer was the original grid model. To improve shape fidelity, the intercalated layers changed every two layers instead of one. The solid infill was designed on Slic3r by selecting solid infill at 30%. This was transferred to Repetir Host and combined to the remaining intercalated code as the bottom layer at height (z) of 0.2mm. The solid infill created a higher surface of the printed design, to ensure layer stacking the heights were adjusted differently for each layer.

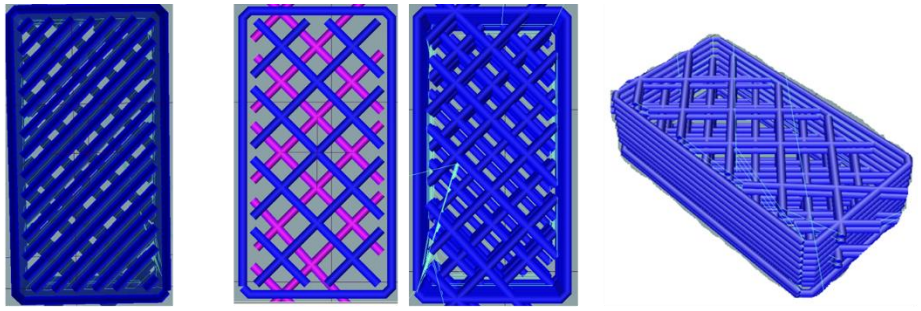

Solid infill layer bottom

Intercalated design

```
156
157 G1 X-1.584 Y-3.792 F2340; move to first infill point
158 M760;
159 G1 F700
160 G1 X1.458 Y-6.834 E0.11950 ; infill
161 G1 X5.396 Y-6.834 F700; move to first infill point
162 G1 F700
163 G1 X-1.584 Y0.146 E0.27421 ; infill
164 G1 X-1.584 Y4.084 F700; move to first infill point
165 G1 F700
166 G1 X5.584 Y-3.084 E0.28160 ; infill
167 G1 X5.584 Y-3.792 F700; move to first infill point
168 G1 F700
169 G1 X2.542 Y-6.834 E0.11950 ; infill
170 G1 X-1.396 Y-6.834  ; infill
171 G1 X5.584 Y0.146 E0.27421 ; infill
172 G1 X5.584 Y4.084  ; infill
173 G1 X-1.584 Y-3.084 E0.28160 ; infill
174 G1 X-1.584 Y0.854  ; infill
175 G1 X5.396 Y7.834 E0.27421 ; infill
176 G1 X1.458 Y7.834  ; infill
177 G1 X-1.584 Y4.792 E0.11950 ; infill
178 G1 X-1.396 Y7.834 F700; move to first infill point
179 G1 F700
180 G1 X5.584 Y0.854 E0.27421 ; infill
181 G1 X5.584 Y4.792 F700; move to first infill point
182 G1 F700
183 G1 X2.542 Y7.834 E0.11950 ; infill
184 M761;
```

Original grid 45 code

```
95 G1 X-1.584 Y-5.792 F2340; move to first infill point
96 M760;
97 G1 F700
98 G1 X1.458 Y-8.834 E0.11950 ; infill
99 G1 X5.396 Y-9.834 F700; move to first infill point
100 G1 F700
101 G1 X-1.584 Y-2.146 E0.27421 ; infill
102 G1 X-1.584 Y2.084 F700; move to first infill point
103 G1 F700
104 G1 X5.584 Y-5.084 E0.28160 ; infill
105 G1 X5.584 Y-1.792 F700; move to first infill point
106 G1 F700
107 G1 X-0.542 Y-8.034 E0.11950 ; infill
108 G1 X-1.396 Y-4.834  ; infill
109 G1 X5.584 Y2.146 E0.27421 ; infill
110 G1 X5.584 Y6.084  ; infill
111 G1 X-1.584 Y-1.084 E0.28160 ; infill
112 G1 X-1.584 Y2.854  ; infill
113 G1 X5.396 Y9.834 E0.27421 ; infill
114 G1 X1.458 Y9.834  ; infill
115 G1 X-1.584 Y6.792 E0.11950 ; infill
116 G1 X-1.396 Y5.834 F700; move to first infill point
117 G1 F700
118 G1 X5.584 Y-1.154 E0.27421 ; infill
119 G1 X5.584 Y2.792 F700; move to first infill point
120 G1 F700
121 G1 X-1.542 Y9.834 E0.11950 ; infill
122
123 M761;
```

Intercalated grid 45 code

Layer	Z Height (mm)
1	0.2
2	0.5
3	1.4
4	1.8
5	2.2
6	2.7
7	3.2
8	3.7
9	4.2
10	4.7

Figure 8. 10 layers code and design. The design of the 10 layers construct contained a base solid infill layer, and the remaining 9 layers were intercalated grid 45 patterns. The intercalated code was developed through trial and error. The table indicates the height used for each layer within the code.

2.4 Coordinates for printing in well-plates

Inherently the code is set for a petri-dish, it was crucial to adjust it for a six- and twelve-well plate environment. In a twelve-well plate the initial origin is in the corner of B2, while in a six-well plate it is located between A2 and B2. A ruler was used to measure distance from initial point of origin to a new desired origin and to obtain the distance between the new point of origin on the following well (Figure 9).

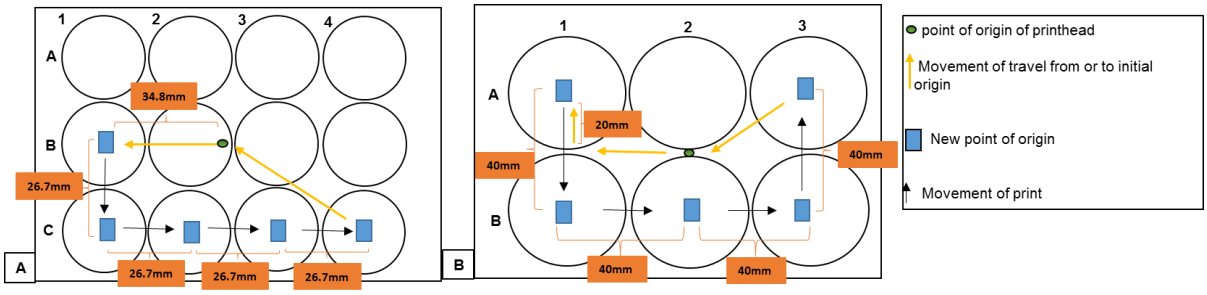

Figure 9. Coordinates for well plates. (a) shows the distance between wells necessary to modify the code to fit constructs in a 12 well-plate. (b) shows the distance between wells necessary to modify the code to fit constructs in a 6 well-plate.

The obtained measurements were input into the code with the horizontal measurements being equivalent to X measurement and vertical to Y. The initial origin provided is (X-43.2, Y-26.7), the first new point of origin(A1) for a six well-plate is (X-40, Y20). To determine this new origin [G92 X0 Y0] was added to the code. Once these coordinates were added, the movement of print was determined by the distance of one well to the other (Table). After print of the final well, the code was redirected to the encrypted origin as an attempt to meet the requirement for a fast printing process. The same principles were applied to create the pattern for a twelve well-plate.

Encrypted Origin	**Well One (A1)**	**Well Two (B1)**	**Well Three (B2)**	**Well Four (B3)**	**Well Five (A3)**	**Back to encrypted origin**
G1 Z30 F700; G0 X0 Y0 G1 X-43.2 Y-26.7 F700 G92 X0 Y0 M117 original origin	G90; use absolute coordinate s G0 Z25; G1 **X-40** **Y20** F700; G92 X0 Y0 ; M117 Well one ;	G0 Z25; G0 X0 Y0; G1 **Y-40** F700; G92 X0 Y0; M117 Well Two;	G0 Z25; G0 X0 Y0; G1 **X40** F700; G92 X0 Y0; M117 Well Three;	G0 Z25; G0 X0 Y0; G1 **X40** F700; G92 X0 Y0; M117 Well Four;	G0 Z25; G0 X0 Y0; G1 **Y40** F700; G92 X0 Y0; M117 Well Five;	G1 Z30 F700; G0 X0 Y0; G1 **X-43.2** **Y26.7** F700; G92 X0 Y0; M117 original origin

Table 4. Implementing measurements to code. The coordinates presented are shown as given by Repetir host. The inserted measurements are highlighted in bold. X refers to a sideways movement, as Y refers to an up or down movement.

2.5 Translation of code to bioprint

Cellink start (Cellink, US), a polyethylene oxide-based bioink and sacrificial material, was used to test the design properties once bioprinted. The bioink was stored at room temperature and extrusion pressured varied from 15-35kpa depending on nozzle diameter.

2.6 Preparation of Bioinks

2.6.1 PEG-DA Alginate

13.7Mm stock solution of NaCl solution was prepared. 1% Irgacure (410896, Sigma) was heated at 40ºC in NaCl for 15 minutes or until a clear solution was obtained. The mixture was brought to room temperature. 20% Poly(ethylene glycol) diacrylate M_n700 (PEG-DA, Sigma) was added, mixed and filtered with a 0.2µm filter for sterility purposes. Alginate (PROTANAL LF 60/10, FMC) was sterilised under UV 265nm for an hour. 12.5% alginate was added to the solution and mixed until homogenous. UV crosslinking was used (365nm).

2.6.2 PEG-DA Alginate-collagen

For addition of collagen, a 316 ml 3X DMEM (Thermo Fisher, UK) solution containing 10% FBS was prepared. 3.6 g of high glucose, powdered DMEM was added to distilled water at room temperature and gently stirred. 1.04g of sodium bicarbonate was added to the medium. pH was adjusted to 0.2-0.3 units below the desired final working pH (7.4) by slowly adding 1M NaoH or 1M HCl. The pH may rise to 0.3 units upon filtration. The medium was filtered with 0.2µm filter into sterile containers and finally FBS was added.

0.5mg/ml of collagen was mixed with 3X DMEM solution prepared. pH was adjusted if necessary. This solution and PEG-DA bioink were kept on ice until they were combined. The collagen-3X DMEM solution composed 10% of the overall final bioink.

2.6.3 PEG-DA Gelatine

1% Irgacure was dissolved in NaCl (13.7Mm) at 40º C until the solution was clear. The solution was brought to room temperature, mixed with 20% PEG-DA and sterilised with 0.2µm filter. Gelatine (Type A porcine skin, Sigma), was sterilised under UV for an hour and 12.5% added into the solution until dissolved.

2.6.4 Preparation of lyophilised GelMA

Dialysis bags preparation: 12 kDa MWCO - 25mm width dialysis bags (Sigma, D9777) were placed under running water for 3-4 hours, that enabled glycerol removal and opening of the bags ready for use.

10% of gelatine was dissolved in PBS at 50ºC and stirred for 10 minutes. Methacrylic anhydride (MA) was added dropwise and at increased stirring speed. To achieve a high degree of function for the solution, 0.6g of MA was added for every 1g of gelatine used. When the solution became clear, after 1-2 hours of stirring, it was transferred into a 50 ml flask and centrifuged for 3 minutes at 3500 xg speed. The supernatant was transferred into a 200ml beaker and the pellet discarded. The obtained solution was mixed with double the volume of distilled water (40ºC) and placed in the dialysis bags.

The dialysis bags were placed in 5L glass flask containing 40ºC distilled water. Metal stirring bars were placed at the bottom. The flask was maintained on top of a hot stirring plate and temperature checks were performed three times daily to ensure temperature was kept at 40ºC. The stirring speed was adjusted to ensure a gentle movement of the bags. The dialysis process was performed for seven days or until the solution was clear. All processes for GelMA preparation were carried inside a chemical safety fume hood.

Upon dialysis completion, pH was adjusted to 7.4 with the NaOH. The solution was filter sterilised and transferred to 5ml tubes. The samples were snap-freezed with liquid nitrogen. The tube caps were pierced, and the samples were placed on a freeze dryer for 4-7 days or until the samples were fully dry. Dryness was achieved when the weight of the samples did not change from one day to the other. Standard caps replaced pierced ones to prevent solution being hydrated during storage. Solutions were kept on -20º C.

2.6.5 Preparation of GelMA bioink

The day before cell encapsulation, a 2.5mg/ml Irgacure solution was prepared by dissolving the powder in PBS and placing the flask on a 70ºC water bath until the solution became clear (5-10 mins). The solution was filtered sterilised.

The desired concentration of GelMA was obtained by using the following calculation:

1.25 x final desired concentration

The desired amount of lyophilised GelMA was measured (5%, 7.5%, 10% or 20%) and PBS was added to four-fifths of the final volume. Irgacure was added into the solution providing a final concentration of 0.5%. The GelMA foam was immersed by the liquid agents, protected from light by using aluminium foil and left to soak overnight at 4ºC enabling full hydration. The following day, the flask containing Irgacure- GelMA was placed on a hot plate at 37ºC and stirred until the solution was dissolved and solvent was clear.

2.6.6 Preparation of 5% GelMA-HA

Following the GelMA protocol, hybrid constructs were created using hyaluronic acid as an attempt to facilitate bioprinting of low viscosity 5% GelMA. In the final Irgacure-GelMA solution, 2.4% HA was added and stirred at 37ºC for 10 minutes.

2.6.7 Preparation of Alginate-nanocellulose (AL/N)

This bioink was obtained from Cellink and is advertised as Cellink bioink. It is crosslinked with 'crosslinking agent' which is also obtained from the company.

2.7 Bioprinting

Inkredible bioprinter was used for printing constructs. The device was turned on, in the panel 'Home Axes' was selected. Next, the well plate was placed in the printbed and calibration of Z axis was performed, 'Move Z' was adjusted to 0.5+ in the panel. After that, the file containing the code could be accessed. Once selected, pressed 'bioprint'. Extrusion pressure could be adjusted by turning a knob located on the right side of the bioprinter.

2.8 Cytotoxicity analysis of PEG-DA Alginate

PEG-DA Alginate models (n=6) were bioprinted, crosslinked and placed directly on pig thymus mscs cultures in 12 well-plates. Additional PEG-DA Alginate models were bioprinted, crosslinked and placed on PBS for 1 and 2 days (n=6 for each day). The constructs were placed in cell culture after day 1 and 2 PBS rinse. Live/ Dead stain was used to analyse results.

2.9 Determining nozzle size and extrusion pressure

Bioinks printability was tested with different nozzle diameters: 22G, 25G and 27G. In regards to extrusion pressure, bioinks preferably needed to be extruded with a pressure lesser than 30kPa.

2.10 Optimal crosslink time

The appropriate crosslinking time was determine through the observation of shape fidelity in constructs and the ability of such to withstand incubation after the crosslinking process.

2.11 Porcine thymus mesenchymal cells isolation

Pig thymus was rinsed twice with PBS in a petri dish, the thymus was transferred into another petri dish to further the cleaning process of the sample. Blood and fat lumps were removed with the aid of scissors and forceps to obtain a cleaner sample. The thymus was cut into 1cm x 1cm pieces and transferred into a tube containing 10ml of collagenase I. The tube was placed in the incubator (37° C) for two hours. The digested tissue was placed in

70 µm cell stainer, in small amounts, and pressed with the base of a syringe to aid the cell isolation. If needed, PBS was added in small amounts to facilitate pressing through filter.Then, the liquid collected from the filtration process was placed into two different T-75 flasks and medium was changed after 48 hours.

2.12 Cell culture

Pig thymus mesenchymal cells were cultured in Dulbeco's Modified Eagle Medium (DMEM) supplemented with 10%FBS, 1% penicillin-streptomyocin; the cells were kept in a humidified incubator of 5% CO2 at 37ºC (Panasonic). The medium was changed every two days.

2.13 Cell passaging

The 10% DMEM solution was removed from the cell culture and the cells were gently washed with 5ml Phosphate Buffer Saline (PBS) twice. 2ml of trypsin was added to the flask and incubated for 5 minutes or until cells detached from the bottom of the flask. 8ml of DMEM was added into the incubated flask and resuspended continuously until all the cells were washed from the bottom. The solution was transferred into a bijou tube and placed under centrifugation for 5 minutes (1500 rpm, 9m·s−2, room temperature). The supernatant was disposed and 6ml of DMEM was added to the tube to resuspend the cell pellet. This solution was then placed in two different flasks, 3 ml each, and the addition of 5ml of DMEM was placed in each flask to obtain a total volume of 8ml in each flask.

2.14 Cell counting

Cell count was performed using an automated cell counter (Countess II FL) .The automated counter was adjusted to the specific type of cells used, porcine thymus- mesenchymal cells. 10 µlof the total solution of the cell passaging process was taken before centrifugation and placed in a slide which was then inserted into the counter providing the total number of cells in the sample.

2.15 Cell encapsulation

Bioinks were placed in the incubator, 37°C, for 5-10 minutes prior to encapsulation process as it ensured these were in liquid state and not solid to enable mixing with cells.

Cell encapsulation was performed by infusing 1 million cells (0.1 ml) into 0.9 ml of GelMA. The infused bioink was placed on ice for 5 minutes to allow the solution to become more viscous prior to crosslinking of each layer. Every layer was crosslinked with UV light (365nm). Medium (DMEM, 10%FBS, 1%P/S) was into wells and changed every 48 hours.

Cell encapsulation for AL/N was performed in similar manner to GelMA, however 1 million cells were added into 1ml of AL/N bioink. The same parameter was used for PEG-DA Alginate without collagen.

To mix the cells with the bioink, a cell mixer from a kit (Cellink) was used. 1ml syringe was used to collect the cell-infused DMEM, while a 12 ml syringe was used to collected the bioink. The upper part of the syringes were carefully placed on a perfectly fitted holding device. The extruding part of the syringes were attached to a cell mixer, which was further attached to a cartridge which goes into the bioprinter. Pressure was exerted on the upper part of the syringes to press the liquids down into the cartridge (Figure 10). The cartridge was placed into bioprinter and commanded to print constructs.

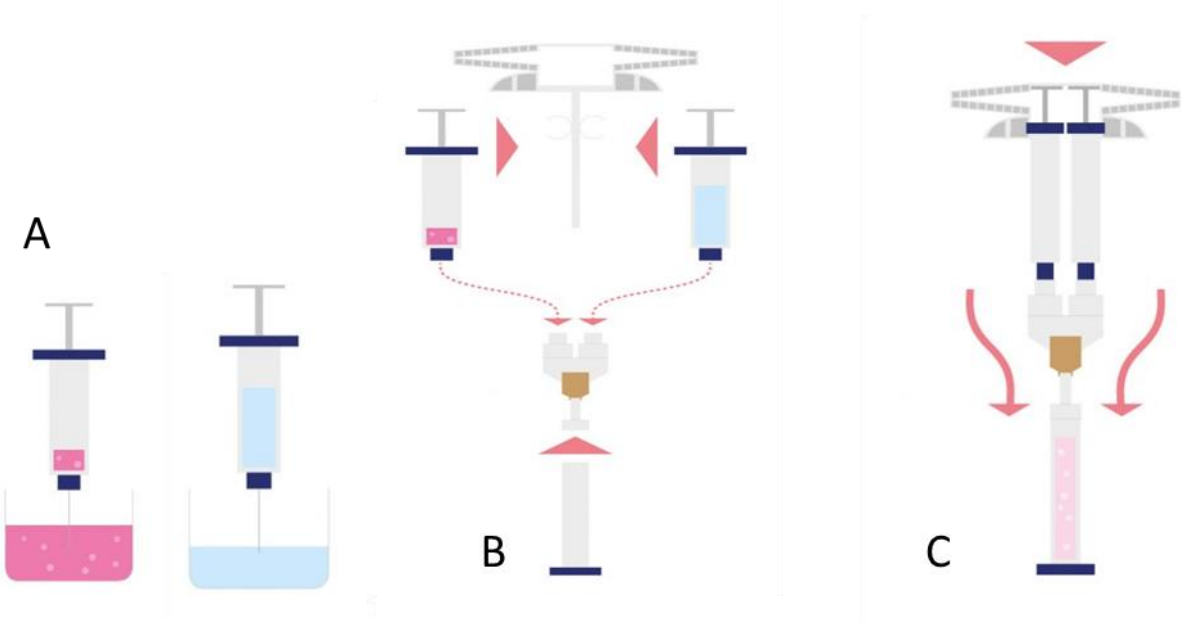

Figure 10. Cell mixer from Cellink. (a) pink fluid represents cell medium and blue represents bioink, both are being collected with different syringes. (b) the syringes are placed on holding device and then attached to cell mixing device. (c) syringes pressure causes content to mix into third syringe. Image adapted from Cellink.

PEG-DA Alginate with collagen constructs were encapsulated with cells after print. Constructs were extruded with a syringe. Each construct used 0.25ml of bioink. After being crosslinked with UV, the constructs were placed in DMEM-containing cells.Each construct was placed in DMEM containing 250,000 cells. The well plates were placed in an orbital shaker and DMEM was changed after 48 hours.

All constructs were crosslinked by UV light, except AL/N which was crosslinked using calcium (crosslinking agent, Cellink). The agent was placed at the end of construct bioprint (not after each layer) and left for 5 minutes. Agent was removed and DMEM was placed in well and plate was incubated.

2.16 Cell Viability Assessment s

DMEM surrounding constructs was removed and lived/dead stain mixture was added. The mixture contained standard volumes of 1000µl of 10% medium in combination with 2µl of ethidium bromide and 0.5µl of calcein. Constructs were incubated for 30 minutes, with standards of incubation of 5% CO_2 at 37°C.

Imaging was performed using Fluorescence microscope Zeiss Axio Observer z1 (Zeiss, Germany) with Zen Blue software. Cell viability assessments were carried at day 1,7,14 and 21 (n=6 for each time point). The percentage of cell viability was determined through (live cells/ total number of cells) x 100.

2.17 Tensile tests

The mechanical properties of constructs were measured with a Universal Testing Machine (Instron, USA). The tensile properties were obtained by performing a uniaxial stretching test, at room temperature 25°C and constructs remained wet which helped the handling of samples. The speed of the crosshead was 5mm/min and the gauge length was 4.5mm. Bluehill 3 was used to gather information from the tensile machine and it provided the measurements for tensile strength at maximum load (n=6) and Young's modulus (n=6)

2.18 Statistical analysis

GraphPad Prism was used for statistical analysis. All data are presented as mean ± SEM. Cell viability and tensile tests through the selected timepoints were assessed using one-way ANOVA, followed by Tukey's post hoc test. Tensile tests comparison between constructs with and without cells was assessed using unpaired t-test. P values <0.05 were considered to be statistically significant.

3 RESULTS

3.1 Translation of G-code to bioprinting using Cellink start

To analyse printing compatibility to code, 3D constructs were initially printed using Cellink start. This product was ideal for code testing as it was easy to use, presented a clear colour which facilitated assessment of the 3D construct and the fact that further crosslinking agents were unnecessary made the overall construct refinement process quicker.

It was observed that the created four-layered construct was successfully printed. It presented good shape fidelity and clear gaps throughout the structure which perfectly resembled the G-code. Additionally, the codes created to adapt print into 6-well and 12-well plates were successful. The 10-layered construct print was not successful. The low viscosity of Cellink start and lack of crosslinking system interfered on the shape fidelity of a more intricate design. Finally, the optimal extrusion pressure with nozzle 27G for Cellink start was found to be 15-25k Pa.

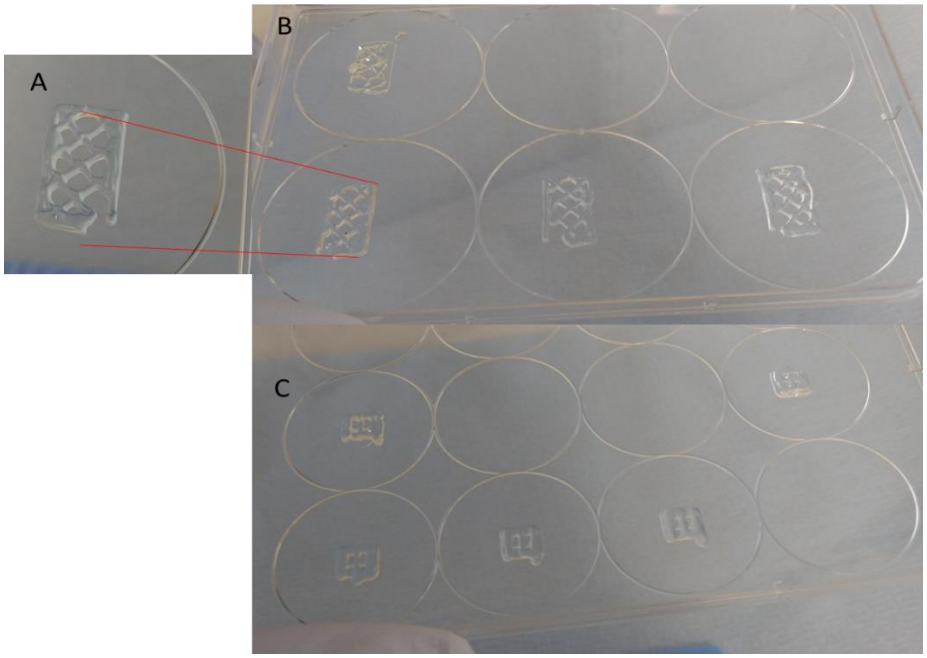

Figure 11. From code into bioprinting. Cellink start was used initially to test the properties of the translation from code to bioprinting. (a) shows the successful bioprint of Grid 45 pattern. (b), (c) shows the successful bioprinting in coordinates in 6 and 12 well plates.

3.2 Optimal nozzle size and pressure for bioinks

The translation of g-code into bioprinting was successful with cellink start, it was important to evaluate the bioprinting process with the chosen bioinks of this project. Therefore, before all

constructs were used for cell viability and tensile analysis, extrusion assessments were carried.

3.2.1 PEG-DA Alginate

It was found that the optimal nozzle size for PEG-DA Alginate was 22G.The use of this nozzle allowed the printing pressure to be between 15-22 kPa also providing an overall smooth printing process without nozzle clogging. The 25G nozzle increased the printing pressure to 30 kPa, consequently bioink extrusion was not continuous and a uniform construct was not achieved. Finally, bioink extrusion was not achieved with 27 gauge, the bioink appeared too viscous for extrusion in a smaller nozzle.

3.2.2 PEG-DA Gelatine

For PEG-DA Gelatine, print trials were performed with all nozzle sizes. However, extrusion was only possible with 22G at a pressure of 25-35 kPa. Extrusion of the bioink resulted in a 3D construct external shape similar to the code design, but the internal gaps of the structure were undefined resulting on a solid rectangular block.

3.2.3 GelMA

For the bioprinting of GelMA, 22G nozzle presented uncontrolled extrusion for most concentrations (5%, 7.5% and 10%). The low viscosity of the bioinks resulted in merged filaments and undefined constructs. It was found that 25G nozzle was ideal for the bioprinting of 7.5%, 10% and 20% GelMA. This nozzle provided a barrier preventing uncontrolled extrusion and created the desired grid pattern in the structure. The optimal pressure which provided a smooth print without clogging was between 10-18 kPa. Nozzle 27G required a higher pressure to allow extrusion, 25-30 kPa, and the bioprinting process was consistently extended due to nozzle clogs. Moreover, the final construct presented poor shape fidelity due to merged filaments.

It was not possible to print 5% GelMA in a grid pattern and four-layered design, the bioink presented low viscosity and despite best efforts to maintain the construct in shape by attempting to slow speed of print, the filaments of the construct consistently merged.

3.2.4 Alginate-nanocellulose (AL/N)

The optimal pressure for AL/N was found to be 10-15 kPa using 27G nozzle. Extrusion occurred with other nozzle sizes, however 27G presented higher shape fidelity than the others. Also, 22G presented higher volume of material extrusion creating a thicker structure with inconsistent shape fidelity prior to the crosslinking stage. 25G nozzle presented the same features mentioned for 22G nozzle, but with a higher degree of shape fidelity prior to crosslinking.

3.3 Optimal crosslinking layer by layer

All bioinks used in this study required a form of crosslinking. Following the success of establishing the optimal extrusion properties for each bioink by printing one layer, the crosslinking properties were tested focusing on optimal time to create a four-layer construct with final good shape fidelity.

3.3.1 PEG-DA

The crosslinking properties of PEG-DA Alginate presented optimal at a 5 seconds UV exposure for each layer. This parameter presented good shape fidelity for the 4 layers print and allowed the construct to withstand incubation without dissolution. 10 seconds of UV exposure for each layer also presented good shape fidelity. However, in the incubation process it became clear that the layers were separating which indicated a non-cohesive construct. 15 seconds UV exposure also created a high shape fidelity construct, but it was clear before incubation that the layers were individually constructed and on the incubation process, the layers were fully separated.

3.3.2 PEG-DA Gelatine

For PEG-DA Gelatine, the optimal UV exposure time was 5 seconds for each layer. Despite not presenting good shape fidelity, the material was able to withstand the incubation process with a solid and homogenous structure. In 10 seconds exposure, the construct presented signs of layer separation before incubation which were confirmed after incubation as the layers were found completely separated on the well-plate. The same applied to 15 seconds UV exposure.

3.3.3 Optimal crosslinking time for 5% GelMA

For 5% GelMA, various attempts were made to obtain a grid structure within the constructs but these were all unsuccessful. The filaments of the constructs always merged before the crosslinking process occurred making it difficult to achieve the desired 3D design. Instead the crosslinking properties were tested with the shape the biomaterial formulated once dispersed on the well plate. The optimal UV exposure time established for this bioink was 20 seconds per layer. This allowed the bioink to withstand incubation without dissolving. 15 seconds exposure presented a stable structure on the well plate when tilted from side to side, but the biomaterial completely dissolved in the incubator after 30 minutes. 10 and 5 seconds exposure presented poor structure stability when the well plate was tilted. The bioink was in liquid state and merged with DMEM prior to the incubation process.

3.3.4 Optimal crosslinking time for 7.5% GelMA

It was found that for 7.5% GelMA constructs the optimal UV exposure time was 20 seconds. This exposure time created a grid patterned construct with homogenous layers and capable of withstanding incubation. 15 seconds of UV exposure presented similar features to 20 seconds, the constructs were solid and withstood incubation for an hour, however, it was observed that after an overnight incubation the constructs became fragmented. 10 seconds exposure created a defined grid pattern but it dissolved during incubation after 30 minutes. 5 seconds exposure for each layer resulted on solid constructs but with merged filaments. However, after placement in incubator these were dissolved within 5 minutes.

3.3.5 Optimal crosslinking time for 10% and 20% GelMA

The optimal UV exposure for 10% GelMA was 15 seconds for each layer and the same was found for 20% GelMA. This exposure time created a cohesive structure for both materials without layer separation and dissolution under incubation. 10 seconds exposure was also explored for these materials and despite this parameter presenting good shape fidelity and incubation endurance. It was observed after overnight incubation that the constructs were partially disintegrated. 5 seconds of incubation created defined constructs but dissolution on the incubation process for both 10% and 20% GelMA.

3.4 The addition of HA to 5%GelMA

The addition of 2.4% HA to GelMA resulted on a faster printing process overall. HA allowed the ice-cooling process in GelMA to be bypassed while still providing good shape fidelity. The uncontrolled nozzle drip which occurred with 5% GelMA concentrations was eliminated as HA provided the bioink a higher viscosity.

3.4.1 Optimal nozzle size and extrusion pressure for GelMA-HA

The printing properties of GelMA-HA presented very successful. The addition of HA to the bioink provided overall easier handling of the solution due to higher viscosity. This addition caused a slight change in the colour of the material, from a clear and transparent solution to a slight opaque. The optimal nozzle for printing this material was 25G at a pressure of 12-20 kPa, these parameters allowed a solid and consistent extrusion of the bioink. Extrusion with 22G nozzle was attempted but the bigger nozzle size created excessive extrusion of material even at lower pressures. In contrast, 27G nozzle presented no extrusion of material up to 40 kPa pressure.

3.4 Final constructs and overall bioprint time

PEG-DA Alginate presented successful shape fidelity(Figure 12 a) and the overall time to print a construct was 3 minutes. PEG-DA Gelatine presented a less than ideal shape fidelity (Figure 12 b), however it was still used to carry analysis, the overall time of print for this construct was also 3 minutes.

5% GelMA presented a poor shape fidelity (Figure 12 c), but cell viability assessments and some tensile tests were performed. The overall time to create 1 construct was 20 minutes. 5%GelMA-HA (Figure 12 d)took considerably less time, 3 minutes. For all remaining GelMA concentrations (Figure 12 e-g) the average time to prepare 1 construct was 25 minutes. It is important to highlight that the constructs were prepared in batches, therefore 6 constructs took 25 minutes preparation. Finally, for AL/N constructs the overall time to prepare a construct wa 7 minutes.

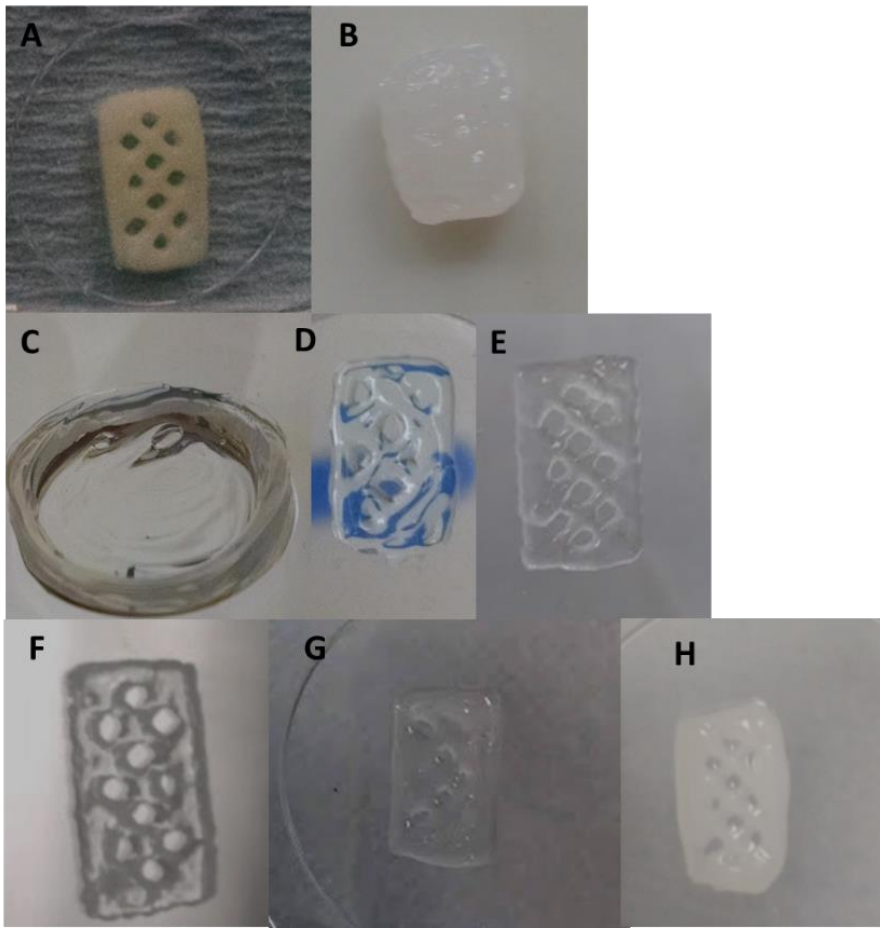

Figure 12. (a) PEG-DA Alginate without collagen. (b) PEG-DA Gelatine. (c) 5% GelMA. (d) 5% GelMA-HA. (e) 7.5% GelMA. (f) 10% GelMA. (g) 20% GelMA. (h) AL/N.

3.5 Cell viability of PEG-DA Alginate

At day 0 and 1 following the bioprinting of cell-seeded PEG-DA Alginate constructs, cell viability assessment was performed. Data was obtained through five images captured from each sample (n=6) in 2.5x and 20x magnification.

PEG-DA Alginate presented 100% cell death in all constructs when observed two hours after the bioprinting process (Figure 13). To understand if cell death was a result of the stress from the bioprinting shortly followed by live and dead stain, the experiment was set again and analysed on day 1.The viability presented on day 1 was 100% cell death. Although, in contrast to day 0 all constructs were found absent of cells. Further analyses showed that by day 1 all cells were located at bottom of the flask rather than being held in the construct.

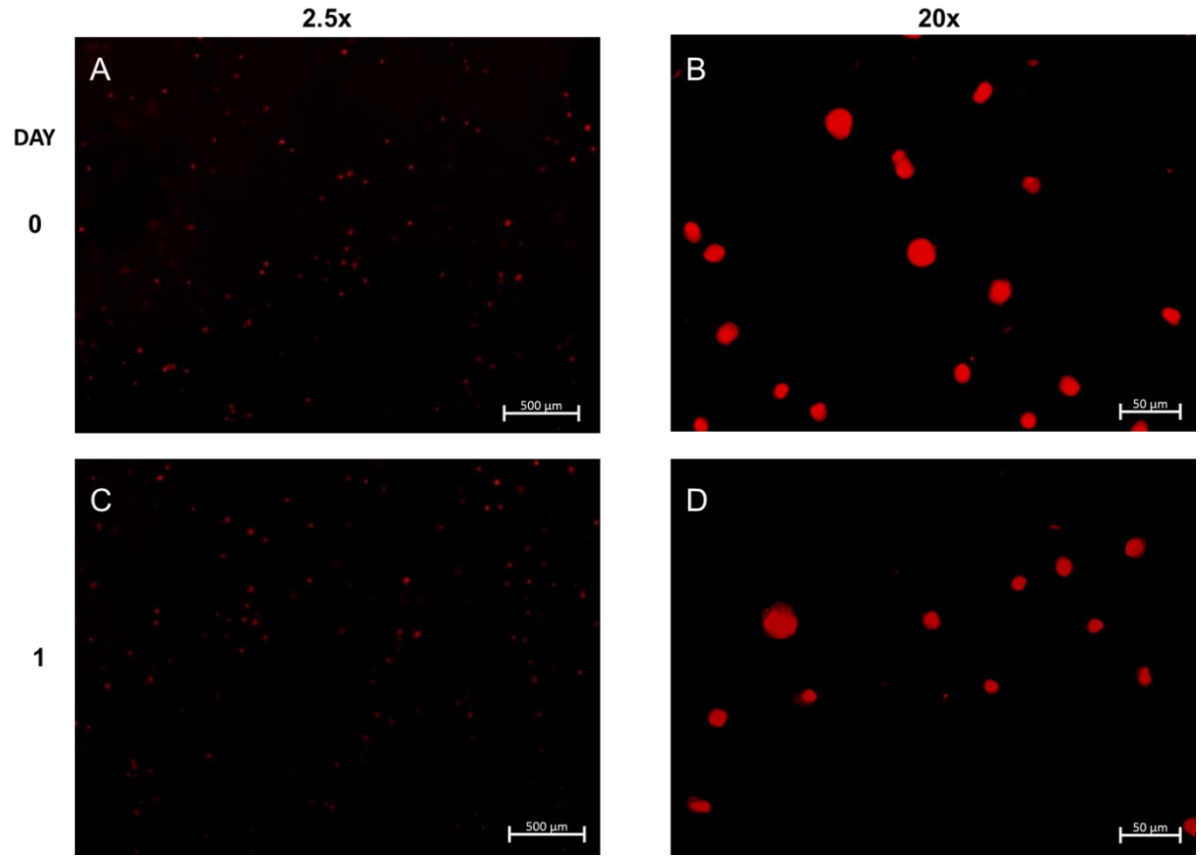

Figure 13. Cell Viability Images of PEG-DA Alginate Constructs. Dead cells (red) were abundant at day 0 **(a and b).** Assessment was done at day 1 in a repeated experiment to determine whether the stress from bioprinting and live/dead stain were causing death. At day 1 **(c and d),** cells were found dead, however there were no cells located within the construct. All cells were found on the bottom of the flask. Scale bar in **a and c** is representative of 500µm. Scale bar in **b and d** is representative of 50µm.

3.6 Cytotoxicity of PEG-DA Alginate

To analyse the factors that led to extensive cell death in PEG-DA Alginate constructs, further analysis with the material were carried. To determine whether PEG-DA Alginate contained toxic substances which caused harm to cells, printed constructs without cells were directly placed in cell culture. For control, untreated cells (absent of constructs) were placed in separate wells for analysis.

At day 1, the control presented 100% cell viability and cells were well attached to the bottom of the flask (Figure 14). In contrast, cell cultures containing PEG-DA Alginate constructs at day 1 presented 100% cell death as seen on previous experiment.

Following these results, further investigation on the properties of the bioink was performed. PEG-DA Alginate constructs (cell-free) were printed and directly placed on PBS. Constructs were either maintained in PBS for 1 or 2 days. After PBS rinse, the constructs were transferred to cell culture for one day and cell viability was analysed.

1-day PBS rinsed constructs presented 75.78 ±3.21 % average viability at day 1 (Figure 15), this was found to be significantly lower than the viability for the control culture. 2-days PBS rinsed constructs presented 91.38 ± 2.52% viability which is significantly higher than 1-day PBS rinse. The cell culture for both set of experiments presented well attached cells to the bottom of the flask and signs of proliferation were observed.

These results demonstrated that PEG-DA Alginate could not be used for direct bioprinting of cells. Instead the bioink could only be seeded with cells after construct print and PBS rinse for 2 days.

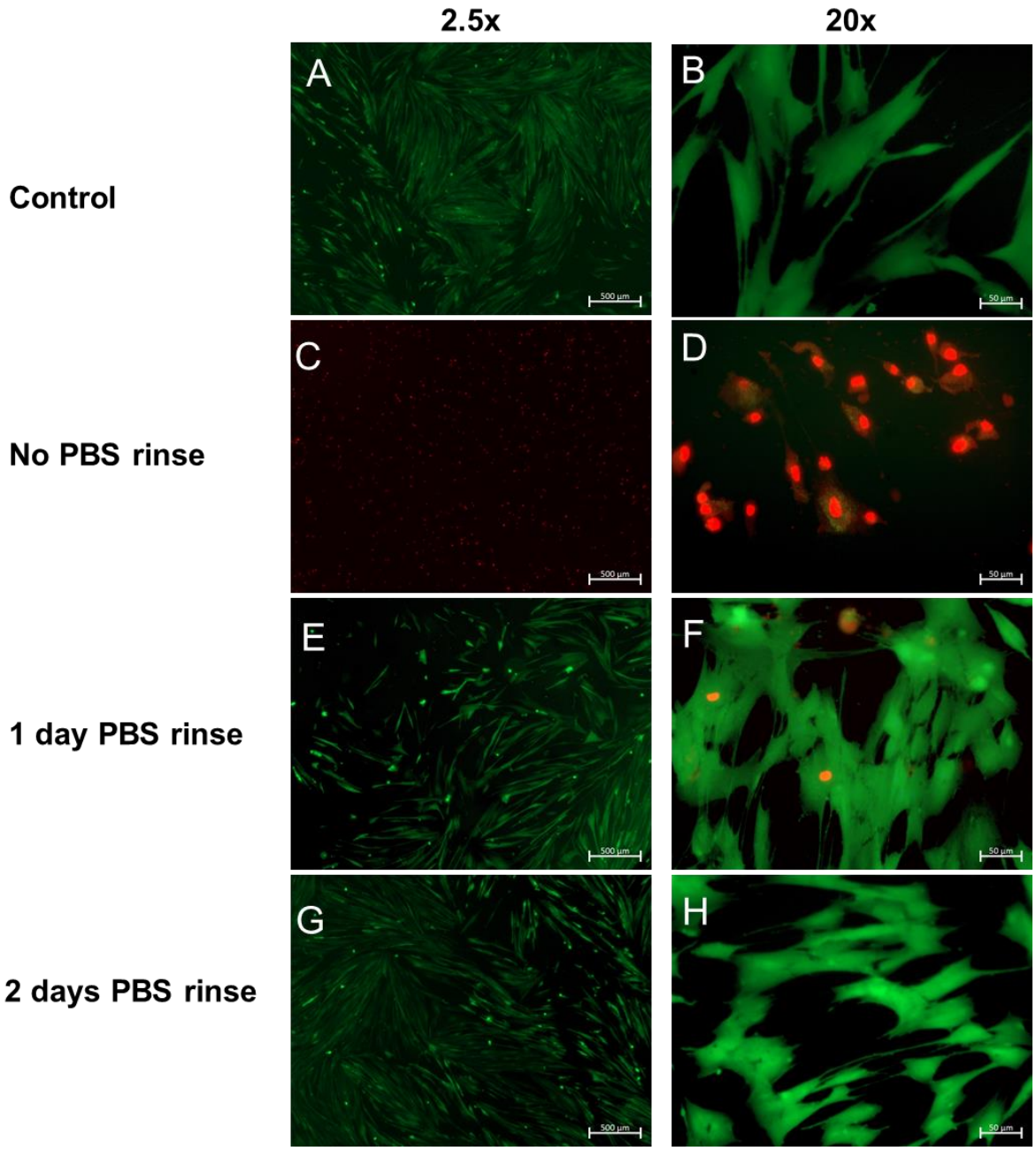

Figure 14. Cell Viability Images of Cytotoxicity of PEG-DA Alginate Constructs. Viable cells (green) were significantly more abundant for constructs rinsed for two days **(g and h)** compared to untreated constructs **(c and d).** Constructs rinsed for one day **(c and d)** also showed a significant increase in cell viability compared to no untreated. A control was used for the experiment **(a and b**), one day rinsed and untreated constructs presented significantly lower viability compared to control. Scale bar in **a, c, e, g** is representative of 500µm. Scale bar in **b, d, f, h** is representative of 50µm.

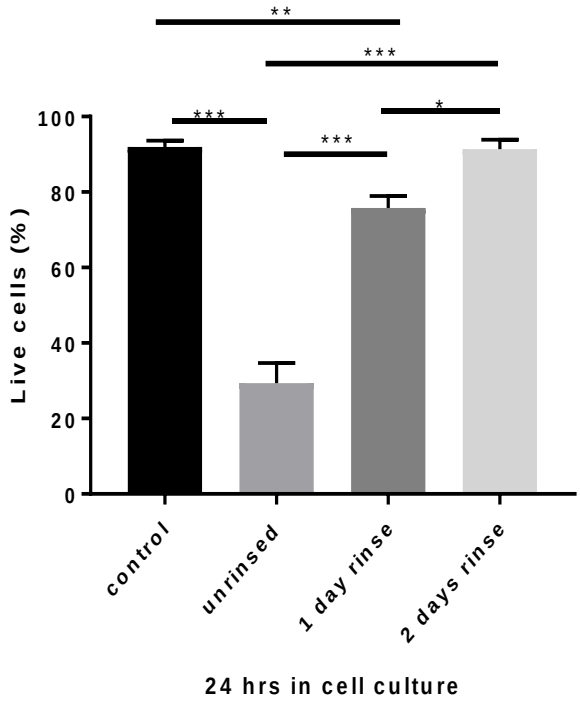

Figure 15. Impact of PBS rinse upon PEG-DA Alginate constructs cytotoxicity. All assessments were performed one day after the construct was implemented into the cell culture. The viability of cell treated with rinsed constructs were significantly higher than samples treated with unrinsed PEG-DA Alginate constructs. The greatest viability was demonstrated with a 2 days PBS-rinse which proved to be similar to the average viability of the control sample. 1 day rinsed constructs presented a significant lower cell viability when compared to control. N=6 per time point. One-way ANOVA followed by Tukey's post hoc test, * $p<0.05$, ** $p<0.01$, *** $p<0.001$. Data presented as mean ± SEM.

3.7 PEG-DA Alginate with collagen: impact of collagen addition to the bioink properties

Following information on the non-adhesive and non-absorptive nature of PEG-DA, the addition of collagen to the bioink was added to PEG-DA Alginate to increase cell attachment properties.

Upon the addition of collagen, the bioink presented a lower viscosity and phase separation prior to printing. Due to the heterogeneous bioink, nozzle clogging was a consistent occurrence with all nozzle sizes. Although less frequent with 22G nozzle, a continuous bioink extrusion was not obtained. Despite poor shape fidelity, it was still important to assess cell viability upon the addition of collagen to the bioink. Therefore, a syringe was used to extrude 0.5 ml of bioink in each well. After crosslinking under UV, the constructs still presented phase separation, but the cured part of the biomaterial withstood incubation allowing viability assessment to be performed.

3.8 Cell Viability of rinsed PEG-DA Alginate-collagen constructs

Following the print of PEG-DA Alginate-collagen constructs and 2 days PBS rinse, cell seeding was performed. 1 million cells were placed in the well of each construct, the wells were placed in a shaker and incubated for 24 hours (day 1). Constructs were cultured in flaks and cell viability assessment was performed at day 1, 7, 14 and 21.

The average cell viability for constructs at day 1, immediately after removal from shaker, was found to be 75.15 ± 0.94 % (Figure 16). At day 7, the average cell viability significantly decreased to 65.54 ± 1.19% and for day 14, the average viability significantly decreased even further to 48.89 ± 1.1% compared to day 7. At day 21, a drastic decrease in viable cells was observed with viability presented at a 5.09 ± 1.176% average, demonstrating an overall significant decrease in viability and presenting over a 93% decline when compared to day 1.

The cells were found to be distributed within the construct surface and inner parts (Figure 17). Most cells were located at the edges of each construct and through the time points, cell death mainly occurred to cells located at the centre.

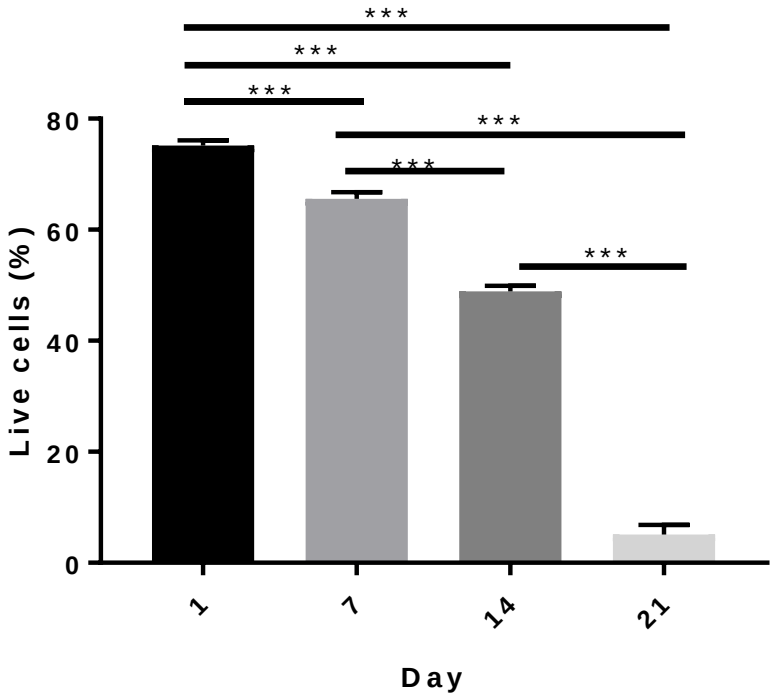

Figure 16. Average Cell Viability of PEG-DA Alginate-collagen constructs overtime. The average viability shows a gradual significant decline overtime with the lowest value at day 21 which dead cells were more abundant. N=6 per timepoint. One-way ANOVA followed by Tukey's post hoc test, *** $p<0.001$. Data presented as mean ± SEM.

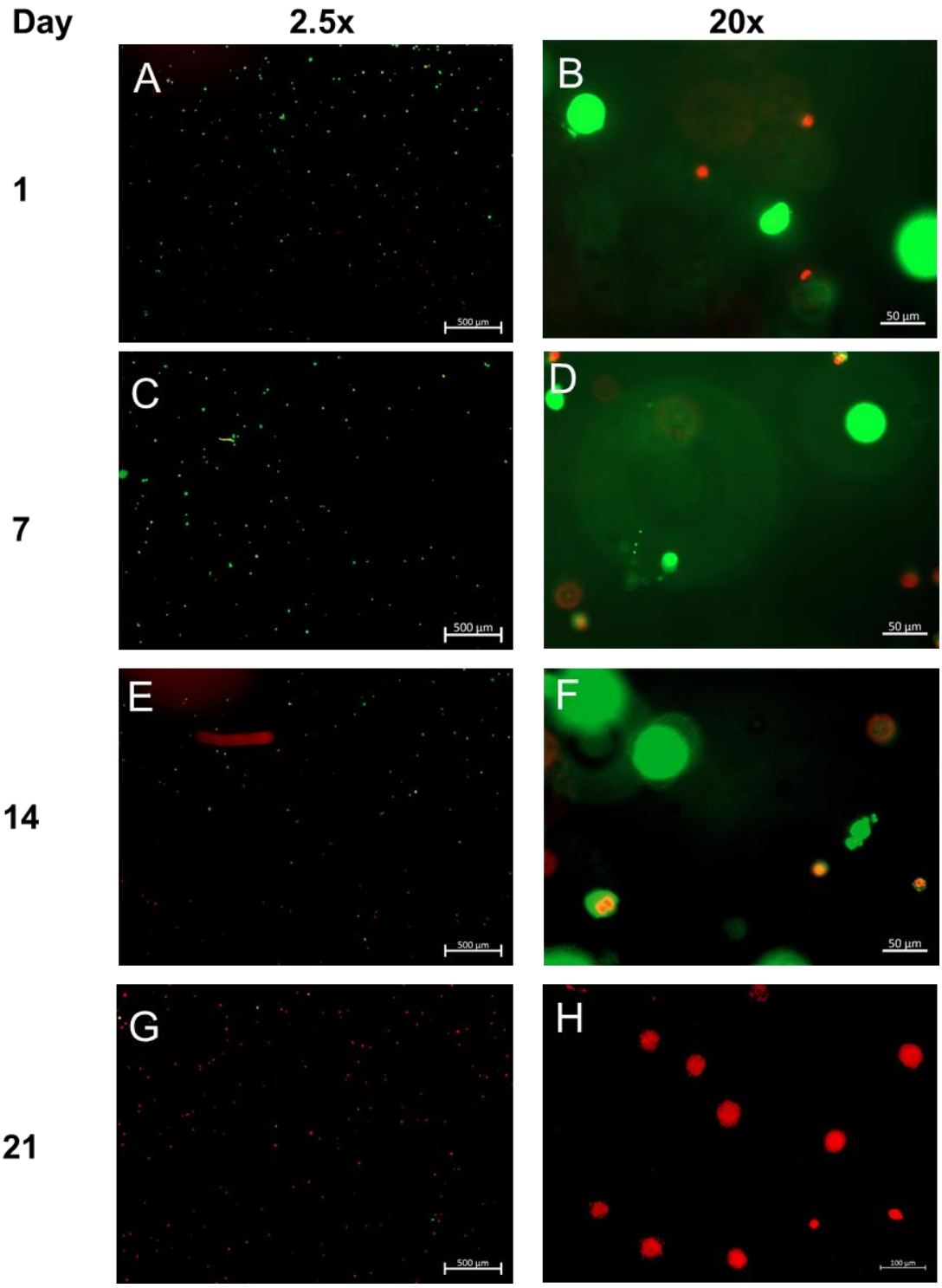

Figure 17. Cell Viability Images of PEG-DA Alginate-Collagen Constructs. Viable cells (green) were abundant on day 1 and 7 following the bioprinting of constructs (a-d). At day 14 more dead cells (red) could be seen than previous day (e and f) and day 21 showed a prominent increase of dead cells (g and h). Out of focus cells demonstrate the cells being on different planes within the constructs (b, d, f and h). Scale bar in **a, c, e, g** is representative of 500µm. Scale bar in **b, d, f, h** is representative of 50µm.

3.9 Cell viability of PEG-DA Gelatine

This bioink was based on PEG-DA Alginate, it was directly printed with cells without PBS rinse. At day 0, all cells within the construct were dead. At day 1, all cells were shown to be dead (Figure 18). However, in contrast to PEG-DA Alginate, the dead cells remained within the construct and no cells were detected at the bottom of the flask at this time point. Despite abundant death, it was clear that more cells were attached to constructs using this bioink than on PEG-DA Alginate with or without collagen. These results led to further interest on naturally sourced biomaterials and animal based bioinks due to enhanced cell attachment properties compared to plant based.

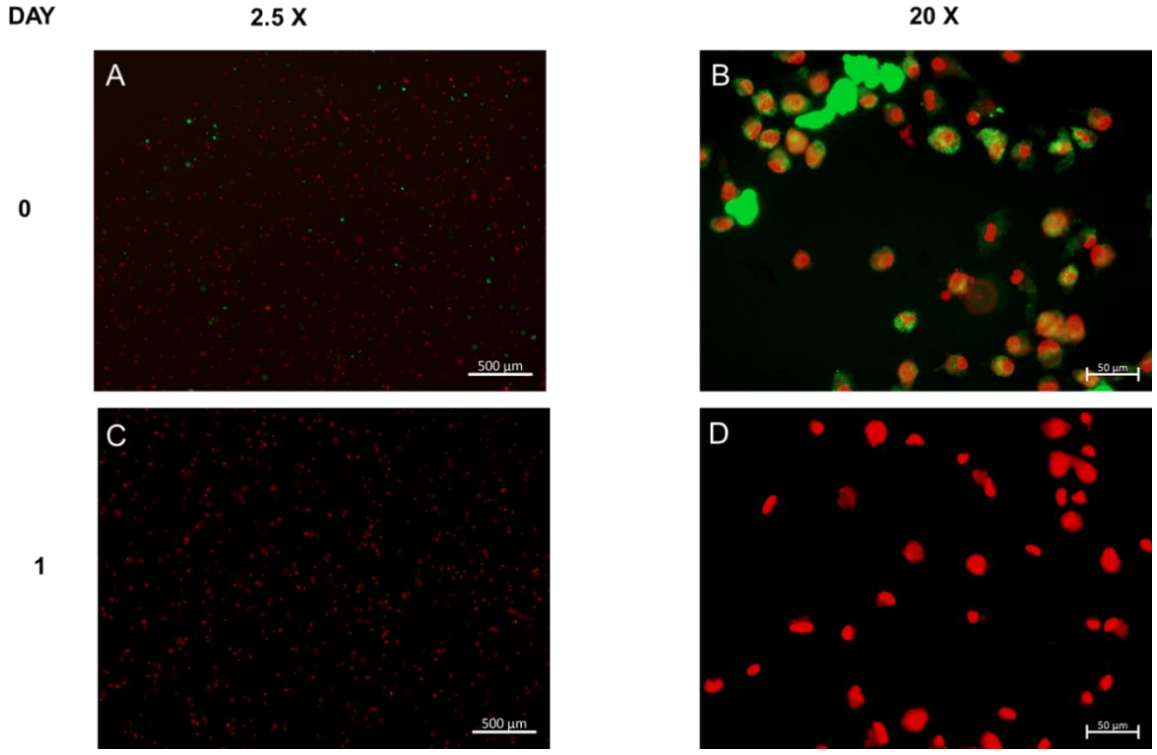

Figure 18. Cell Viability Images of PEG-DA Gelatine constructs. Dead cells (red) were abundant on day 0, two hours after bioprinting (a-b). The red centre in the outer green cells signify that all cells are dead independent of the green dye (b). At day 1, all cells were dead as expected to the results from day 0, however the dead cells remained attached to the constructs. Scale bar in **a and c** is representative of 500µm. Scale bar in **b and d** is representative of 50µm.

3.10 Cell viability of 5% GelMA constructs

Following the bioprinting of 5% GelMA constructs, cell viability assessments were performed at day 1, 7, 14 and 21 in similar manner to previous bioinks.

The average cell viability for 5% GelMA constructs at day 1 was 81.38 ± 4.02% (Figure 19). At day 7, cell viability demonstrated a slight increase to 89.08 ± 2.67%, though this increase was no significant. At day 14, average viability was 88.28 ± 2.62% which was slightly lower than day 7. At day 21, cell viability slightly decreased to 87.13 ± 2.98%, not significantly. Day 21 showed approximately a 7% increase in viability compared to day 1.

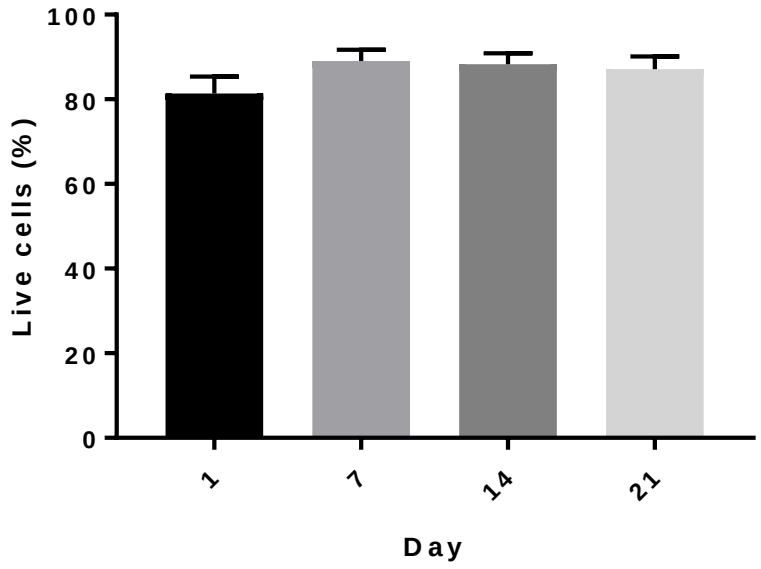

Figure 19. Average cell viability of 5% GelMA constructs. From day 1 to consecutive timepoints, the cell viability slightly increase but not significantly. N=6 per timepoint. One-way ANOVA. Data presented as mean ± SEM.

Overall, 5% GelMA presented good cell viability throughout 21 days (Figure 20). Moreover, the transparent nature of the material along with the flat structure formed due to unsuccessful 3D grid pattern enabled a clearer imaging of cells within the material. At day 1, it was observed clear spindle-shaped cells with good spread throughout the entire surface of the material. At day 7, the cells appeared just as confluent and well distributed like day 1, the same was true for days 14 and 21. In addition to great cell viability, there were no signs of cell migration outside of the material. The bottom of the flask consistently presented no signs of cells.

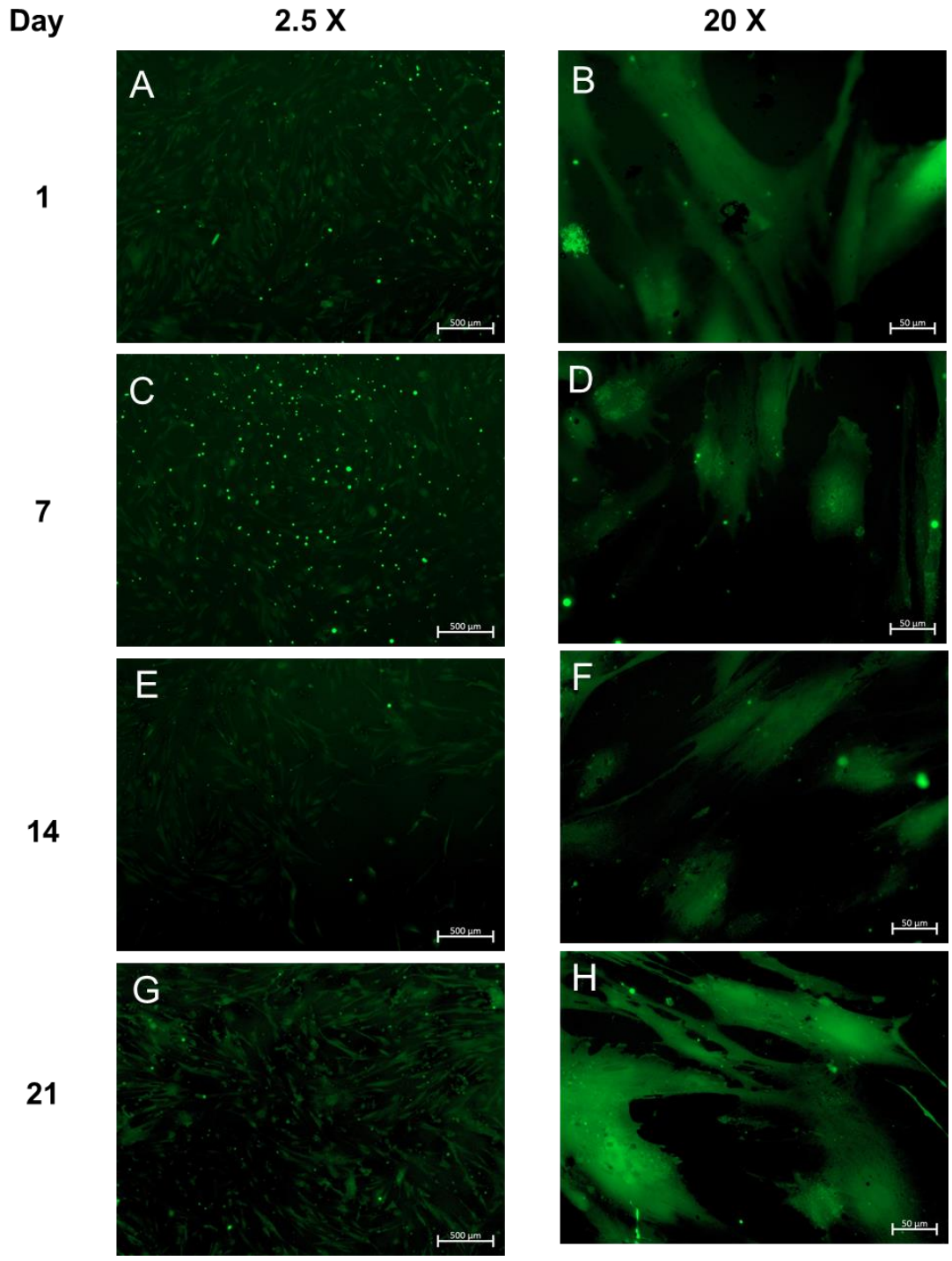

Figure 20. Cell Viability Images of 5% GelMA constructs. Viable cells (green) were abundant all throughout the timepoints. A spindle-like structure of the cells were observed throughout all timepoints. Scale bar in **a, c, e, g** is representative of 500µm. Scale bar in **b, d, f, h** is representative of 50µm.

3.11 Cell viability for 5% GelMA-HA

Due to the inability to obtain a 3D grid pattern with 5% GelMA, 2.4% hyaluronic acid was added into the solution to assist with the stability of the structure. Assessments were performed to determine if the addition of HA and 3D grid pattern affected cell viability. These assessments were performed in a similar manner to the previous experiments.

The average cell viability for 5% GelMA-HA constructs at day 1 was 78.35 ± 3.63% (Figure 21). For day 7, the average cell viability increased to 81.91 ± 3.28%, but this increase was not statistically significant. At day 14, the average cell viability was 79.77 ± 4.21% which is slightly lower than day 7 but the change was not found to be significant. At day 21, the average cell viability was 84.83 ± 3.95% which is indicated an 8.27% increase in viability when compared to day 1 assessment.

The cells were distributed within the layers of the grid pattern and surface (Figure 22). During the 21 days of assessment the cells demonstrated good distribution, although it was difficult to determine the uniformity of the distribution. Moreover, cell migration did not occur from the biomaterial into the bottom of the flask.

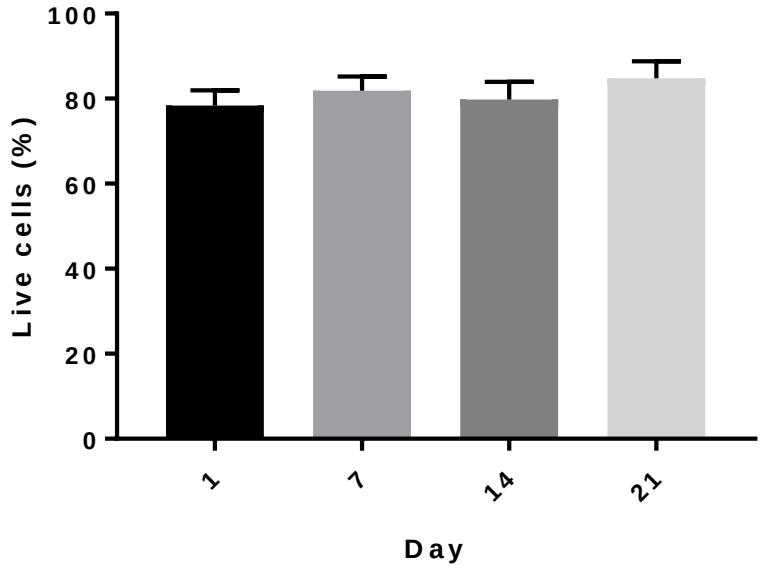

Figure 21. Average cell viability for 5% GelMA-HA constructs. From day 1 to consecutive timepoints, the cell viability increased but not significantly. Day 21 presented the highest viability. N=6 per timepoint. One-way ANOVA. Data presented as mean ± SEM.

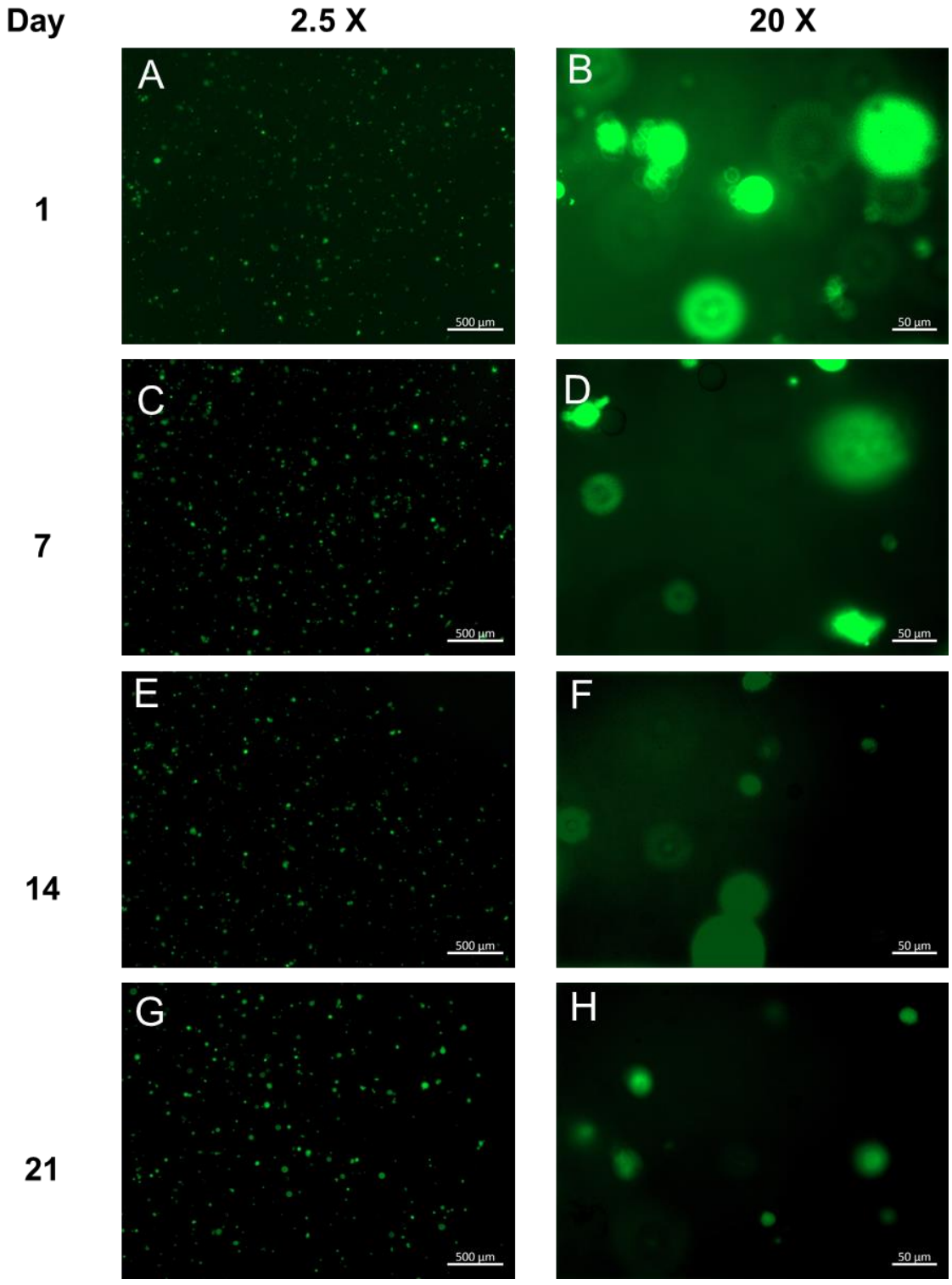

Figure 22. Cell Viability Images of 5% GelMA-HA constructs. Viable cells (green) were abundant throughout all timepoints. Out of focus images show that the cells were located within different planes in the constructs (b, d, f and h). Scale bar in **a, c, e, g** is representative of 500µm. Scale bar in **b, d, f, h** is representative of 50µm.

3.12 Cell viability for 7.5% GelMA

Following the difficulty to create a 3D grid pattern with 5% GelMA, it was important to determine if an increase in concentration of GelMA would allow better stability of the construct. As previously mentioned, the increase to 7.5% GelMA was successful for shape stability. The next stage was to assess cell viability for this modified bioink. All assessments were performed at a similar manner to previous experiments.

The average cell viability for 7.5% GelMA constructs at day 1 was 85.97 ± 2.74%. Cell viability gradually decreased throughout the timepoints assessed. At day 7, cell viability slightly decreased to 75.45 ± 3.95, this decrease was not significant. The decrease in cell viability for days 14 (70.85 ± 4.92%) and 21 (64.67 ± 2.06%) were considered statistically significant when compared to day 1. Day 21 presented the most significant decrease in viability compared to day 1.

The cells were well spread within the construct layers and surface. In contrast to 5% GelMA imaging, the cells in this biomaterial were not captured on a spindle-shaped form. The 3D construct made it difficult to obtain focused images of cells in higher resolution, but this difficulty shows that cells were located at different planes in the construct (b-h).

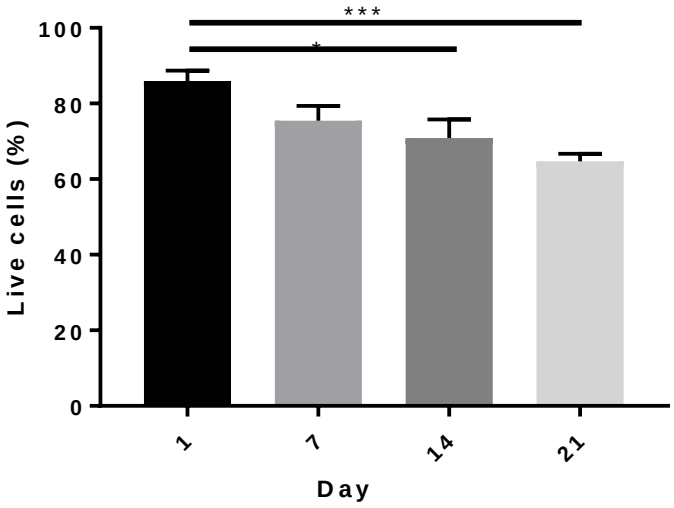

Figure 23. Average cell viability of 7.5% GelMA constructs. Cell viability gradually decreased overtime. The change in viability was only considered significant from day 14 onwards. N=6 per timepoint. One-way ANOVA. Followed by Tukey's post hoc test, * $p<0.05$. Data presented as mean ± SEM.

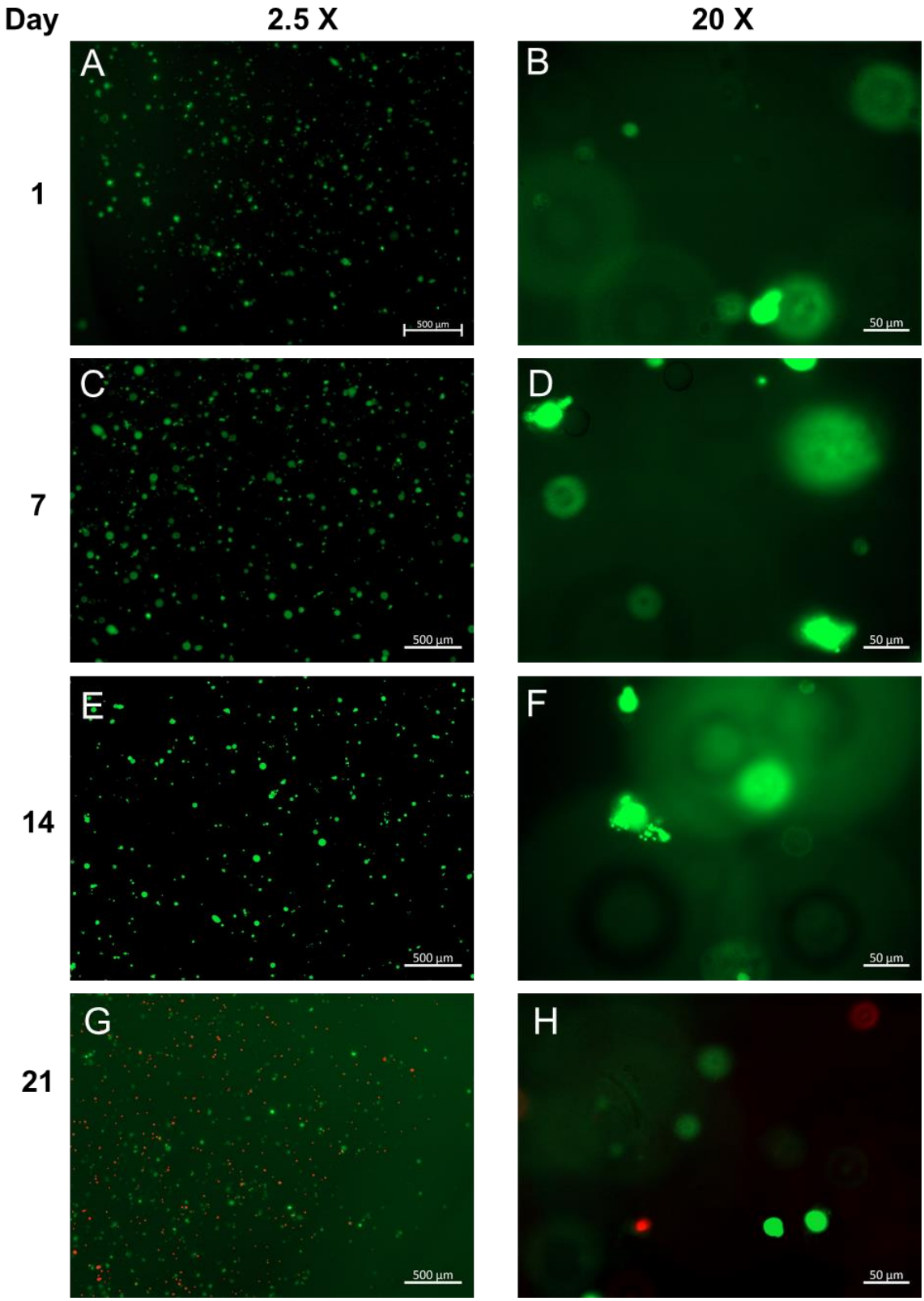

Figure 24. Cell Viability Images of 7.5% GelMA constructs. Viable cells (green) were abundant from day 1 to 14 (a, b, c, d, e and f). At day 21, some dead (cells) were observed. Out of focus cells demonstrate that cells were in different planes in the constructs (b, d, f, h). Scale bar in **a, c, e, g** is representative of 500µm. Scale bar in **b, d, f, h** is representative of 50µm.

3.13 Cell viability for 10% GelMA

10% GelMA constructs were cultured for 21 days and cell viability assessments were performed to analyse the impact of the increase of GelMA concentration in the cells. Cell viability presented highest at day 1 with 85.03 ± 3.48% live cells within the construct. In the subsequent timepoints, viability significantly decreased when compared to day 1. At day 7, cell viability was 72.75 ± 3.96% and at day 14, the average cell viability was 69.84 ± 2.69%. Day 21 presented the lowest cell viability, 58.44 ± 1.41%. In comparison to day 7, the decrease in viability of day 21 was significantly lower.

Throughout 21 days the cells were well spread within the construct. Again, the cells were captured out of focus due to difficulty of imaging in 3D plane, but that shows that the cells were spread within different layers in the construct. The bottom of the flask was also observed, and no major sign of cell migration was detected.

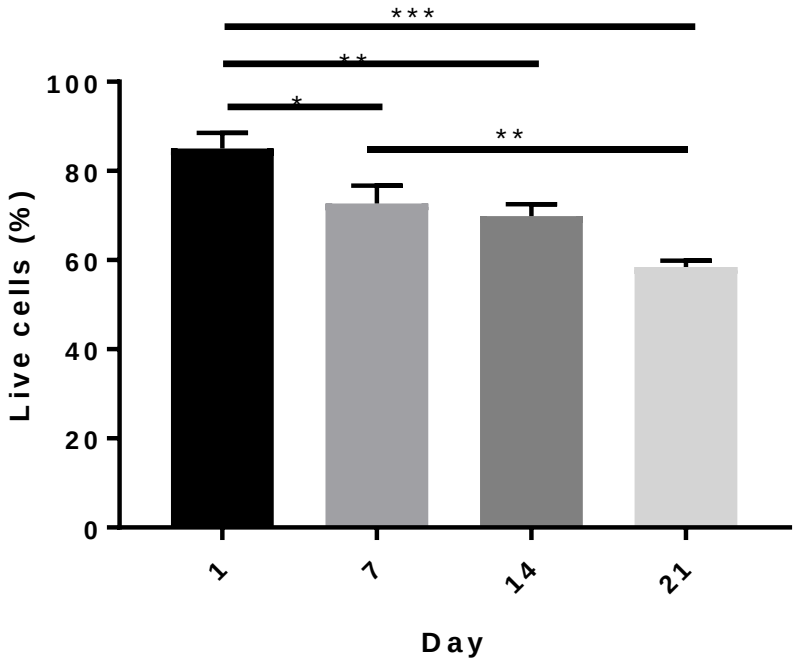

Figure 25. Average cell viability of 10% GelMA constructs. Cell viability significantly declined overtime. N=6 per timepoint. One-way ANOVA followed by Tukey's post hoc test, *p<0.05, **p<0.01 and ***p<0.001. Data presented as mean ± SEM.

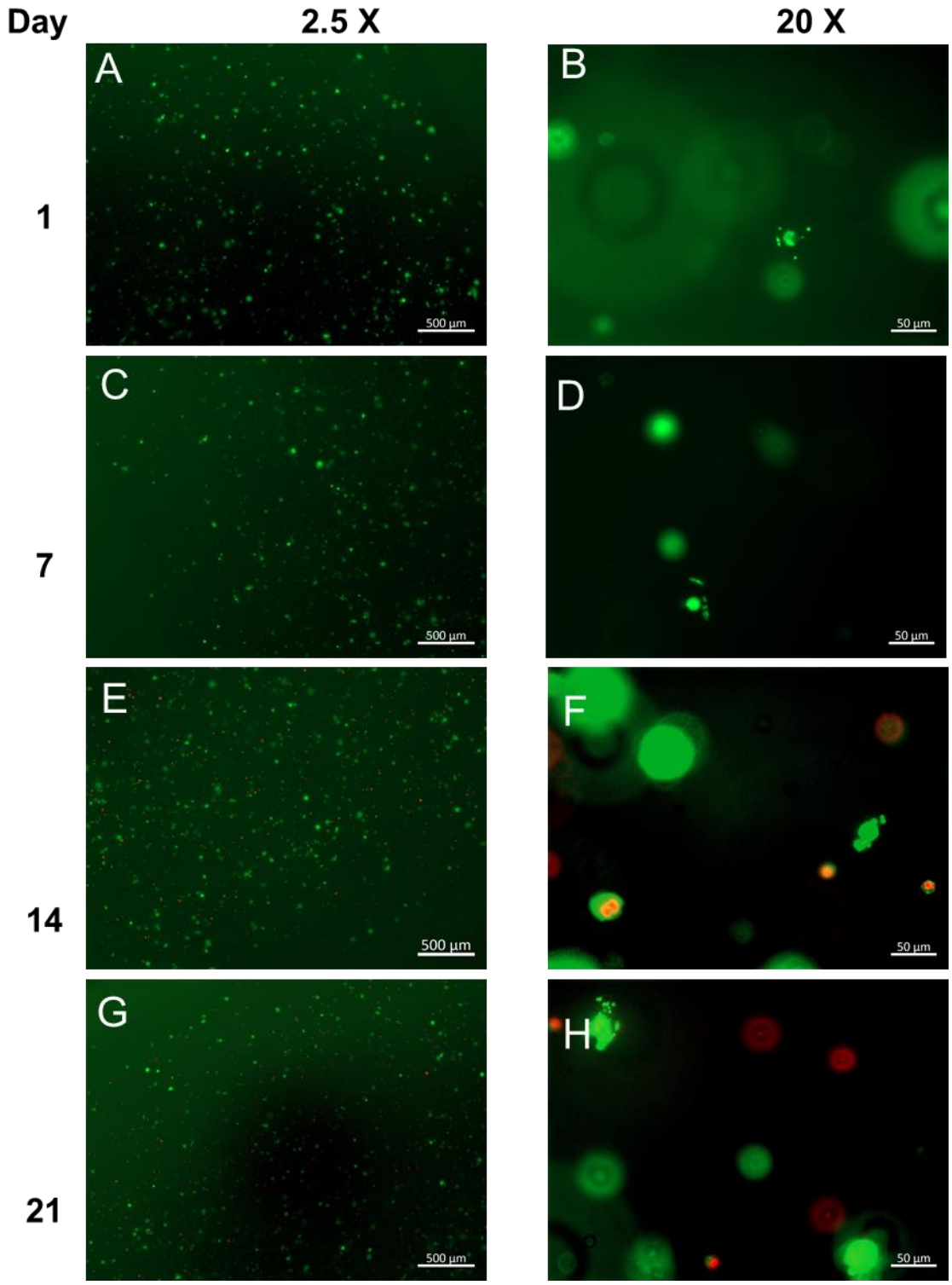

Figure 26. Cell Viability Images of 10% GelMA constructs. Viable cells (green) were abundant mostly abundant on day 1 and 7 (a-d). At day 14 (e and f) , it was observed more dead cells than on previous day and the same applied for day 21 (g and h). Out of focus cells demonstrate that cells were in different planes in the constructs **(b, d, f, h)**. Scale bar in **a, c, e, g** is representative of 500µm. Scale bar in **b, d, f, h** is representative of 50µm.

3.14 Cell viability for 20% GelMA

At day 1, there was 100% cell death in 20% GelMA constructs. The cells were found still attached to constructs (Figure 27).

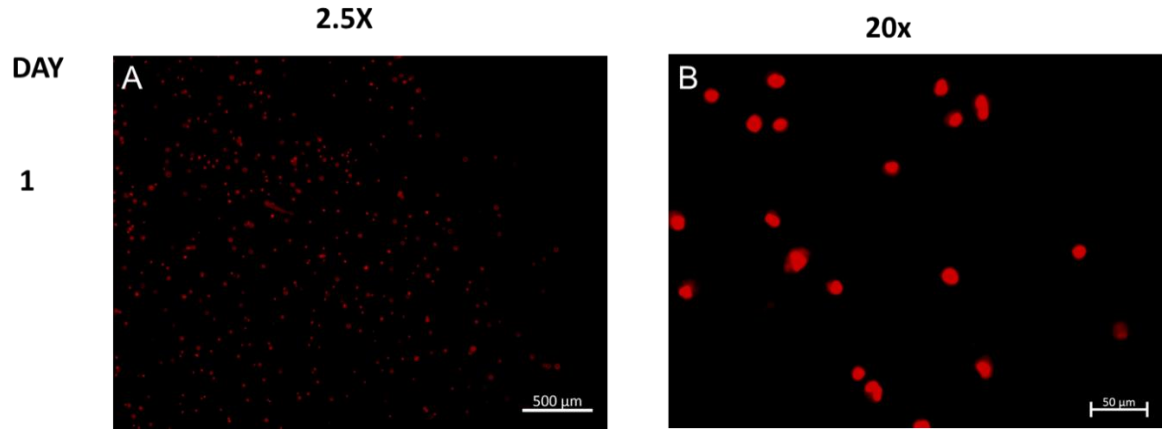

Figure 27. Dead cells (red) are abundant on day 1. Scale bar in **a** is representative of 500µm. Scale bar in **b** is representative of 50µm.

3.15 Cell viability for AL/N

The last set of experiments focused on animal-based biomaterials. Having previously assessed cell viability in synthetic biomaterials, PEG-DA, it was important to analyse cell viability using alginate alone. AL/N was used for bioprinting constructs and cell viability was analysed for 21 days.

Throughout the 21 days assessment, viable cells remained abundant. At day 1, the cell viability for AL/N constructs was 83.16 ± 4.03% (Figure 28). The viability presented a slight increase for day 7, 84.65 ± 4.38% within the constructs. Interestingly at day 7, it was observed that some cells had migrated to the bottom of the flask, although these were not quantified. At day 14, it was observed that most cells within the construct migrated to the bottom of the flask. Cell viability was quantified for the cells located at the bottom of the flask, 82.99 ± 5.12. At this time point, 62 live cells were counted within the construct and no dead cells. At day 21, even less cells were found within the constructs, at this timepoint cell viability for cells located at the

bottom of the flask was 81.21 ± 5.18%. Overall, the cell viability variance for timepoints was not significant.

The imaging for AL/N constructs was performed with fluoresce and light microscopy (Figure 29). The use of light microscopy enabled the instant feedback on cell migration prior to staining capturing images of cells located on the bottom of the flask Figure (c,f,I,l). Live cells were captured at day 1 and 7 and live cells were clearly abundant within the constructs. However, not many cells were seen within constructs for the following timepoints even when the constructs were further dissected into smaller pieces to enable easier microscope analysis. Fluorescence images of cells located at the bottom of the flask were captured and used for cell viability quantification.

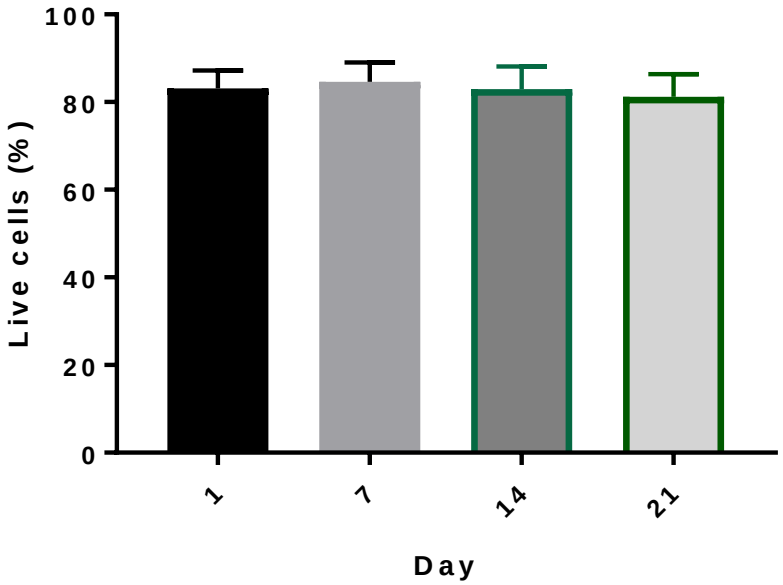

Figure 28. Average cell viability for AL/N constructs. The average cell viability remained nearly constant. Highlighted green bars indicate the cell viability from the bottom of the flask as the cells migrated from the construct at that point. N=6 per timepoint. One-way ANOVA. Data presented as mean ± SEM.

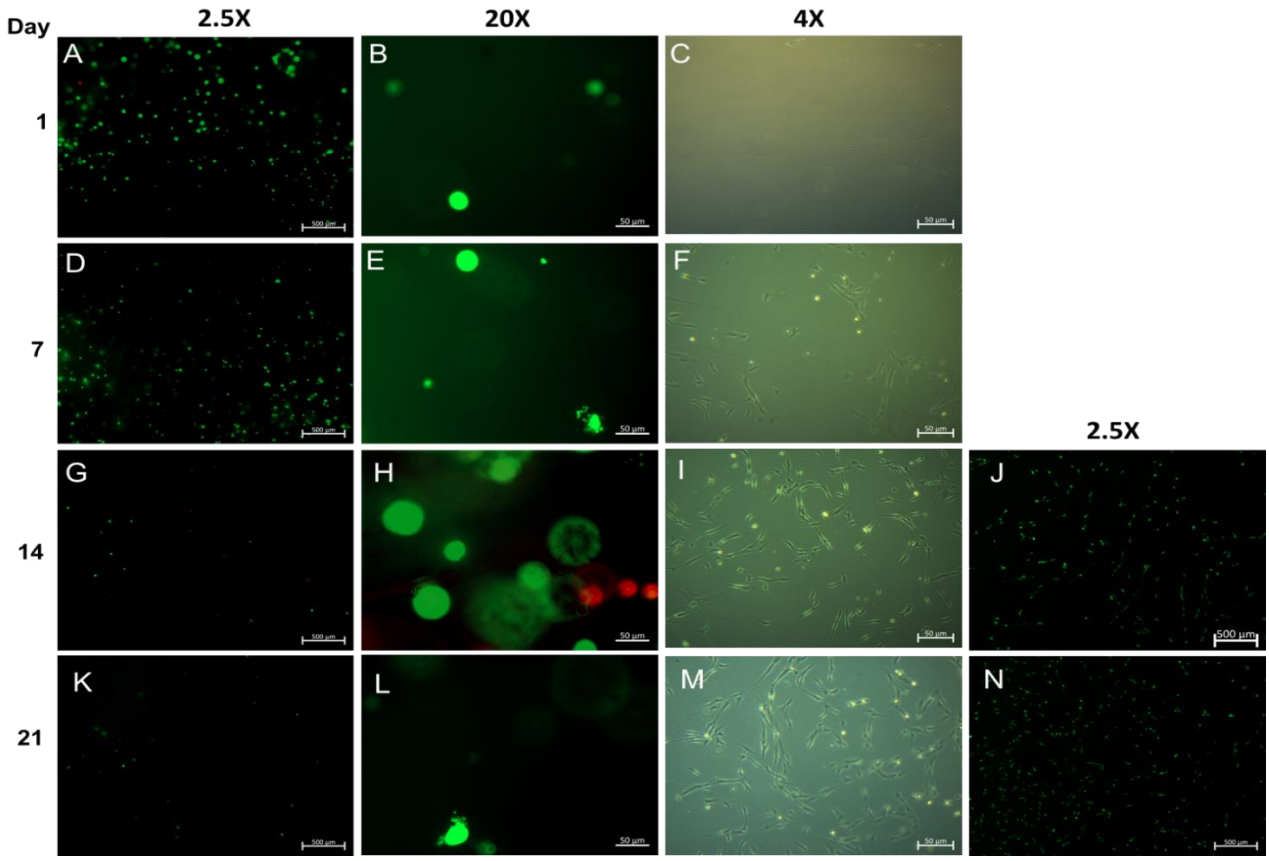

Figure 29. Cell Viability Images of AL/N constructs. At day 1, viable cells (green) were abundant and well spread through the constructs (a-b), at this point no cell migration to the bottom of flask was detected (c). Day 7 presented good viability (d and e) and some signs of cell migration was detected (f). At day 14, not many cells remained within the constructs, most migrated to the bottom of the flask at that point (l and j) and the same thing applies for day 21 (k-n). 4x images were obtain through light microscopy while 2.5x and 20x were obtained through fluorescence microscopy. Out of focus cells demonstrate that cells were located in different planes in the constructs **(b, e, h, l)**. Scale bar in **a, c, d, f, g, i, j, k, m and n** is representative of 500µm. Scale bar in **b, e, h and l** is representative of 50µm.

3.16 AL/N as delivery tool for CorMatrix

The previous results demonstrated that by day 14 all cells migrated from the alginate constructs to the bottom of the flask. To further explore the uses of the biomaterial, Alginate Cellink constructs were used as a cell delivery tool to CorMatrix. This investigation was

performed to assess cell viability and to analyse cell spread through the surface of CorMatrix. The assessments were performed at day 14.

At day 21, cell viability for cells within the area of CorMatrix was 98.02 ± 3.98%. The cells presented a clear spindle-like shape although in proximity to adjacent cells. It was observed that most cells which migrated from alginate constructs preferred to stick to the bottom of the flask rather than the CorMatrix. Moreover, most cells that attached to CorMatrix did not present good spread throughout the surface. The cells mainly attached to two apical edges of the CorMatrix, leaving the centre completely absent of cells.

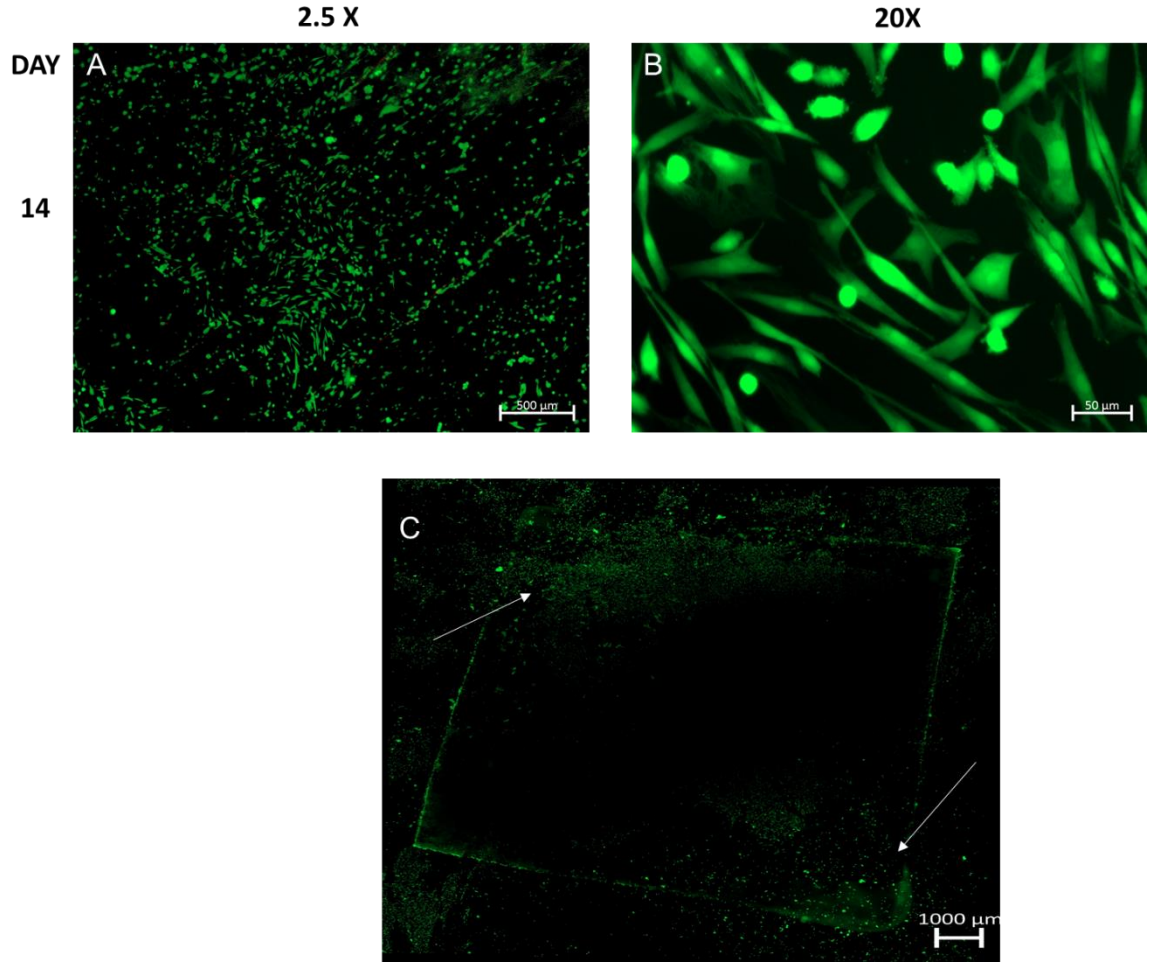

Figure 30. Cell Viability Images of CorMatrix. At day 14, cell migration occurred from alginate construct into the CorMatrix as expected. Viable cells (green) were abundant (a) and presented a spindle-like structure (b). Cell distribution within the CorMatrix was poor as the cells attached to the corners of the material, leaving the middle absent of cells (c). Scale bar in **a** representative of 500µm. Scale bar in **b** is representative of 50µm. Scale bar in c is representative of 1000µm.

3.17 Cell viability of 10-layered AL/N constructs in Non-Adherent Plastic Well

All cell viability assessments were previously performed in 4 layered constructs. Further investigation of cell viability in larger constructs is important as it provides insight whether tissue engineered constructs can sustain live cells for a relevant time period. Therefore, 10 layered Alginate Cellink constructs were created and bioprinted directly with cells in an intercalated grid pattern shape. Moreover, given the previous results demonstrating cell migration from constructs with Alginate, non-adherent well plates were used to observe cell migration. Cell viability and migration were assessed in a similar manner to previous experiments.

At day 1, the average viability presented for 10 layered 'Cellink bioink' constructs was 84.26 ± 3.16%. At day 7, the cell viability slightly increased to 84.3 ± 3.42 and suffered a slight decrease at day 14 which showed 81.79 ± 2.96% cell viability (Figure 31). At day 14 all cells were found in suspension (Figure 32). The slight variances in cell viability were not considered statistically different. At day 21, cell death was abundant.

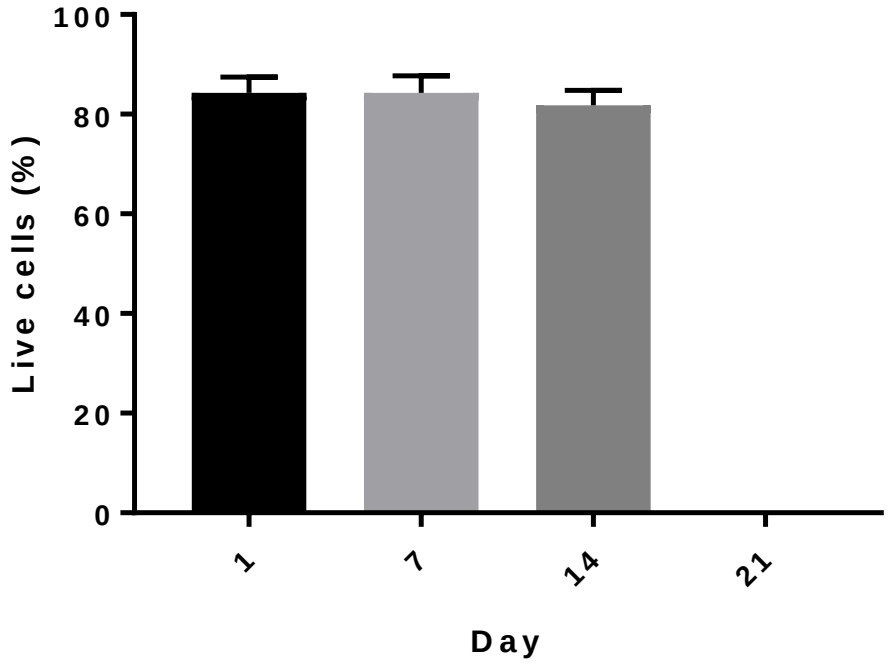

Figure 31. Average cell viability for 10 layered Alginate constructs. The average cell viability presented no significant changes from day 1-14. However, at day 21 all cells were dead within the construct. N=6 per timepoint. One-way ANOVA. Data presented as mean ± SEM.

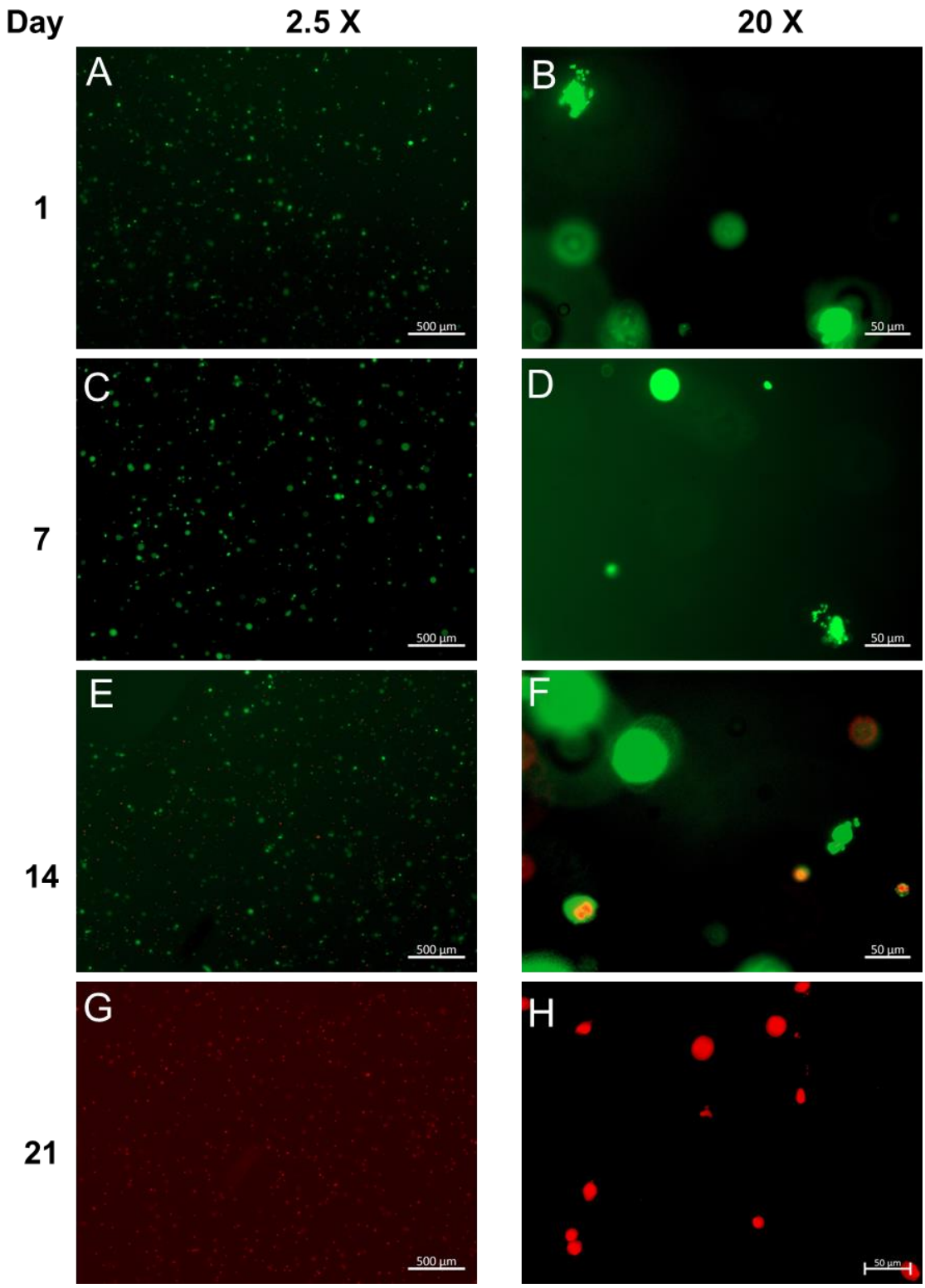

Figure 32. Cell Viability Images of 10 layered Alginate constructs. Viable cells (green) were abundant from day 1 until 7 within constructs (a-d). At day 14, all cells were found in suspension and by day 21 all cells were dead (red). Out of focus cells demonstrate that cells were in different planes in the constructs **(b and d)**. Scale bar in **a, c, e, g** is representative of 500µm. Scale bar in **b, d, f, h** is representative of 50µm.

3.18 Biomechanical analysis of PEG-DA Alginate constructs

It has been previously determined that PEG-DA Alginate required PBS rinse to provide a suitable environment for cell survival. Also, it was mentioned that without the presence of collagen, PEG-DA is non-absorptive leading to poor cell attachment. Following this information, biomechanical assessments for PEG-DA Alginate constructs were performed solely on cell-free constructs. It was important to obtain this information as PEG-DA Alginate-collagen constructs did not provide good shape fidelity.

The average tensile strength presented by PEG-DA Alginate constructs was the highest at Day 1 showing 1956 ± 119.1 kpa (Figure 33). In the subsequent time points, tensile strength significantly decreased over 60% from the initial value obtained. Day 21 presented the lowest average tensile strength, 562.5 ± 20.92 kpa. There was no significant difference in tensile strength among day 7, 14 and 21.

In addition to the tensile strength, the elasticity potential of PEG-DA Alginate was analysed. Overall, there were no significant variations on the elasticity potential shown by this biomaterial. At day 1, the average Young's Moduli was 145.2 ± 49.75 kpa, the Modulus for the following days decrease until day 21 which was 94.94 ± 4.56 kpa.

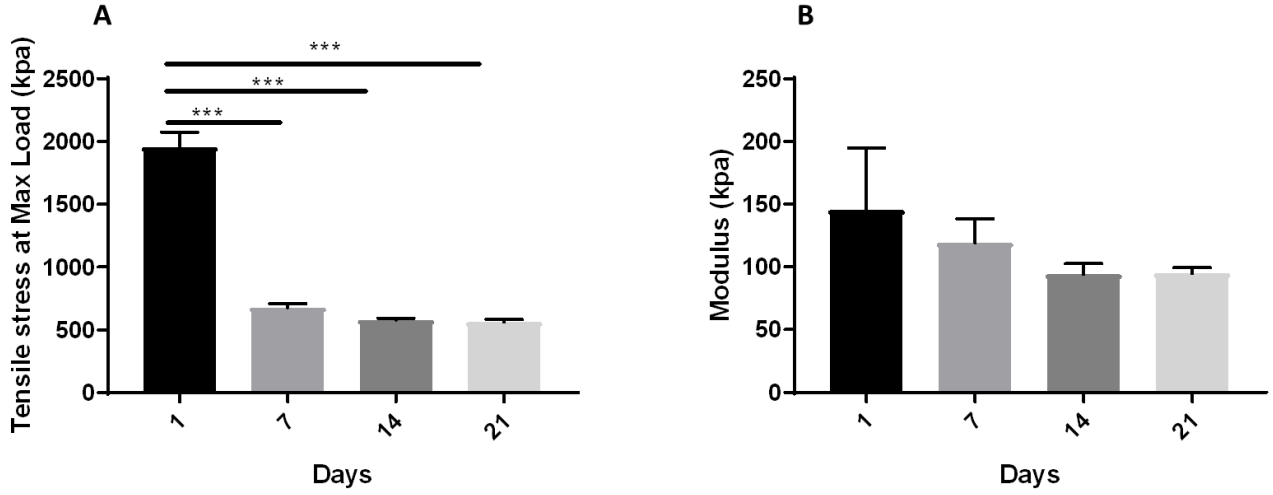

Figure 33. Biomechanical properties of PEG-DA Alginate constructs. Tensile strength at Maximum load significantly decreased overtime **(a)**. The elasticity potential of the material also decreased overtime however not significantly **(b)**. N=6. One-way ANOVA followed by Tukey's post hoc test,*** P<0.001. Data presented as mean ± SEM.

3.19 Biomechanical analysis of 5% GelMA constructs

As previously recorded, 5% GelMA constructs were unable to present the desired 3D grid pattern. Despite the poor shape fidelity on the structure obtained, biomechanical properties for the biomaterial without cells were obtained.

The average tensile strength for 5% GelMA constructs at day 1 was 151.7 ± 54.75 kpa (Figure 34). In the subsequent time points the tensile strength decreased for the constructs but not significantly. The lowest value for tensile strength was obtained at day 21, 103.21 ± 7.64 kpa.

The elastic properties of the material were also analysed. At day 1, the average Young's moduli was 41.64 ±11.14 kpa. At day 7, the values obtained for Young's modulus slightly increased to 50.41 ± 3.61. In the following time points, the elastic properties recordings decreased. The lowest modulus obtained was at day 21 presenting a 24.13 ± 2.29 kpa, this was a significant decrease compared to day 7.

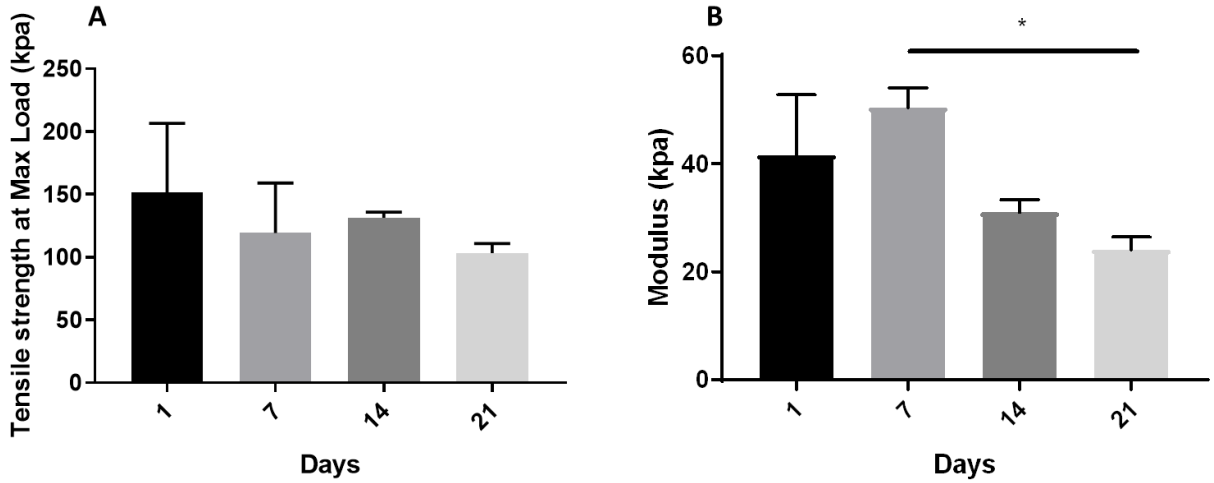

Figure 34. Biomechanical properties of 5% GelMA constructs. Tensile strength of the constructs deceased overtime, however the decrease was not significant **(a)**. The elasticity of the material decreased overtime and day 21 presents a significantly lower elasticity potential when compared to day 7 **(b)**. N=6 per time point. One-way ANOVA followed by Tukey's post hoc test, * $P<0.05$. Data presented as mean ± SEM.

3.20 Tensile strength at Maximum Load for 5% GelMA-HA constructs with and without cells

5% GelMA- HA constructs have previously presented good shape fidelity before and after cell incorporation within the structure. Biomechanical properties were analysed for this biomaterial in a similar manner as the previous tested materials. Further, the analysis was carried with and without the presence of cells within the construct to obtain information on the effect of cells on tensile strength and elastic properties in a construct.

The tensile strength for 5% GelMA-HA constructs without cells was highest at day 1 presenting an average of 958.9 ± 236 kpa strength (Figure 35). In the following time points, the tensile strength of the constructs gradually decreased, however, not significantly. Day 21 presented the lowest tensile strength, 621.1 ± 65.29 which shows approximately a 65% decrease in strength compared to day 1.

The tensile strength for 5% GelMA-HA constructs with cells was also highest at day 1 presenting a 438.6 ± 112.1 kpa strength at maximum load. The subsequent time points demonstrated a gradual decrease in tensile strength of the constructs, however these variations were not considered statically significant. Day 21 also presented the lowest tensile strength, 153.9 ± 47.45 kpa which is approximately a 64.9% decrease in strength compared to day 1.

The comparison at day 1 of tensile strength between constructs with and without cells demonstrated that 5% GelMA-HA constructs with cells present lower tension endurance than constructs without cells. Although, the constructs containing cells presented 54.2% decline in tensile strength this discrepancy was not quite significant.

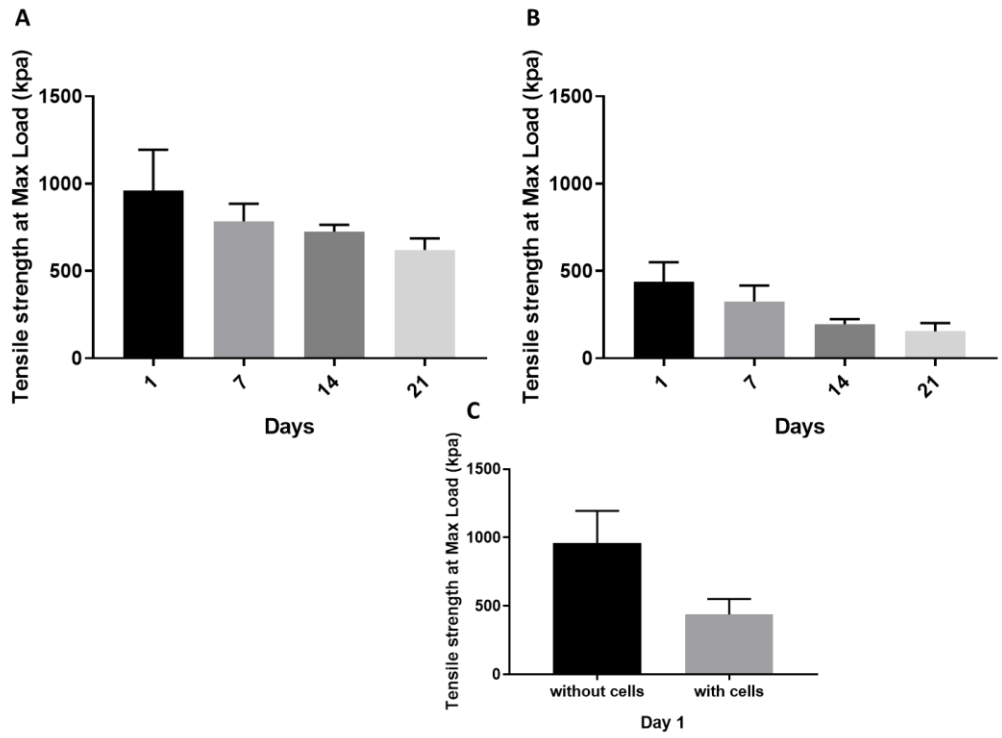

Figure 35. Tensile stress at Maximum Load for 5% GelMA- HA constructs with and without cells. Tensile strength decreases overtime for constructs with and without cells (a,b). Day 1 comparison shows that the tensile strength of construct with the presence of cells is reduced, however this decrease is not quite significant (p=0.0745**, c**). One-way ANOVA was used for analysis of construct with and without cells overtime. Unpaired t test was used for day 1 comparison. Data presented as mean ± SEM.

3.21 Young's Modulus for 5% GelMA-HA constructs

The elasticity potential of 5%GelMA-HA constructs without cells showed the highest at day 1 with 184.0 ± 12.93 kpa (Figure 36). The modulus decreased over time reaching the lowest at day 21, 100.8 ± 16.26 kpa, which was significantly lower compared to day 1. The decrease in the elastic potential of the constructs was not considered significantly different from day 7 to 21.

5% GelMA-HA constructs with cells showed a similiar gradual decrease to the constructs without cells. At day 1, the average moduli was 88.61 ± 25.67 kpa and in the subsequent time points the elastic potential decreased but these variances were not considered statistically significant. Day 21 presented the lowest elasticity potential, 29.44 ± 15.14 kpa.

The day 1 comparison of the constructs with and without cells demonstrated that the presence of cells within the biomaterial significantly decreases the elasticity potential of the constructs.

Constructs without cells presented an approximate 52% decrease in its elasticity potential compared to construct without cells.

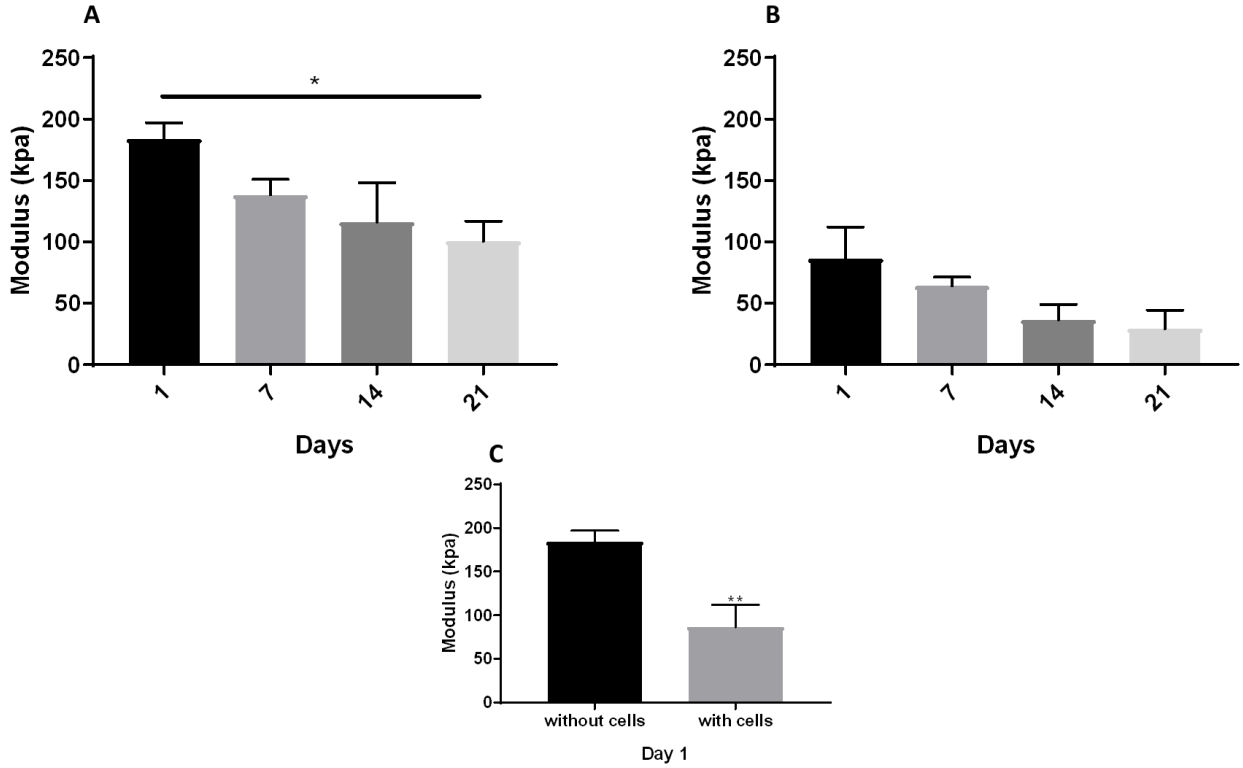

Figure 36. Young's Modulus of 5% GelMA-HA for constructs with and without cells. The elasticity capacity of the constructs gradually decreased overtime with the difference only being significant at day 21 **(a)**. For constructs with cells the decrease was gradual, however not significant **(b)**. The day 1 comparison showed that the presence of cells decreases the elasticity capacity of the constructs significantly **(c)**. N=6 per timepoint. One-way ANOVA followed by Tukey's post hoc was used for analysis of moduli overtime. Unpaired t-test was used for day 1 comparison, * $P<0.05$, ** $P<0.01$. Data presented as mean ± SEM.

3.22 Tensile strength at Maximum Load for 7.5% GelMA constructs

For 7.5% GelMA constructs without cells, the average tensile strength presented at day 1 was 1416.1 ± 54.44 kpa (Figure 37). At day 7, the tensile strength decreased to 1175.2 ± 295.7 kpa, but at day 14 the values obtained for tensile strength slightly increased to 1356.6 ± 76.44

kpa. Day 21 presented the lowest tensile endurance with 1132.4 ± 115.2 kpa. All the variances in tensile strength for these constructs were not considered statistically significant.

Following investigation, constructs containing cells demonstrated decreased tensile strength compared to constructs without cells. 7.5% GelMA constructs with cells presented 356.0 ± 3.42 kpa tensile strength at day 1. The subsequent time points demonstrated a gradual decrease in tensile strength, however this decrease on strength was considered significant from day 14 onwards. At day 14 the tensile strength was 185.7 ± 49.73 kpa, followed by a further significant decrease in construct strength on day 21 which presented 110.0 ± 43.21 kpa.

The day 1 comparison between 7.5% GelMA constructs with and without cells demonstrated that the presence of cells within the constructs significantly decrease the tensile strength by approximately 75%.

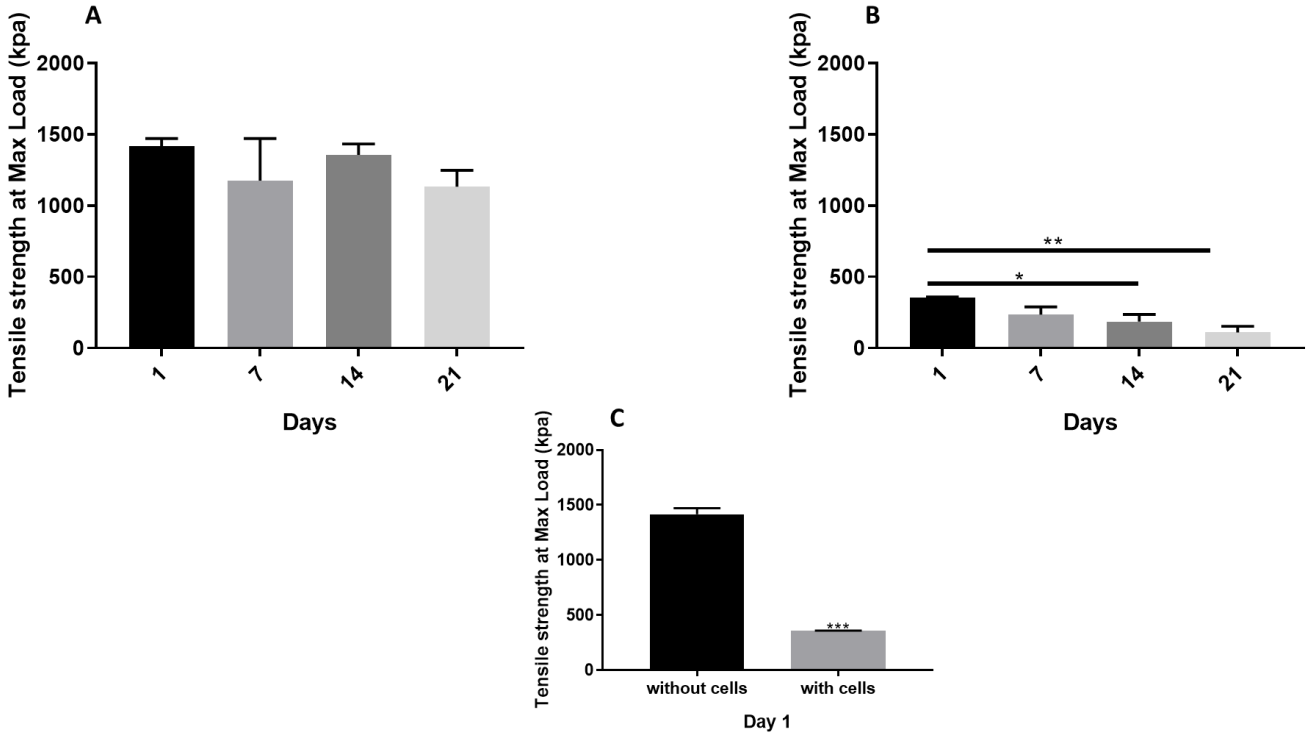

Figure 37. Tensile stress at Maximum Load of 7.5% GelMA constructs with and without cells. The tensile strength for constructs without cells presented no significant changes overtime (a). Constructs with cells showed a gradual decrease in tensile strength overtime with a significant decrease on days 14 and 21 (b). Day 1 comparison demonstrated that the presence of cells significantly decreases the tensile strength of the constructs (c). N=6 per timepoint. One-way ANOVA was used for analysis of constructs with and without cells overtime, Tukey's post hoc test was used for constructs with cells. Unpaired t-test was used for day 1 comparison. *p<0.05, **p<0.01, ***p< 0.0001. Data presented as mean ± SEM.

3.23 Young's Modulus for 7.5% GelMA constructs

The average moduli for 7.5% GelMA constructs without cells at day 1 was 183.1 ± 22.9 kpa (Figure 38). In the following time points, the elasticity capacity of the constructs decrease but the changes were not statistically sigificant. The lowest elasticity potential was recorded at day 21, which showed a moduli of 131.0 ± 17.30 kpa.

For 7.5% GelMA constructs with cells, the best elasticity potential was at day 1 which showed a moduili of 95.24 ± 7.64 kpa. The elasticity potential of the constructs decreased overtime and this decrease was deemed signficant starting at day 14 which presented a moduli of 37.30 ± 10.70kpa. The lowest elasticity capacity was shown at day 21 with a moduli of 27.24 ± 5.29 kpa, this was considered significantly lower than the elasticity shown at day 1 and 7.

The day 1 comparison for this biomaterial also showed that the presence of cells significantly decreases the elasticity potential of the constructs. The presence of cells within the constructs caused an approximate 47.98% decrease in elasticity.

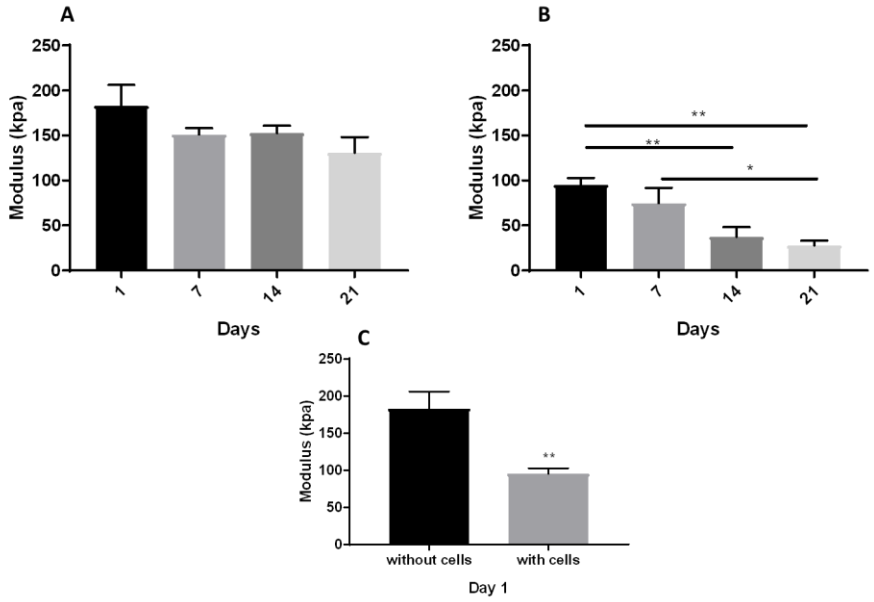

Figure 38. Young's Modulus of 7.5% GelMA constructs with and without cells Constructs without cells showed a gradual decrease on the elasticity, however not significant **(a)**. Constructs with cells showed a decrease in elasticity significantly (b). The day 1 comparison demonstrated the significant decrease in elasticity the presence of cells cause to constructs (c). N=6 per time point. One-way ANOVA was used for analysis of constructs with and without cells overtime. Unpaired t-test was used for day 1 comparison, ** P<0.01, * P<0.05. Data presented as mean ± SEM.

3.24 Tensile strength at Maximum Load for 10% GelMA constructs

Overall the tensile strength presented by 10% GelMA constructs without cells did not present any significant differences (Figure 39). At day 1, the average value for tensile strength obtained was 1383.7 ± 74.20 kpa. At day 7, the tensile strength slightly decreased to 1073.2 ± 317.7, however at day 14 the values obtained for tensile strength were slightly higher, 1265.8 ± 101.1 kpa. At day 21, the average tensile strength presented was 1086.3 ± 122.5 kpa.

For 10% GelMA constructs with cells, the tensile strength significantly decreased overtime compared to day 1. The highest value for tensile strength was presented at day 1, 413.7 ± 41.52 kpa. In the subsequent time points, the tensile endurance of the constructs decreased and the lowest recorded strength was at day 21 with 139.5 ± 45.19 kpa.

The day 1 comparison for 10% GelMA constructs with and without cells demonstrated that the presence of cells significantly decreases the tensile endurance of constructs. The disparity in tensile strength obtained at day 1 comparison was of 70%.

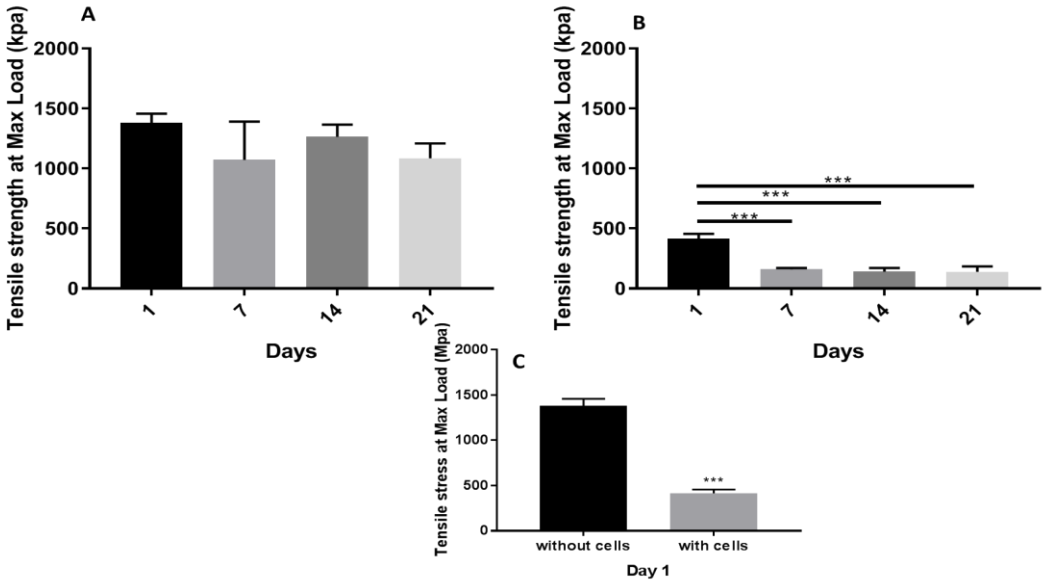

Figure 39. Tensile stress at Maximum Load of 10% GelMA constructs with and without cells. The tensile strength for constructs without cells presented a decrease, however not significantly **(a)**. Constructs with cells presented an overall significant decrease overtime in comparison to day 1 **(b)**. The day 1 comparison highlighted the significant decrease in strength cells cause to constructs **(c)**. N=6 per time point. One-way ANOVA followed by Tukey's post hoc test was used for analysis of constructs with and without cells overtime. Unpaired t-test was used for day 1 comparison, *** P<0.001. Data presented as mean ± SEM.

3.25 Young's Modulus for 10% GelMA constructs

The elasticity potential of 10% GelMA constructs without cells did not significantly varied on the analysed time points. The highest elasticity potential was shown at day with a moduli of 184.4 ± 23.10 kpa (Figure 40). In a similar manner to previous biomaterials analysed, the elasticity potential of these constructs also decreased overtime. The lowest elasticity potential was shown at day 21 with a moduli of 132.10 ± 17.44 kpa.

For constructs with cells, there was an overall significant decrease on elasticity potential overtime when compared to day 1. At day 1, the moduli obtained was 103.9 ± 12.43 kpa which showed the highest elasticity potential. Day 21 showed the lowest elasticity potential with a recorded moduli of 49.78 ± 5.53 kpa.

The day 1 comparisons showed again that the presence of cells decreases the overall elasticity potential for the constructs. The integration of cells within 10% GelMA caused a significant 43.65% decrease in its elasticity potential.

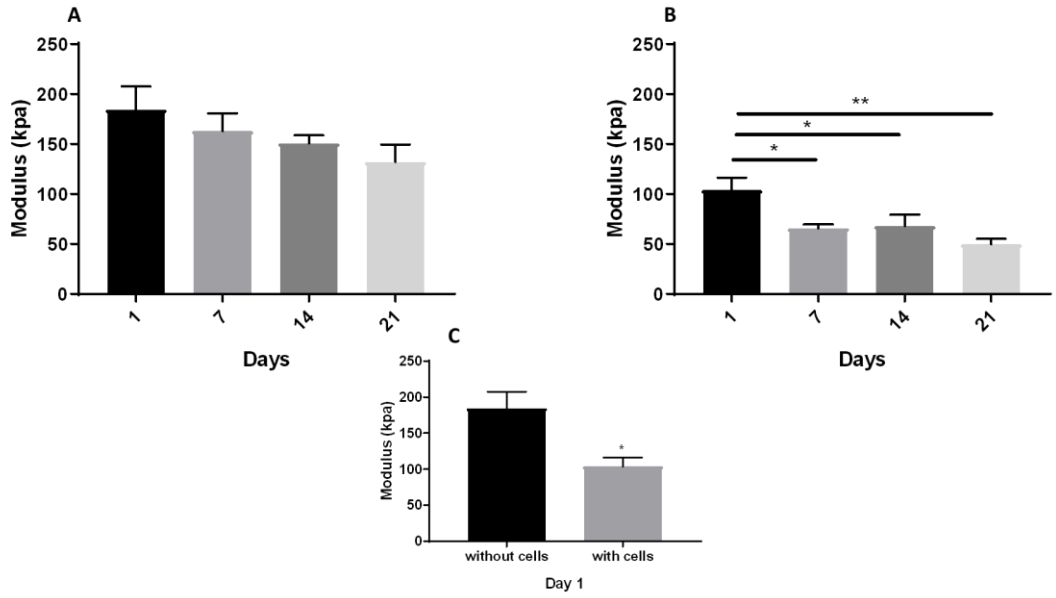

Figure 40. Young's Modulus of 10% GelMA constructs with and without cells. Constructs without cells showed a gradual decrease on elasticity, but not significantly **(a)**. In contrast, constructs with cells showed a significant decrease in elasticity overtime **(b)**. The day 1 comparison showed a significant decrease in elasticity for constructs with cells (c). N=6 per time point. One-way ANOVA was used for analysis of constructs with and without cells. Unpaired t-test used for day 1 comparison, * $P<0.05$, ** $P<0.01$. Data presented as mean ± SEM.

3.26 Tensile strength at Maximum Load for AL/N constructs

AL/N constructs without cells presented an average tensile strength of 2981.17 ± 463.9 kpa at day 1. The tensile strength presented a gradual decline over the subsequent time points. At day 7, the tensile strength slightly decreased to 2320 ± 89.30 kpa but not significantly (Figure 41). At day 14, the tensile strength recorded for constructs further decreased to 1748.3 ± 104.7 kpa, this was considered significant lower in comparison to day 1. The lowest values for tensile endurance were presented at day 21, 1250.1 ± 76.74 kpa. The tensile strength for day 21 was significantly lower when compared to day 1 and day 7.

AL/N constructs containing cells presented an average tensile strength at day 1 of 1823.8 ± 369.7 kpa. After day 1 the tensile strength of the constructs decreased overtime, but this decrease in strength was only considered significant starting on day 14. At day 14, the average tensile strength presented was 785.9 ± 80.27 kpa which was significantly lower when compared to day 1. Moreover, day 21 also presented a significant decrease in tensile strength when compared to day 1, 660.8 ± 52.82 kpa.

The day 1 comparison between constructs with and without cells demonstrate that the presence of cells significantly decreases the tensile strength of the constructs. For AL/N constructs the decline of tensile strength was of approximately 38.8%.

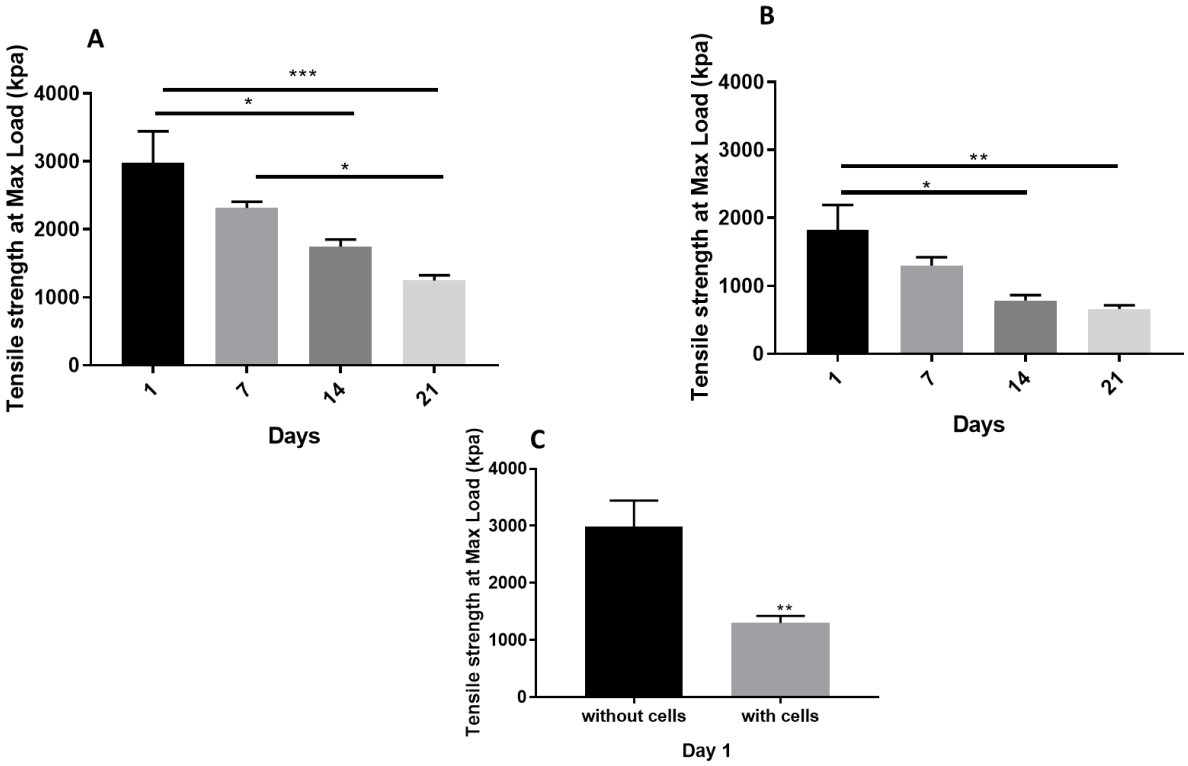

Figure 41. Tensile strength at Maximum Load of AL/N constructs with and without cells. Constructs without cells presented a significant decrease on tensile strength overtime (a). Constructs with cells also presented a significant decrease in tensile strength overtime (b). Day 1 comparison showed how the presence of cells significantly decreases the strength of constructs (c). N=6 per timepoint. One-way ANOVA followed by Tukey's post hoc test for analysis of constructs with and without cells overtime. Unpaired t-test was used for day 1 comparison, * P<0.05, ** P<0.01, *** P<0.001. Data presented as mean ± SEM

3.27 Young's Modulus for AL/N constructs

The highest elastic potential for Alginate constructs without cells was presented at day 1 with a modulus of 400.3 ± 119.8 kpa (Figure 42). The elasticity potential decreased overtime however the variances were not deemed statistically signficant. The lowest elasticity potential was presented at day 21 with a moduli of 176.1 ± 14.84 kpa.

For constructs with cells, the elasticity potential decreased in a similar manner seen to previous biomaterials overtime, but this decrease was not considered significant. The highest elastic potential for alginate constructs with cells was shown at day 1 with a modulus of 241.3

± 68.27 kpa. At day 21, the lowest elastic potential was obtained with a moduli of 110.2 ± 14.0 kpa.

The day 1 comparison for constructs with and without cells demonstrated that the presence of cells within alginate constructs does not affect the elasticity potential of the biomaterial significantly. Despite not significant, the presence of cells caused a 39.72% decrease on the elasticity potential of the constructs.

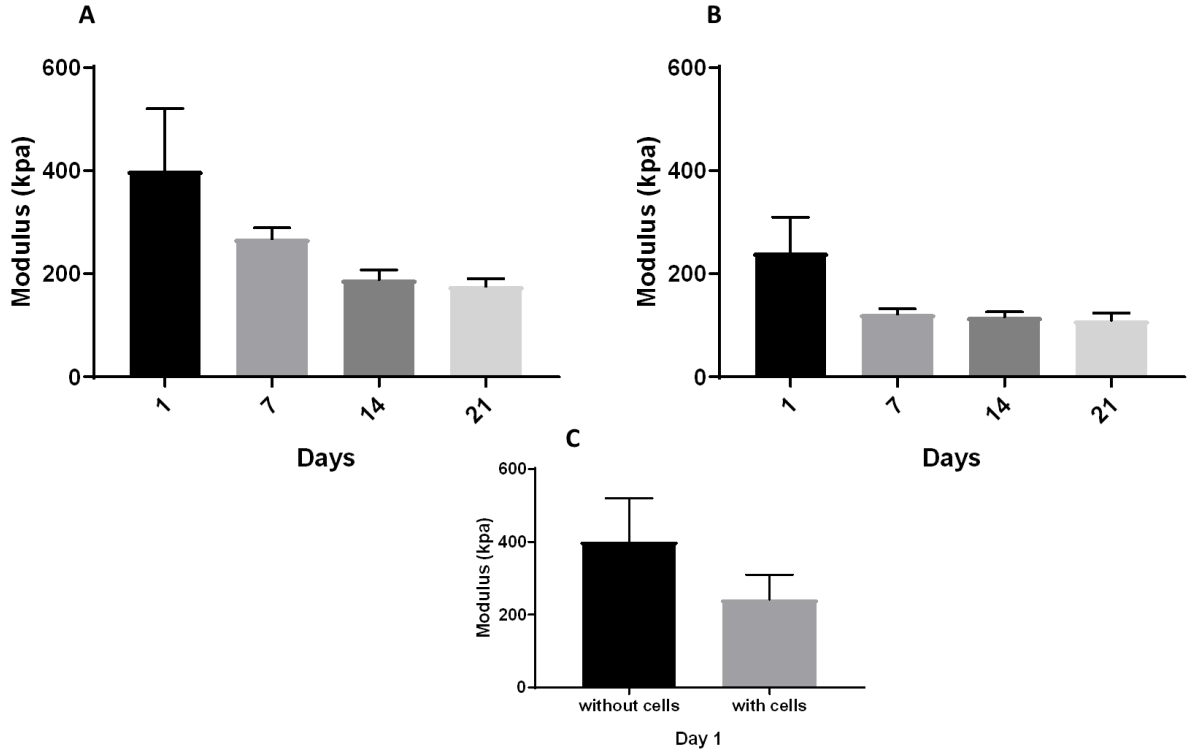

Figure 42. Young's Modulus of Alginate Cellink constructs with and without cells. Constructs with **(b)** and without cells **(a)** showed a gradual decrease in elasticity capacity, however not significantly. Day 1 comparison demonstrated that the presence of cells decrease the elasticity of constructs but not significantly **(c)**. N=6 per time point. One-way ANOVA was used for analysis of constructs with and without cells overtime. Unpaired t-test was used for day 1 comparison. Data presented as mean ± SEM.

3.28 Scanning Electron Microscopy

The structure of the constructures varied (Figure 43). PEG-DA Alginate seemed to have the most distinct characteristics compare other constructs. The pores for this biomaterial does not look as crumbly as the others. 5% and 7.5% GelMA seem to have similar structure, fibre-like and crumbled. The same applies for AL/N constructs, except that the space in between pores seem wider.

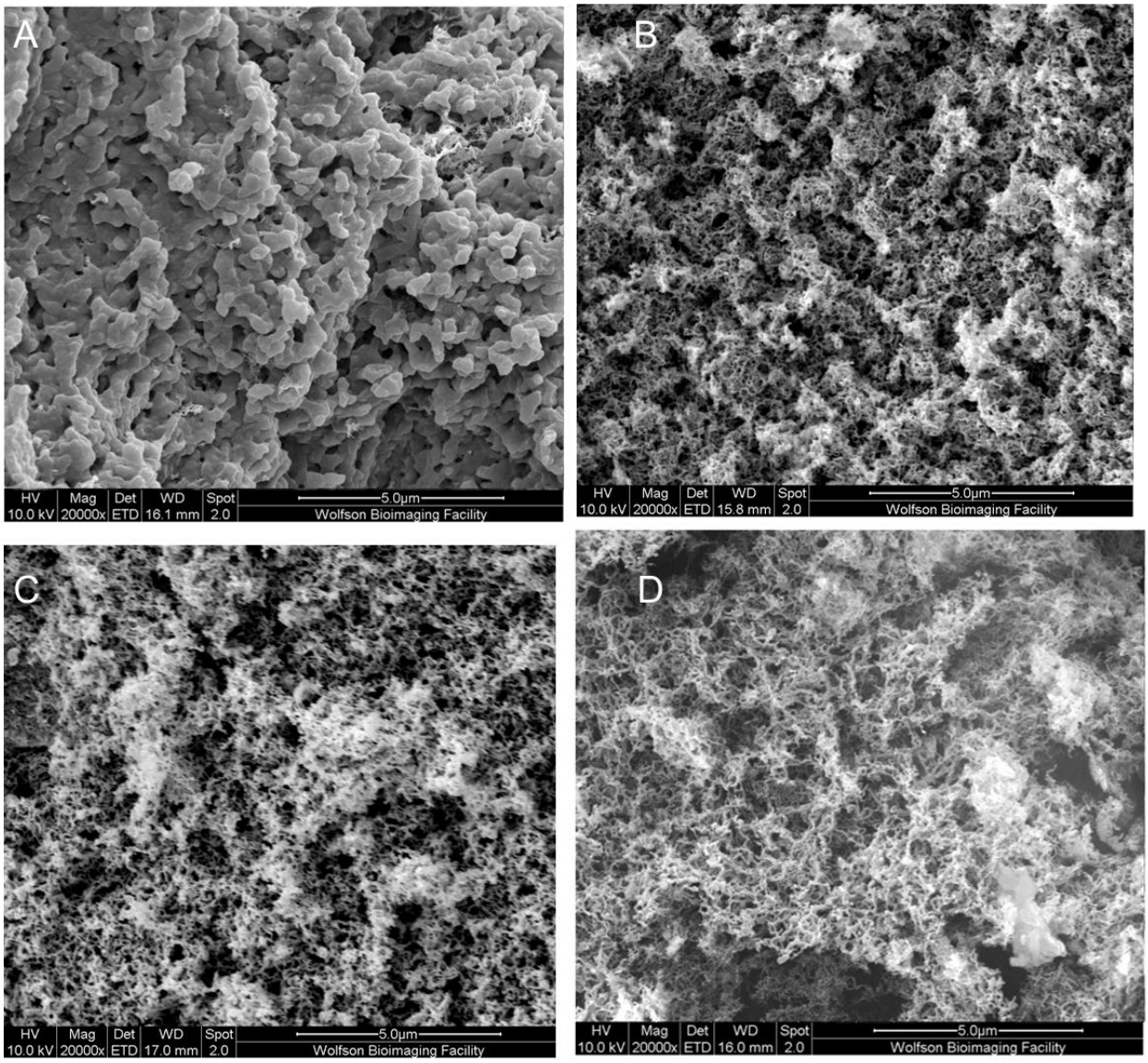

Figure 43. Representative SEM imaging of constructs (a) Images of PEG-DA Alginate with collagen constructs shows the pores within the structure of the biomaterial. (b) Shows 7.5% GelMA fibre-like structure with gap in between, the same applies for 5% GelMA-HA. (d) Imaging of AL/N constructs shows a wider spread of fibrous-like structure and gaps. N=4,Scale bar= 5µm.

4 DISCUSSION

Tissue engineering provides different methodologies to aid with CHD treatment, 3D bioprinting transformed the field of TE as it provides approaches which are speedy, controlled and precise compared to other manufacturing methods available (Yu et al., 2018). This project focused on

the formulation of bioinks and explored the efficacy of the biomaterials to support cell viability when used in combination with 3D bioprinting. Moreover, biomechanical analysis was performed to establish potential application of constructs and compare these to native heart tissue.

4.1 Printability and Cell viability

4.1.1 PEG-DA based bioinks

PEG-DA has been used for biomedical applications as it is non-toxic, presents easy manipulation and is biocompatible (Mazzoccoli et al., 2010). The easy manipulation of the material has been beneficial for cardiovascular research as heart structures (aortic valve and vessels) can be successfully obtained with this material at a relatively fast speed (Zhang et al., 2015a, Hockaday et al., 2012).

This work aimed initially to investigate the ability of PEG-DA to support cell viability through a directly seeded bioprint method when coupled with Alginate. The printability of PEG-DA Alginate was fast, provided great shape fidelity and nozzle clogging was not observed with the bioink. However, abundant cell death was obtained with a direct seeded print. Upon further investigation, it was established that shear stress of the bioprinting process was not the cause of abundant cell death. It was found that the lack of PBS rinse on PEG-DA Alginate constructs greatly impacted cell viability. It has been previously shown that PEG degradation can be toxic to cells and PEG-variants despite being more biocompatible can also carry on toxic properties of PEG (Murali et al., 2015). Therefore, the elimination of the toxic properties of the biomaterial is necessary before cell implantation.

PEG-DA intrinsically presents poor cell adhesion properties (Browning et al., 2014), coupling the biomaterial with Alginate and Gelatine is a method of enhancing cell attachment properties for constructs. It was observed that cells in PEG-DA Alginate (unrinsed) detached from constructs soon after death, by day 1. Cells from PEG-DA Gelatine, were also abundantly dead but these remained in the at day 1. This highlights the advantage of using animal-based bioinks over plant-based biomaterials. In animal-based biomaterials, cells demonstrate better attachment as the biomaterial naturally provides ECM signals and receptors to facilitate proliferation and the adhesion process. Alginate is negatively charged which impacts the ability to readily absorb proteins and it lacks ligands to which cells can bind to (Genes et al., 2004).

From the findings mentioned above, the investigation for cell viability was tailored to minimise cytotoxicity (through PBS rinse before seeding the constructs with cells) and the addition of collagen was introduced to PEG-DA Alginate to enhance cell adhesion in constructs. Cell

viability was greatly improved in constructs presenting over 50% viability consistently for 14 days. There were no signs of cell migration to the bottom of the flaks.

The cell implantation process was performed through the use of an orbital shaker which has proven to provide good cell spread and viability in 3D models. Although, the use of a bioreactor or spinner flask for cell seeding might have provided better cell attachment to constructs (Griffon et al., 2011). To further induce cell attachment to constructs and prevent cell migration to the bottom of the flask, low attachment plates were used throughout this experiment. However, research suggests that low attachment plates have no impact on the ability of cells to further attach to 3D constructs. Instead, cells are maintained in a suspended state and form spheroids over attachment to the biomaterial (Comley, 2017, Sant and Johnston, 2017, Shin et al., 2004).

The abundant cell death obtained at day 21 for PEG-DA Alginate with collagen can be due to the poor shape fidelity of constructs upon the addition of collagen. PEG-DA extrusion is sensitive to salt concentration (Hockaday et al., 2012). Despite best efforts, the final bioink consistently clogged nozzles and extrusion was not possible. Instead, the bioink was extruded using a syringe and crosslinked after each 'layer' extruded. Consequently, the final constructs did not present passageways for nutrient exchange which is vital for cell survival within 3D models (Song et al., 2009).

Other research groups have used PEG-DA Alginate with collagen successfully. These formulated various models including an aortic valve which was able to maintain cell viability for 21 days (Hockaday et al, 2012; Hong et al, 2015). Despite contact with one of the groups and following their guidelines to produce the bioink with collagen, I was still unable to produce a homogenous bioink to improve shape fidelity.

4.1.2 GelMA based bioinks

GelMA has been widely used for cardiovascular research for the fabrication of cardiac patches, myocardial tissue constructs and as a cell delivery vehicle for heart tissue (Klotz et al., 2016; Shin, et al, 2016). This biomaterial has great biocompatibility with cells as it contains an abundance of proteins and integrin-binding motifs that promote cells adhesion and migration. This study investigated shape fidelity of constructs dependant on GelMA concentration and the impact of different concentrations in cell viability.

The poorest shape fidelity was demonstrated with 5% GelMA which proved unable to translate into the desired grid construct. Nonetheless, cell viability was analysed and this concentration presented the highest overall viability for the biomaterial, despite the constructs not presenting gaps within the structure to enhance nutrient exchange. The dimensions of the constructs from

this concentration were not measured, but were appropriate for maintaining cell viability for 21 days.

5% GelMA was the only bioink to present spindle-shaped cells under microscopy. This is attributed to the final constructs presenting a flat structure compared to taller grid constructs, providing targeted focus in microscopy. Low concentrations of GelMA (≤ 5%) have shown to create spontaneous organisation of cells. In such environment cells have higher ability to elongate, migrate and form networks with neighbouring cells than in higher concentrations (Nichol et al., 2010).

According to Loesnerr et. al, 2016 the recommended GelMA concentration for Mscs is 5% followed by UV exposure at 33 seconds in total. In this project, UV exposure was set to 20 seconds per layer. This resulted in constructs able to withstand incubation and providing good results for cell viability compared to other concentrations and biomaterials. Also, the recommended cell seeding density for Mscs in 5% GelMA is $1x10^6$ cells per ml, this parameter was used in this project.

Despite presenting great cell viability, the printing process of the bioink was not smooth. GelMa is thermosensitive and the bioprinter used in this project lacks temperature management properties. That lead to a prolonged biopriting process; before printing each construct the viscosity of the bioink needed to be assessed (by eye) to determine if it was a viscosity which would create grid patterns, or if room temperature had set the bioink to a high viscosity which would not allow print. The same issue has been previously reported in literature, and it has been established that concentrations of GelMA lower than 20% present difficulties to create a uniform-3D model (Colosi et al., 2016, Pepelanova et al., 2018).

5% GelMA was coupled with hyaluronic acid to improve printability of the bioink. This hybrid bioink provided good shape fidelity for constructs and a grid pattern was obtained. Interestingly, the addition of HA enabled the placement of the plate on ice after each layer printed to be bypassed. This gelation process uses the innate properties of gelatine that solidifies under 35ºC to obtain a good shape fidelity for each layer prior to UV exposure (Jaipan et al., 2017), but the process is time consuming.

The cell viability for GelMA-HA was only 2.3% lower than 5% GelMA at day 21. The microscopy images for this biomaterial present cells in circular shapes. The cells in constructs are spread across different planes, therefore the focus of cells was hard to obtain. The same is true for the following biomaterials in this project.

The printability of 7.5%, 10% and 20% GelMA was greatly improved, with the UV exposure time set for each concentration the printing process was relatively fast. Although, 7.5% and

10% still required placement of the plate in ice to stabilise each layer prior to crosslinking. 20% presented good dispersion and created a model which was robust.

It was observed that as the concentrations for the bioink increased, the cell viability at day 21 decreased. 10% GelMA presented a lower cell viability than 7.5% GelMA by approximately 6.2% and in comparison to 5% GelMA it presented an approximate 29% lower cell viability. Progressing to a concentration of 20%, cell death was abundant from day 1.

As mentioned before, a 5% concentration is ideal for mscs. Upon increase of the concentration to 10% the recommended cell model to use are chondrocytes and a 20% concentration is usually used for carcinoma cells and tumour studies (Lee et al., 2016). As the concentration increases, shape fidelity also increases but at the cost of a stiffer construct. Stiffer constructs tend to have a decreased pore size and cell migration becomes limited (Loessner et al., 2016) A study showed cell survival and attachment suffered a 50% decrease as the result of an increase in GelMA concentration from 5% to 20% (Wu et al., 2019).

4.1.3 Alginate- nanocellulose

This bioink provided easy printability in all nozzle sizes and no clogging issues. It was also the fastest printing process demonstrated among all bioinks. The viscosity of the biomaterial allowed all layers to be printed within constructs without intermittent crosslinking. Calcium was only added to constructs at the final stage of the process, prior to DMEM addition.

Alginate can vary in molecular weight and viscosity but can be difficult to use in 3D constructs as it can become rigid throughout the printing process and without thermal properties in a bioprinter, the process can become tiresome. Nanocellulose provides high mechanical strength and thermal stability to alginate. A hybrid AL/N hydrogel presents increased cell proliferation compared to constructs composed solely of alginate (Siqueira et al, 2019). It has also been reported that nanocellulose improves controlled release of cells for alginate hydrogels (Nascimento et al., 2018).

In this project, AL/N demonstrated over 80% cell viability through 21 days. These results validate the extensive literature on the high biocompatibility of alginate and cellulose (Tam et al., 2011, Lee and Mooney, 2012, Sun and Tan, 2013). However, cell migration began at day 7 and by day 14 most cells were found in the bottom of the flask. The inability of constructs to adhere to cells for an extended period highlights the potential of alginate and cellulose based materials to be used as delivery tools (Nahar et al., 2017). In this case the constructs would not be expected to assimilate native structures; these would be expected to degrade after their function has been completed (Halib et al., 2017).

The controlled release of cells is a valuable feature for cardiac tissue engineering. Alginate and nano-cellulose are great tools for cell, protein and growth factor delivery. Blood vessel formation has been detected in mouse models through the use of this hybrid biomaterial by the sustained release of vascular endothelial growth factor (Camci-Unal et al., 2014). Moreover, alginate has been used as cardiac patch for cardiomyocyte delivery and vascularisation in myocardial infarction mouse models. The results showed live cardiomyocytes, myofiber formation and an increased presence of gap junctions even after complete patch degradation (Kaiser and Coulombe, 2015). These are promising features for CHD treatment.

In regards to cell release, from the microscopy images obtained it can be said that a sustained cell release was maintained for 14 days. Alginate microspheres in drug delivery studies, were shown to release 80% of content within the first 100 hours, while alginate-cellulose microspheres released 20%. Both released a high surge of content upon construct degradation after 30 days (Lin et al., 2011). Other studies were able to maintain drug and cell release for three months with hybrid constructs (Lin and Dufresne, 2014, Leslie et al., 2013).

To further investigate cell viability within alginate-nanocellulose, a 10 layered construct was created. Additionally, a low attachment well plate was used to observe if it would have an impact on cell migration. Some cells were found floating in media, outside constructs, from day 7. At day 14 all cells were in suspension and by day 21 all cells were dead. The results indicate that low attachment plates had no further impact on cell attachment to constructs, instead cells were kept in a suspended state and presented a circular shape. The abundant cell death can be due to the lack of nutrient in DMEM, as the medium was not changed for 14 days for fear of losing cell migration occurance.

In future, instead of leaving the constructs in the same medium, the constructs should be placed in a new well with DMEM every 48 hours. This will ensure that the cells in constructs are receiving nutrients while the cells (if any) in the previous flask can be used for a more accurate quantification on cell migration for AL/N constructs with more specific time points. This way lack of nutrients from DMEM could be ruled out as the potential cause of cell death.

One of the aims of this particular investigation was to analyse cell viability in a bigger construct with intercalated gaps for nutrient exchange. Cell survival was maintained for 7 days within the constructs, however due to the propensity for cell migration this biomaterial was inadequate to carry out a 21-day analysis from the onset. GelMA would provide a good environment for cells in bigger constructs but the translation from code to design would be compromised due to the low viscosity of the bioink. This could lead to cell death as there would not be gaps for nutrient exchange. PEG-DA Alginate would be ideal to carry this analysis,

however the addition of collagen is necessary to maintain extended cell viability and unfortunately the printing process with this bioink was not successful.

AL/N was also used to analyse cell spread from constructs to CorMatrix. The results for cell spreadibility within the material was poor. Most cells attached to the corners of the CorMatrix leaving the middle cell-free. This can potentially be attributed to the detachment of construct from CorMatrix after two days. CorMatrix is highly biocompatible and the reason why cells preferred to attach to the corner of the material is unknow. This behaviour is usually observed in hydrogel constructs which do not present appropriate inner networks to allow nutrient diffusion. In such cases, cells prefer outer parts of the constructs which allows them to be closer to medium. However, CorMatrix is 0.3 µm thick which falls within the possible nutrient exchange range, 200µm (Mosala Nezhad et al., 2016).

4.2 Biomechanical properties

The aim of this investigation was to design constructs with the potential to treat CHD. In tissue engineering it is important to create designs which are able to withstand their intended application (Zhu and Marchant, 2011). Tensile strength and modulus of the biomaterials provide insight of their potential cardiovascular application.

Overall the incorporation of cells significantly decreased the tensile strength and elasticity potential of constructs. It has been widely reported the decrease of strength in constructs after cell implantation, this can be attributed to degradation of material upon swelling and degree of crosslinking of materials prior to incubation (Billiet et al., 2014). However, there has been studies in which constructs demonstrated an increase in elasticity and/or stiffness upon cell implantation. This phenomenon is more common in hydrogels which have matured under bioreactor conditions, as in this environment cells are more likely to reorganise fibre interaction and produce higher levels of extracellular matrix. More often, constructs tend to decrease the tensile strength but increase their elastic potential overtime (Hu and Athanasiou, 2005, Wakatsuki and Elson, 2003).

4.2.1 Alginate-nanocellulose

AL/N presented the highest tensile strength and elastic potential compared to all other biomaterials in this study. The results demonstrated that AL/N constructs significantly decreased their tensile strength overtime with and without cells, but maintained its elastic potential. The decrease in mechanical properties in alginate-based bioinks is dependent on the alginate polymer used and method in which it was processed, but most alginate-based hydrogels show a significant decrease in mechanical properties within the first 7 days (Drury et al., 2004). In this study, the decrease of tensile strength was only significant from day 14

with and without cells. This day coincides with the migration of cells from constructs, but this factor is not mainly responsible for the biomechanical change as the same pattern is observed in constructs without cells.

The constructs created in this investigation present positive potential for implantation. Constructs with (≈1823 kpa) and without cells (≈2981 kpa) presented superior tensile strength to human aortic and pulmonary valve structures at day 1 (Table 1). The average strength for AL/N constructs at day 21 without cells is approximately 28% lower than the tensile strength of a human aortic valve, ≈1740kpa. If cells are incorporated, this disparity increases by approximately 62% at day 21. In terms of elasticity, the constructs created in this study are not as extensible as the native heart structures mentioned above, independent of cell incorporation. The highest modulus results obtained was at day 1 (≈440 kpa), this represents a 2% modulus capacity of a human aortic valve.

4.2.2 PEG-DA Alginate (without collagen)

PEG-DA Alginate constructs were only tested without cells. The constructs presented second higest tensile strength at day 1, however by day 21 it showed tensile strength superior only to 5% GelMA constructs which were the weakest. Interestingly, this biomaterial contained the highest amount of photo-initiator, 1% Irgacure 2959, and the shortest UV exposure per layer. Higher concentration of photo-initiator helps biomaterials to set with shorter UV exposure times, but often these lead to stiffer constructs and cell death (Kandhaker et. al, 2016). Overtime the elastic potential for PEG-DA Alginate was reduced but presented similar potential to GelMA based constructs.

Hockaday et. al, 2012 analysed stress- strain and modulus relationship for various concentrations of PEG-DA Alginate constructs, including the same bioink used in this study without collagen. The biomechanical tests carried in that study were performed right after bioprint and crosslinking of samples which differs from this study as measurements were carried one day after bioprint. Hockaday obtained 74.6 ± 1.5 kpa modulus for 8mm diameter and 7mm width samples, created with biopsy punches. In this study, constructs were 7.5 x 15 x 2 mm in size and demonstrated nearly twice more extensibility potential at day 1 (145.2 ± 49.75 kpa).

Chen et. al, 2018 analysed the tensile strength PEG-DA constructs 70 x 20 x 0.5 in size. These constructs presented 130-fold higher tensile strength after print (18980 ± 1.11kpa) compared to PEG-DA Alginate constructs created in this study. In Chen's study, 3% of 2,4,6-trimethyl benzoyl diphenyl phosphine oxide was used as photoinitiator and their samples were cured under UV for 1 minute twice (Chen et al., 2018). These features are considerably different than the parameters used in this study.

Overall the biomechanical results obtained in this study demonstrate great potential for cardiovascular use. The tensile strength for PEG-DA Alginate at day 1 (1956 ± 119.1 kpa) without cells demonstrated slightly superior results to the average tensile strength of aortic valves in human hearts, 1740 ± 0.29 kpa (Table 1). However, at day 21 the tensile strength demonstrated by constructs were 30-fold weaker than a human aortic valve. The constructs in this study demonstrated to be less extensible and compliant than aortic and pulmonary valves for both humans and pigs, but demonstrated similar extensive potential to more specific anatomical regions such as aortic leaflets (≈54kpa), aortic (≈140-180 kpa) and pulmonary root (≈50-85 kpa) in humans (Hockaday et al., 2012, Mavrilas and Missirlis, 1991).

PEG is a synthetic biomaterial which can be modified to present more suitable mechanical strength, material porosity and degradation rates. PEG hydrogels have been used for cardiac tissue implants and have prevented LV dilation and remodelling in mice. Moreover, it has been shown to promote blood vessel formation and tissue growth when used in combination with cells (Domenech et al., 2016). Due to the extreme versatility of this material, the constructs created in this study can be further optimised to increase tensile strength and elasticity to better suit the potential for heart use. That said, the constructs show positive potential to be used as cardiac patches to correct holes in heart of CHD patients.

4.2.3 GelMA

Gelatine is denatured collagen, but the material still contains crucial factors for cell adhesion and nutrient absorption. The addition of methacrylate to the substance allows further mechanical manipulation of the biomaterial through photo-crosslinking (Zhu et al., 2019). This study has shown a consistent record of good cell viability for GelMA concentrations ranging from 5% to 10%. However, the biomechanical properties for the constructs have shown to vary significantly dependant on GelMA concentration.

5% GelMA presented printability difficulties and inability to create a 3D grid construct. Consequently, this biomaterial presented significantly lower tensile strength compared to all other materials at day 1 without cells and remained the weakest overtime. As for modulus, initially this concentration presented similar elasticity to all other biomaterials except AL/N, but overtime the biomaterial demonstrated inferior elastic potential to all. As previously mentioned, lower concentrations of GelMA present lower shape fidelity and consequently poorer mechanical properties. There are two main ways in which research improves the mechanical properties of GelMA: 1. Include thermoplastic co-depostion or mixing hyaluronic acid and 2. Increasing GelMA concentration (Pepelanova et. al, 2018). In this study we explored both.

The use of hyaluronic acid evidently provided benefits for shape fidelity of the constructs. This hybrid biomaterial presented superior tensile strength and elastic potential overtime compared

to 5%GelMA. Moreover, the addition of HA allowed biomechanical properties measurements with cells which was not possible with 5% GelMA as the biomaterial was too weak to manipulate into biomechanical testing. The increased concentration GelMA constructs (7.5% and 10%) presented similar elastic potential to 5% GelMA-HA overtime with and without cells. Tensile strength among increased concentration GelMA groups and 5% GelMA-HA with cells demonstrated similar strengths, but without cells GelMA-HA presented significantly lower strength overtime. The addition of cells to constructs lowers tensile strength as demonstrated in the previous experiments (Drury et al., 2004, Vedadghavami et al., 2017), this study presented the same characteristics. However, as 7.5% and 10% GelMA constructs demonstrated over 90% decrease in tensile strength from when analysed without cells at day 1 to day 21 with cells, GelMA-HA constructs presented a slightly lower disparity, 84%. This potentially suggests that HA is a beneficial addition to biomaterials as it helps constructs maintain higher tensile strength overtime.

During GelMA preparation various factors can influence its mechanical properties: degree of functionalisation of amino acids, source of gelatine and crosslinking manipulation used within experiment. Crosslinking manipulation can vary on the type of photo-initiator used, concentration of photo-initiator and light intensity for crosslink (O'Connell et al., 2018).

In this study, Irgacure-2959 was used on all biomaterials which were chemically crosslinked, but the concentration of the photoinitiator was maintained only for GelMA-based biomaterials. The crosslinking time for 10% GelMA constructs was 15 seconds per layer while all other concentrations were exposed to 20 seconds of UV. Although it has been shown that UV exposure time can cause a decrease in cell viability, these changes are dependant on GelMA concentrations and intensity received from constructs by the 365nm UV used. These factors are translated into this study as 10% GelMA has lesser UV exposure time, but lower cell viability overall within GelMA-based constructs. In terms of biomechanical properties, constructs tend to become stiffer with higher concentration and UV exposure time (Pahoff et. al, 2018) but in this study tensile strength was maintained slightly lower for 10% GelMA constructs in comparison to 7.5% GelMA while the elastic potential was slightly higher than other GelMA-based biomaterials overtime.

GelMA has presented similar biomechanical properties to PEG-DA Alginate with the advantage of a good cell viability record. Therefore, these constructs have potential use for CHD treatment as they present alike properties to certain anatomical heart regions such as aortic and pulmonary leaflets.

4.3 Limitations of this study

4.3.1 Alternative imaging methodologies

The imaging used in this study could be improved by enhanced microscopy techniques to provide a clear 3D positioning of cells. The main microscope used in this study, Zeiss Axio Observer z1, can provide greater depth of field by using Z-projection/ stacks. This method captures various images from the object at different distances providing a clear- focused image. In this instance, the 3D positioning of cells can be clearly seen instead of unfocused-blurred images in the background which were obtained (Sartori et al., 2007).

Confocal microscopy is an additional technique that allows improved 3D imaging for hydrogels. In fluorescence microscopy the constructs receive an even spread of light, all parts of a sample can be excited simultaneously which results on the fluorescence captured by a photodetector. The focal plane for imaging is wider which can result on blurred background due to surrounding reflection. Confocal microscopy operates by single point illumination and has a narrower focal plane. Fluorescence gathered by the sample is filtered through a pinhole which rejects light from areas outside the focal plane. The point of illumination can be as small as the wavelength of light, 0.5 µm, which helps create a clear image (Nwaneshiudu et al., 2012).

4.3.2 Proliferation assessment

5% GelMA constructs presented an increase on live cells in comparison to day 1, these results show that the biomaterial is highly capable of supporting viability. However, these do not provide information on the proliferative state of cells within the constructs.

A well-established method for cell proliferation assessment in hydrogels is metabolic activity assays (Bradshaw et al., 2014; Gering et al., 2019; Kisiday et al., 2002; Schmalz et al., 2014; Tyliszczak et al., 2017). Cell proliferation causes lactate dehydrogenase to increase activity during proliferation and this causes a decrease on tetrazolium salts, this change in activity allows read of absorbance on a spectrophotometer and microplate reader to determine cell proliferation. Common tetrazolium salts are MTS, MTT and XTT; these vary in sensitivity and toxicity to cells. MTT is used as enpoint analysis as it is toxic to cells while the other assays can be used in continuing experiments (Bradshaw et al., 2014; Gering et al., 2019; Kisiday et al., 2002; Schmalz et al., 2014; Tyliszczak et al., 2017).

4.3.3 Degradation analysis

Due to the numerous applications hydrogels can provide (eg. drug or cell delivery, tissue fabrication), the mechanism of degradation for the biomaterial in use needs to be considered and tailored to the function of the construct created. There are two main methods of

degradation: 1. Hydrolysis and enzymatic degradation. 2. Introduction biofunctional molecules in crosslinking to aid degradation in vivo (Lee et al., 2004). This study did not explore rate and method of degradation of the different hydrogels created. That would provide additional information on the application of constructs and insight for refinement of hydrogel production aiming for a controlled degradation.

5 CONCLUSION

AL/N demonstrated high biocompatibility and superior tensile strength and modulus than all other biomaterials in this study. However, complete cell migration at day 14 highlights the potential for cell delivery rather than a long-term structure. PEG-DA Alginate presents advantageous features for tissue engineering as it is a synthetic biomaterial which can be more easily manipulated to modify biomechanical properties. However, in this investigation it presented similar tensile strength and modulus to GelMA constructs while presenting inferior cell biocompatibility. GelMA constructs presented great cell viability through 21 days maintaining great cell attachment. Tensile strength and modulus were inferior to results obtained by AL/N, however this material shows more potential for a long-term structure than the others.

Though few tensile strength and modulus results presented minor similarities to native heart structures. It is important to to highlight that most constructs presented a drastic reduction in strength and modulus once cells were incorporated. Therefore, the constructs developed in this study are best suited as cell delivery vehicles rathen than long-term structures.

6 REFERENCES

AKAGI, T. 2015. Current concept of transcatheter closure of atrial septal defect in adults. J Cardiol, 65, 17-25.

AKUTSU, H., COWAN, C. A. & MELTON, D. 2006. Human Embryonic Stem Cells. Methods in Enzymology. Academic Press.

ALLEN, H. D., SHADDY, R. E., PENNY, D. J., CETTA, F. & FELTES, T. F. 2016. Moss and Adams' heart disease in infants, children, and adolescents : including the fetus and young adult, Philadelphia, Wolters Kluwer.

ANDERSON, R. H., WEBB, S., BROWN, N. A., LAMERS, W. & MOORMAN, A. 2003. Development of the heart: (2) - Septation of the atriums and ventricles. Heart, 89, 949-958.

ANTOINE, E. E., VLACHOS, P. P. & RYLANDER, M. N. 2014. Review of Collagen I Hydrogels for Bioengineered Tissue Microenvironments: Characterization of Mechanics, Structure, and Transport. Tissue Engineering Part B-Reviews, 20, 683-696.

APITZ, C., WEBB, G. D. & REDINGTON, A. N. 2009. Tetralogy of Fallot. The Lancet, 374, 1462-1471.

ARBEITER, D., GRABOW, N., WESSARGES, Y., STERNBERG, K. & SCHMITZ, K. P. 2012. Suitability of porcine pericardial tissue for heart valve engineering: Biomechanical properties.

AVILA RODRÍGUEZ, M. I., RODRÍGUEZ BARROSO, L. G. & SÁNCHEZ, M. L. 2018. Collagen: A review on its sources and potential cosmetic applications. Journal of Cosmetic Dermatology, 17, 20-26.

AVOLIO, E., CAPUTO, M. & MADEDDU, P. 2015. Stem cell therapy and tissue engineering for correction of congenital heart disease. Front Cell Dev Biol, 3, 39.

AXPE, E. & OYEN, M. L. 2016. Applications of Alginate-Based Bioinks in 3D Bioprinting. International Journal of Molecular Sciences, 17.

BAKHSHANDEH, B., ZARRINTAJ, P., OFTADEH, M. O., KERAMATI, F., FOULADIHA, H., SOHRABI-JAHROMI, S. & ZIRAKSAZ, Z. 2017. Tissue engineering; strategies, tissues, and biomaterials. Biotechnol Genet Eng Rev, 33, 144-172.

BERGER, J., REIST, M., MAYER, J. M., FELT, O., PEPPAS, N. A. & GURNY, R. 2004. Structure and interactions in covalently and ionically crosslinked chitosan hydrogels for biomedical applications. European Journal of Pharmaceutics and Biopharmaceutics, 57, 19-34.

BERTHIAUME, F., MAGUIRE, T. J. & YARMUSH, M. L. 2011. Tissue Engineering and Regenerative Medicine: History, Progress, and Challenges. 2, 403-430.

BHATIA, S. 2016. Natural Polymers vs Synthetic Polymer. Natural Polymer Drug Delivery Systems: Nanoparticles, Plants, and Algae. Cham: Springer International Publishing.

BIANCO, P. & ROBEY, P. G. 2001. Stem cells in tissue engineering. Nature, 414, 118.

BILLIET, T., GEVAERT, E., DE SCHRYVER, T., CORNELISSEN, M. & DUBRUEL, P. 2014. The 3D printing of gelatin methacrylamide cell-laden tissue-engineered constructs with high cell viability. Biomaterials, 35, 49-62.

BISHOP, E. S., MOSTAFA, S., PAKVASA, M., LUU, H. H., LEE, M. J., WOLF, J. M., AMEER, G. A., HE, T.-C. & REID, R. R. 2017. 3-D bioprinting technologies in tissue engineering and regenerative medicine: Current and future trends. Genes & Diseases, 4, 185-195.

BOEHM, T. & SWANN, J. B. 2013. Thymus involution and regeneration: two sides of the same coin? Nature Reviews Immunology, 13, 831.

BOLAND, T., TAO, X., DAMON, B. J., MANLEY, B., KESARI, P., JALOTA, S. & BHADURI, S. 2007. Drop-on-demand printing of cells and materials for designer tissue constructs. Materials Science & Engineering C-Biomimetic and Supramolecular Systems, 27, 372-376.

Bradshaw, M., Ho, D., Fear, M. W., Gelain, F., Wood, F. M., & Iyer, K. S. (2014). Designer self-assembling hydrogel scaffolds can impact skin cell proliferation and migration. Scientific Reports, 4, 6903. https://doi.org/10.1038/srep06903

BRICKNER, M. E., HILLIS, L. D. & LANGE, R. A. 2000. Congenital Heart Disease in Adults. 342, 334-342.

BRINSTER, D. R. & PATEL, J. A. 2014. The use of CorMatrix extracellular matrix for aortic root enlargement. Journal of cardiothoracic surgery, 9, 178-178.

BROWN, C. 2019. The Normal Fetal circulation, http://leedscongenitalhearts.com/sections/view/77/the-normal-fetal-circulation.

BROWNING, M. B., GUIZA, V., RUSSELL, B., RIVERA, J., CERECERES, S., HOOK, M., HAHN, M. S. & COSGRIFF-HERNANDEZ, E. M. 2014. Endothelial cell response to chemical, biological, and physical cues in bioactive hydrogels. Tissue Eng Part A, 20, 3130-41.

BURKE, M., CARTER, B. M. & PERRIMAN, A. W. 2017. Bioprinting: uncovering the utility layer-by-layer. 1, 165-179.

CAMCI-UNAL, G., ANNABI, N., DOKMECI, M. R., LIAO, R. & KHADEMHOSSEINI, A. 2014. Hydrogels for cardiac tissue engineering. Npg Asia Materials, 6, e99.

CAMCI-UNAL, G., CUTTICA, D., ANNABI, N., DEMARCHI, D. & KHADEMHOSSEINI, A. 2013. Synthesis and characterization of hybrid hyaluronic acid-gelatin hydrogels. Biomacromolecules, 14, 1085-92.

CHEN, F.-M. & LIU, X. 2016. Advancing biomaterials of human origin for tissue engineering. Progress in polymer science, 53, 86-168.

CHEN, J.-Y., HWANG, J. V., AO-IEONG, W.-S., LIN, Y.-C., HSIEH, Y.-K., CHENG, Y.-L. & WANG, J. 2018. Study of Physical and Degradation Properties of 3D-Printed Biodegradable, Photocurable Copolymers, PGSA-co-PEGDA and PGSA-co-PCLDA. 10, 1263.

COLOSI, C., SHIN, S. R., MANOHARAN, V., MASSA, S., COSTANTINI, M., BARBETTA, A., DOKMECI, M. R., DENTINI, M. & KHADEMHOSSEINI, A. 2016. Microfl uidic Bioprinting of

Heterogeneous 3D Tissue Constructs Using Low-Viscosity Bioink. Advanced Materials, 28, 677-684.

COMLEY, J. 2017. Spheroids Rapidly Becomeing a Preferred 3D Cell Culture Format [Online]. Drug Discovery World

COURTNEY, J. A., CNOTA, J. F. & JONES, H. N. 2018. The Role of Abnormal Placentation in Congenital Heart Disease; Cause, Correlate, or Consequence? Front Physiol, 9.

COVAS, D. T., PANEPUCCI, R. A., FONTES, A. M., SILVA, W. A., ORELLANA, M. D., FREITAS, M. C. C., NEDER, L., SANTOS, A. R. D., PERES, L. C., JAMUR, M. C. & ZAGO, M. A. 2008. Multipotent mesenchymal stromal cells obtained from diverse human tissues share functional properties and gene-expression profile with CD146+ perivascular cells and fibroblasts. Experimental Hematology, 36, 642-654.

CRICK, S. J., SHEPPARD, M. N., HO, S. Y., GEBSTEIN, L. & ANDERSON, R. H. 1998. Anatomy of the pig heart: comparisons with normal human cardiac structure. 193, 105-119.

DAVIES, J. E., WALKER, J. T. & KEATING, A. 2017. Concise Review: Wharton's Jelly: The Rich, but Enigmatic, Source of Mesenchymal Stromal Cells. 6, 1620-1630.

DERAKHSHANFAR, S., MBELECK, R., XU, K., ZHANG, X., ZHONG, W. & XING, M. 2018. 3D bioprinting for biomedical devices and tissue engineering: A review of recent trends and advances. Bioactive Materials, 3, 144-156.

DOMENECH, M., POLO-CORRALES, L., RAMIREZ-VICK, J. E. & FREYTES, D. O. 2016. Tissue Engineering Strategies for Myocardial Regeneration: Acellular Versus Cellular Scaffolds? Tissue Eng Part B Rev, 22, 438-458.

DRURY, J. L., DENNIS, R. G. & MOONEY, D. J. 2004. The tensile properties of alginate hydrogels. Biomaterials, 25, 3187-3199.

ECHAVE, M. C., SAENZ DEL BURGO, L., PEDRAZ, J. L. & ORIVE, G. 2017. Gelatin as Biomaterial for Tissue Engineering. Curr Pharm Des, 23, 3567-3584.

EL OMAR, R., BEROUD, J., STOLTZ, J. F., MENU, P., VELOT, E. & DECOT, V. 2014. Umbilical Cord Mesenchymal Stem Cells: The New Gold Standard for Mesenchymal Stem Cell-Based Therapies? Tissue Engineering Part B-Reviews, 20, 523-544.

FEINBERG, A. W., ALFORD, P. W., JIN, H., RIPPLINGER, C. M., WERDICH, A. A., SHEEHY, S. P., GROSBERG, A. & PARKER, K. K. 2012. Controlling the contractile strength of engineered cardiac muscle by hierarchal tissue architecture. Biomaterials, 33, 5732-5741.

FRANTZ, C., STEWART, K. M. & WEAVER, V. M. 2010. The extracellular matrix at a glance. J Cell Sci, 123, 4195-200.

FRIEDMAN, A. H. & FAHEY, J. T. 1993. The transition from fetal to neonatal circulation: normal responses and implications for infants with heart disease. Semin Perinatol, 17, 106-21.

FRIEDMAN, R., BETANCUR, M., BOISSEL, L., TUNCER, H., CETRULO, C. & KLINGEMANN, H. 2007. Umbilical Cord Mesenchymal Stem Cells: Adjuvants for Human Cell Transplantation. Biology of Blood and Marrow Transplantation, 13, 1477-1486.

FUKUDA, K. 2001. Development of Regenerative Cardiomyocytes from Mesenchymal Stem Cells for Cardiovascular Tissue Engineering. 25, 187-193.

GARCIA, J., YANG, Z., MONGRAIN, R., LEASK, R. L. & LACHAPELLE, K. 2018. 3D printing materials and their use in medical education: a review of current technology and trends for the future. 4, 27-40.

GENES, N. G., ROWLEY, J. A., MOONEY, D. J. & BONASSAR, L. J. 2004. Effect of substrate mechanics on chondrocyte adhesion to modified alginate surfaces. Archives of Biochemistry and Biophysics, 422, 161-167.

Gering, C., Koivisto, J. T., Parraga, J., Leppiniemi, J., Vuornos, K., Hytönen, V. P., Miettinen, S., & Kellomäki, M. (2019). Design of modular gellan gum hydrogel functionalized with avidin and biotinylated adhesive ligands for cell culture applications. PLOS ONE, 14(8), e0221931. https://doi.org/10.1371/journal.pone.0221931

Goodwin, C. J., Holt, S. J., Downes, S., & Marshall, N. J. (1995). Microculture tetrazolium assays: a comparison between two new tetrazolium salts, XTT and MTS. Journal of Immunological Methods, 179(1), 95–103. https://doi.org/10.1016/0022-1759(94)00277-4

GRANT, E. K. & BERGER, J. T. 2016. Use of Pulmonary Hypertension Medications in Patients with Tetralogy of Fallot with Pulmonary Atresia and Multiple Aortopulmonary Collaterals. Pediatr Cardiol, 37, 304-12.

GRIFFIN, M., PREMAKUMAR, Y., SEIFALIAN, A., BUTLER, P. E. & SZARKO, M. 2016. Biomechanical Characterization of Human Soft Tissues Using Indentation and Tensile Testing. Journal of visualized experiments : JoVE, 54872.

GRIFFITH, L. G. & NAUGHTON, G. 2002. Tissue Engineering--Current Challenges and Expanding Opportunities. 295, 1009-1014.

GRIFFON, D. J., ABULENCIA, J. P., RAGETLY, G. R., FREDERICKS, L. P. & CHAIEB, S. 2011. A comparative study of seeding techniques and three-dimensional matrices for mesenchymal cell attachment. J Tissue Eng Regen Med, 5, 169-79.

GUILLEMOT, F., GUILLOTIN, B., FONTAINE, A., ALI, M., CATROS, S., KÉRIQUEL, V., FRICAIN, J.-C., RÉMY, M., BAREILLE, R. & AMÉDÉE-VILAMITJANA, J. 2011. Laser-assisted bioprinting to deal with tissue complexity in regenerative medicine. MRS Bulletin, 36, 1015-1019.

GUO, X. F., BAI, Y., ZHANG, L., ZHANG, B., ZAGIDULLIN, N., CARVALHO, K., DU, Z. M. & CAI, B. Z. 2018. Cardiomyocyte differentiation of mesenchymal stem cells from bone marrow: new regulators and its implications. Stem Cell Research & Therapy, 9, 12.

HALIB, N., PERRONE, F., CEMAZAR, M., DAPAS, B., FARRA, R., ABRAMI, M., CHIARAPPA, G., FORTE, G., ZANCONATI, F., POZZATO, G., MURENA, L., FIOTTI, N., LAPASIN, R., CANSOLINO, L., GRASSI, G. & GRASSI, M. 2017. Potential Applications of Nanocellulose-Containing Materials in the Biomedical Field. 10, 977.

HASAN, A., RAGAERT, K., SWIESZKOWSKI, W., SELIMOVIĆ, Š., PAUL, A., CAMCI-UNAL, G., MOFRAD, M. R. K. & KHADEMHOSSEINI, A. 2014. Biomechanical properties of native and tissue engineered heart valve constructs. Journal of Biomechanics, 47, 1949-1963.

HOCKADAY, L. A., KANG, K. H., COLANGELO, N. W., CHEUNG, P. Y., DUAN, B., MALONE, E., WU, J., GIRARDI, L. N., BONASSAR, L. J., LIPSON, H., CHU, C. C. & BUTCHER, J. T. 2012. Rapid 3D printing of anatomically accurate and mechanically heterogeneous aortic valve hydrogel scaffolds. Biofabrication, 4, 035005.

HOWARD, D., BUTTERY, L. D., SHAKESHEFF, K. M. & ROBERTS, S. J. 2008. Tissue engineering: strategies, stem cells and scaffolds. 213, 66-72.

HU, J. C. & ATHANASIOU, K. A. 2005. Low-density cultures of bovine chondrocytes: effects of scaffold material and culture system. Biomaterials, 26, 2001-2012.

IACOBAZZI, D., SWIM, M. M., ALBERTARIO, A., CAPUTO, M. & GHORBEL, M. T. 2018. Thymus-Derived Mesenchymal Stem Cells for Tissue Engineering Clinical-Grade Cardiovascular Grafts. Tissue Eng Part A, 24, 794-808.

JAIN, R. K., AU, P., TAM, J., DUDA, D. G. & FUKUMURA, D. 2005. Engineering vascularized tissue. Nat Biotechnol, 23, 821-3.

JAIPAN, P., NGUYEN, A. & NARAYAN, R. J. 2017. Gelatin-based hydrogels for biomedical applications. MRS Communications, 7, 416-426.

KAISER, N. J. & COULOMBE, K. L. K. 2015. Physiologically inspired cardiac scaffolds for tailored in vivo function and heart regeneration. Biomedical materials (Bristol, England), 10, 034003-034003.

KALSCHEUER, H., ONOE, T., DAHMANI, A., LI, H.-W., HÖLZL, M., YAMADA, K. & SYKES, M. 2014. Xenograft Tolerance and Immune Function of Human T Cells Developing in Pig Thymus Xenografts. 192, 3442-3450.

KANNAN, R. Y., SALACINSKI, H. J., SALES, K., BUTLER, P. & SEIFALIAN, A. M. 2005. The roles of tissue engineering and vascularisation in the development of micro-vascular networks: a review. Biomaterials, 26, 1857-75.

KIM, Y. K., PARK, J. A., YOON, W. H., KIM, J. & JUNG, S. 2016. Drop-on-demand inkjet-based cell printing with 30-μm nozzle diameter for cell-level accuracy. Biomicrofluidics, 10, 064110-064110.

Kisiday, J., Jin, M., Kurz, B., Hung, H., Semino, C., Zhang, S., & Grodzinsky, A. J. (2002). Self-assembling peptide hydrogel fosters chondrocyte extracellular matrix production and cell division: Implications for cartilage tissue repair. Proceedings of the National Academy of Sciences, 99(15), 9996–10001. https://doi.org/10.1073/PNAS.142309999

KLABUNDE, R. E. 2012. Cardiovascular physiology concepts, Philadelphia, PA, Lippincott Williams & Wilkins/Wolters Kluwer.

KLOTZ, B. J., GAWLITTA, D., ROSENBERG, A., MALDA, J. & MELCHELS, F. P. W. 2016. Gelatin-Methacryloyl Hydrogels: Towards Biofabrication-Based Tissue Repair. Trends in Biotechnology, 34, 394-407.

KO, H. C., MILTHORPE, B. K. & MCFARLAND, C. D. 2007. Engineering thick tissues--the vascularisation problem. Eur Cell Mater, 14, 1-18; discussion 18-9.

KOBAYASHI, E., HISHIKAWA, S., TERATANI, T. & LEFOR, A. T. J. T. R. 2012. The pig as a model for translational research: overview of porcine animal models at Jichi Medical University. 1, 8.

KRAMPERA, M., SARTORIS, S., LIOTTA, F., PASINI, A., ANGELI, R., COSMI, L., ANDREINI, A., MOSNA, F., BONETTI, B., REBELLATO, E., TESTI, M. G., FROSALI, F., PIZZOLO, G., TRIDENTE, G., MAGGI, E., ROMAGNANI, S. & ANNUNZIATO, F. 2007. Immune Regulation by Mesenchymal Stem Cells Derived from Adult Spleen and Thymus. 16, 797-810.

LASCHKE, M. W. & MENGER, M. D. 2016. Prevascularization in tissue engineering: Current concepts and future directions. Biotechnol Adv, 34, 112-21.

LEE, B. H., LUM, N., SEOW, L. Y., LIM, P. Q. & TAN, L. P. 2016. Synthesis and Characterization of Types A and B Gelatin Methacryloyl for Bioink Applications. 9, 797.

LEE, D., ZHANG, H. & RYU, S. 2018. Elastic Modulus Measurement of Hydrogels. In: MONDAL, M. I. H. (ed.) Cellulose-Based Superabsorbent Hydrogels. Cham: Springer International Publishing.

LEE, K. Y. & MOONEY, D. J. 2012. Alginate: properties and biomedical applications. Progress in polymer science, 37, 106-126.

Lee, K. Y., Bouhadir, K. H., & Mooney, D. J. (2004). Controlled degradation of hydrogels using multi-functional cross-linking molecules. Biomaterials. https://doi.org/10.1016/j.biomaterials.2003.09.030

LELOVAS, P. P., KOSTOMITSOPOULOS, N. G. & XANTHOS, T. T. 2014. A comparative anatomic and physiologic overview of the porcine heart. J Am Assoc Lab Anim Sci, 53, 432-8.

LESLIE, S. K., COHEN, D. J., SEDLACZEK, J., PINSKER, E. J., BOYAN, B. D. & SCHWARTZ, Z. 2013. Controlled release of rat adipose-derived stem cells from alginate microbeads. Biomaterials, 34, 8172-8184.

LEVICK, J. R. 2010. An introduction to cardiovascular physiology. 5th ed. ed. London: Hodder Arnold.

LI, W. C., YU, M. H., ZHANG, H. M., WANG, H. Q., XI, G. M., YAO, B. C., DENG, Z. H. & ZENG, Y. J. 2008. Biomechanical properties of ascending aorta and pulmonary trunk in pigs and humans. Xenotransplantation, 15, 384-9.

LIN, N. & DUFRESNE, A. 2014. Nanocellulose in biomedicine: Current status and future prospect. European Polymer Journal, 59, 302-325.

LIN, N., HUANG, J., CHANG, P. R., FENG, L. & YU, J. 2011. Effect of polysaccharide nanocrystals on structure, properties, and drug release kinetics of alginate-based microspheres. Colloids and Surfaces B: Biointerfaces, 85, 270-279.

LIN, Y.-H., LIANG, H.-F., CHUNG, C.-K., CHEN, M.-C. & SUNG, H.-W. 2005. Physically crosslinked alginate/N,O-carboxymethyl chitosan hydrogels with calcium for oral delivery of protein drugs. Biomaterials, 26, 2105-2113.

LIN, Z. B., QIAN, B., YANG, Y. Z., ZHOU, K., SUN, J., MO, X. M. & WU, K. H. 2015. Isolation, Characterization and Cardiac Differentiation of Human Thymus Tissue Derived Mesenchymal Stromal Cells. Journal of Cellular Biochemistry, 116, 1205-1212.

LOESSNER, D., MEINERT, C., KAEMMERER, E., MARTINE, L. C., YUE, K., LEVETT, P. A., KLEIN, T. J., MELCHELS, F. P. W., KHADEMHOSSEINI, A. & HUTMACHER, D. W. 2016. Functionalization, preparation and use of cell-laden gelatin methacryloyl-based hydrogels as modular tissue culture platforms. Nature Protocols, 11, 727-746.

LOKMIC, Z., STILLAERT, F., MORRISON, W. A., THOMPSON, E. W. & MITCHELL, G. M. 2007. An arteriovenous loop in a protected space generates a permanent, highly vascular, tissue-engineered construct. Faseb j, 21, 511-22.

MAJUMDER, S., PODDAR, R. & CHATTERJEE, S. 2016. Novel design of pneumatic based bio-printing device. Materials Today: Proceedings, 3, 3186-3193.

MANO, J. F., SILVA, G. A., AZEVEDO, H. S., MALAFAYA, P. B., SOUSA, R. A., SILVA, S. S., BOESEL, L. F., OLIVEIRA, J. M., SANTOS, T. C., MARQUES, A. P., NEVES, N. M. & REIS, R. L. 2007. Natural origin biodegradable systems in tissue engineering and regenerative medicine: present status and some moving trends. Journal of the Royal Society, Interface, 4, 999-1030.

MARTIN, C. & SUN, W. 2012. Biomechanical characterization of aortic valve tissue in humans and common animal models. J Biomed Mater Res A, 100, 1591-9.

Mauri, E., Sacchetti, A., Vicario, N., Peruzzotti-Jametti, L., Rossi, F., & Pluchino, S. (2018). Evaluation of RGD functionalization in hybrid hydrogels as 3D neural stem cell culture systems. Biomater. Sci., 6(3), 501–510. https://doi.org/10.1039/C7BM01056G

MAVRILAS, D. & MISSIRLIS, Y. 1991. An approach to the optimization of preparation of bioprosthetic heart valves. Journal of Biomechanics, 24, 331-339.

MAZZOCCOLI, J. P., FEKE, D. L., BASKARAN, H. & PINTAURO, P. N. 2010. Mechanical and cell viability properties of crosslinked low- and high-molecular weight poly(ethylene glycol) diacrylate blends. Journal of biomedical materials research. Part A, 93, 558-566.

McGowan, E. M., Alling, N., Jackson, E. A., Yagoub, D., Haass, N. K., Allen, J. D., & Martinello-Wilks, R. (2011). Evaluation of cell cycle arrest in estrogen responsive MCF-7 breast cancer cells: Pitfalls of the MTS assay. PLoS ONE, 6(6). https://doi.org/10.1371/journal.pone.0020623

MOORMAN, A., WEBB, S., BROWN, N. A., LAMERS, W. & ANDERSON, R. H. 2003. Development of the heart: (1) - Formation of the cardiac chambers and arterial trunks. Heart, 89, 806-814.

MOSALA NEZHAD, Z., PONCELET, A., DE KERCHOVE, L., FERVAILLE, C., BANSE, X., BOLLEN, X., DEHOUX, J.-P., EL KHOURY, G. & GIANELLO, P. 2016. CorMatrix valved conduit in a porcine model: long-term remodelling and biomechanical characterization†. Interactive CardioVascular and Thoracic Surgery, 24, 90-98.

MOSTEFA-KARA, M., BONNET, D., BELLI, E., FADEL, E. & HOUYEL, L. 2015. Anatomy of the ventricular septal defect in outflow tract defects: similarities and differences. J Thorac Cardiovasc Surg, 149, 682-8.e1.

MULLER, M., BECHER, J., SCHNABELRAUCH, M. & ZENOBI-WONG, M. 2015. Nanostructured Pluronic hydrogels as bioinks for 3D bioprinting. Biofabrication, 7, 035006.

MURALI, V. S., WANG, R., MIKORYAK, C. A., PANTANO, P. & DRAPER, R. 2015. Rapid detection of polyethylene glycol sonolysis upon functionalization of carbon nanomaterials. 240, 1147-1151.

MURPHY, S. V. & ATALA, A. 2014. 3D bioprinting of tissues and organs. Nat Biotechnol, 32, 773-85.

NAHAR, K., HOSSAIN, M. K. & KHAN, T. A. 2017. Alginate and Its Versatile Application in Drug Delivery. Journal of Pharmaceutical Sciences and Research, 9, 606.

NAIR, K., GANDHI, M., KHALIL, S., YAN, K., MARCOLONGO, M., BARBEE, K. & SUN, W. 2009. Characterization of cell viability during bioprinting process.

NASCIMENTO, D. M., NUNES, Y. L., FIGUEIRÊDO, M. C. B., DE AZEREDO, H. M. C., AOUADA, F. A., FEITOSA, J. P. A., ROSA, M. F. & DUFRESNE, A. 2018. Nanocellulose nanocomposite hydrogels: technological and environmental issues. Green Chemistry, 20, 2428-2448.

NELSON, J. S., HEIDER, A., SI, M. S. & OHYE, R. G. 2016. Evaluation of Explanted CorMatrix Intracardiac Patches in Children With Congenital Heart Disease. Ann Thorac Surg, 102, 1329-35.

NEREM, R. M. 2010. Regenerative medicine: the emergence of an industry. Journal of the Royal Society, Interface, 7 Suppl 6, S771-S775.

NICHOL, J. W., KOSHY, S. T., BAE, H., HWANG, C. M., YAMANLAR, S. & KHADEMHOSSEINI, A. 2010. Cell-laden microengineered gelatin methacrylate hydrogels. Biomaterials, 31, 5536-5544.

Nwaneshiudu, A., Kuschal, C., Sakamoto, F. H., Rox Anderson, R., Schwarzenberger, K., & Young, R. C. (2012). Introduction to confocal microscopy. Journal of Investigative Dermatology. https://doi.org/10.1038/jid.2012.429

O'CONNELL, C. D., ZHANG, B., ONOFRILLO, C., DUCHI, S., BLANCHARD, R., QUIGLEY, A., BOURKE, J., GAMBHIR, S., KAPSA, R., DI BELLA, C., CHOONG, P. & WALLACE, G. G. 2018. Tailoring the mechanical properties of gelatin methacryloyl hydrogels through manipulation of the photocrosslinking conditions. Soft Matter, 14, 2142-2151.

OHYE, R. G., SCHRANZ, D. & D'UDEKEM, Y. 2016. Current Therapy for Hypoplastic Left Heart Syndrome and Related Single Ventricle Lesions. Circulation, 134, 1265-1279.

ORETO, L., MANDRAFFINO, G., MANURI, L., SAITTA, M. B., AGATI, S., ZITO, C., IORIO, F. S., CARERJ, S. & GUCCIONE, P. 2018. Atrial septal defect morphology and stenting in hypoplastic left heart syndrome after hybrid palliation. Cardiol Young, 28, 252-260.

PADALINO, M., QUARTI, A., ANGELI, E., FRIGO, A., VIDA, V., POZZI, M., GARGIULO, G. & STELLIN, G. 2015. Early and mid-term clinical experience with extracellular matrix scaffold for congenital cardiac and vascular reconstructive surgery: A multicentric Italian study.

PECK, M., DUSSERRE, N., MCALLISTER, T. N. & L'HEUREUX, N. 2011. Tissue engineering by self-assembly. Materials Today, 14, 218-224.

PENNY, D. J. & VICK, G. W. 2011. Ventricular septal defect. The Lancet, 377, 1103-1112.

PEPELANOVA, I., KRUPPA, K., SCHEPER, T. & LAVRENTIEVA, A. 2018. Gelatin-Methacryloyl (GelMA) Hydrogels with Defined Degree of Functionalization as a Versatile Toolkit for 3D Cell Culture and Extrusion Bioprinting. 5, 55.

PEREZ-NEGUERUELA, C., CARRETERO, J., MAYOL, J. & CAFFARENA, J. M. 2017. Surgical closure of multiple large apical ventricular septal defects: how we do it. Cardiol Young, 27, 588-591.

PICAZO-ANGELIN, B., ZABALA-ARGUELLES, J. I., ANDERSON, R. H. & SANCHEZ-QUINTANA, D. 2018. Anatomy of the normal fetal heart: The basis for understanding fetal echocardiography. Annals of Pediatric Cardiology, 11, 164-173.

PRESNELL, L. B., BLANKENSHIP, A., CHEATHAM, S. L., OWENS, G. E. & STAVESKI, S. L. 2015. An Overview of Pulmonary Atresia and Major Aortopulmonary Collateral Arteries. World J Pediatr Congenit Heart Surg, 6, 630-9.

RODRIGUES, M. S., A.C.; AGUAS, A.P.; GRANDE, N.R. 2005. The coronary circulation of the pig heart: Comparison with the human heart. Eur. J. Anat., 9, 67-87.

ROUWKEMA, J., RIVRON, N. C. & VAN BLITTERSWIJK, C. A. 2008. Vascularization in tissue engineering. Trends in Biotechnology, 26, 434-441.

SANT, S. & JOHNSTON, P. A. 2017. The production of 3D tumor spheroids for cancer drug discovery. Drug Discovery Today: Technologies, 23, 27-36.

Sartori, A., Gatz, R., Beck, F., Rigort, A., Baumeister, W., & Plitzko, J. M. (2007). Correlative microscopy: Bridging the gap between fluorescence light microscopy and cryo-electron tomography. Journal of Structural Biology, 160(2), 135–145. https://doi.org/10.1016/j.jsb.2007.07.011

Schmalz, G., Gröppl, F., Hiller, K.-A., & Galler, K. M. (2014). Three-Dimensional Human Cell Cultures for Cytotoxicity Testing of Dental Filling Materials. Acta Stomatologica Croatica, 48(2), 99–108. https://www.ncbi.nlm.nih.gov/pubmed/27688353

SCHUURMAN, W., LEVETT, P. A., POT, M. W., VAN WEEREN, P. R., DHERT, W. J. A., HUTMACHER, D. W., MELCHELS, F. P. W., KLEIN, T. J. & MALDA, J. 2013. Gelatin-Methacrylamide Hydrogels as Potential Biomaterials for Fabrication of Tissue-Engineered Cartilage Constructs. Macromolecular Bioscience, 13, 551-561.

SHERIDAN, M. H., SHEA, L. D., PETERS, M. C. & MOONEY, D. J. 2000. Bioabsorbable polymer scaffolds for tissue engineering capable of sustained growth factor delivery. Journal of Controlled Release, 64, 91-102.

SHIN, H., ZYGOURAKIS, K., FARACH-CARSON, M. C., YASZEMSKI, M. J. & MIKOS, A. G. 2004. Attachment, proliferation, and migration of marrow stromal osteoblasts cultured on biomimetic hydrogels modified with an osteopontin-derived peptide. Biomaterials, 25, 895-906.

SIAN PINCOTT, E. & BURCH, M. 2011. Indications for heart transplantation in congenital heart disease. Curr Cardiol Rev, 7, 51-8.

SOBHANI, A., KHANLARKHANI, N., BAAZM, M., MOHAMMADZADEH, F., NAJAFI, A., MEHDINEJADIANI, S. & SARGOLZAEI AVAL, F. 2017. Multipotent Stem Cell and Current Application. Acta Med Iran, 55, 6-23.

SONG, Y. S., LIN, R. L., MONTESANO, G., DURMUS, N. G., LEE, G., YOO, S. S., KAYAALP, E., HAEGGSTROM, E., KHADEMHOSSEINI, A. & DEMIRCI, U. 2009. Engineered 3D tissue models for cell-laden microfluidic channels. Anal Bioanal Chem, 395, 185-93.

SPORCLE 2016. Human heart, https://www.sporcle.com/games/timmylemoine1/heart-anatomy-pc

STORY, L. & RUTHERFORD, M. 2015. Advances and applications in fetal magnetic resonance imaging. The Obstetrician & Gynaecologist, 17, 189-199.

STRADINS, P., LACIS, R., OZOLANTA, I., PURINA, B., OSE, V., FELDMANE, L. & KASYANOV, V. 2004. Comparison of biomechanical and structural properties between human aortic and pulmonary valve. Eur J Cardiothorac Surg, 26, 634-9.

SUN, J. & TAN, H. 2013. Alginate-Based Biomaterials for Regenerative Medicine Applications. Materials (Basel), 6, 1285-1309.

SUNDARAMURTHI, D., RAUF, S. & HAUSER, C. 2016. 3D bioprinting technology for regenerative medicine applications.

TAM, S. K., DUSSEAULT, J., BILODEAU, S., LANGLOIS, G., HALLE, J. P. & YAHIA, L. 2011. Factors influencing alginate gel biocompatibility. J Biomed Mater Res A, 98, 40-52.

Tyliszczak, B., Drabczyk, A., Kudłacik-Kramarczyk, S., Bialik-Wąs, K., & Sobczak-Kupiec, A. (2017). In vitro cytotoxicity of hydrogels based on chitosan and modified with gold nanoparticles. Journal of Polymer Research, 24(10), 153. https://doi.org/10.1007/s10965-017-1315-3

VASQUEZ, A. F. & LASALA, J. M. 2013. Atrial septal defect closure. Cardiol Clin, 31, 385-400.

VEDADGHAVAMI, A., MINOOEI, F., MOHAMMADI, M. H., KHETANI, S., REZAEI KOLAHCHI, A., MASHAYEKHAN, S. & SANATI-NEZHAD, A. 2017. Manufacturing of hydrogel biomaterials with controlled mechanical properties for tissue engineering applications. Acta Biomater, 62, 42-63.

WAKATSUKI, T. & ELSON, E. L. 2003. Reciprocal interactions between cells and extracellular matrix during remodeling of tissue constructs. Biophys Chem, 100, 593-605.

WEBSTER, S. & DE WREEDE, R. 2016. Embryology at a glance, Chichester, Wiley Blackwell.

WU, Y., XIANG, Y., FANG, J., LI, X., LIN, Z., DAI, G., YIN, J., WEI, P. & ZHANG, D. 2019. The influence of the stiffness of GelMA substrate on the outgrowth of PC12 cells. 39, BSR20181748.

YU, C., ZHU, W., SUN, B., MEI, D., GOU, M. & CHEN, S. 2018. Modulating physical, chemical, and biological properties in 3D printing for tissue engineering applications. 5, 041107.

YU, Y., MONCAL, K. K., LI, J., PENG, W., RIVERO, I., MARTIN, J. A. & OZBOLAT, I. T. 2016. Three-dimensional bioprinting using self-assembling scalable scaffold-free “tissue strands” as a new bioink. Scientific Reports, 6, 28714.

ZAIDI, S. & BRUECKNER, M. 2017. Genetics and Genomics of Congenital Heart Disease. Circ Res, 120, 923-940.

ZHANG, G. 2012. Biomimicry in biomedical research. Organogenesis, 8, 101-102.

ZHANG, L., PEI, Y. F., WANG, L., LIAO, M. F., LU, Q. S., ZHUANG, Y. F., ZHANG, S. M. & JING, Z. P. 2012. Dramatic decrease of aortic longitudinal elastic strength in a rat model of aortic dissection. Ann Vasc Surg, 26, 996-1001.

ZHANG, W., LIU, X.-C., YANG, L., ZHU, D.-L., ZHANG, Y.-D., CHEN, Y. & ZHANG, H.-Y. 2013. Wharton’s jelly-derived mesenchymal stem cells promote myocardial regeneration and cardiac repair after miniswine acute myocardial infarction. 24, 549-558.

ZHANG, X., XU, B., PUPERI, D. S., YONEZAWA, A. L., WU, Y., TSENG, H., CUCHIARA, M. L., WEST, J. L. & GRANDE-ALLEN, K. J. 2015a. Integrating valve-inspired design features into poly(ethylene glycol) hydrogel scaffolds for heart valve tissue engineering. Acta biomaterialia, 14, 11-21.

ZHANG, X., ZHANG, Y. J. C. B. & BIOPHYSICS 2015b. Tissue Engineering Applications of Three-Dimensional Bioprinting. 72, 777-782.

ZHAO, L. J., HAN, B., ZHANG, J. J., YI, Y. C., JIANG, D. D. & LYU, J. L. 2018. Transcatheter closure of congenital perimembranous ventricular septal defect using the Amplatzer duct occluder 2. Cardiol Young, 28, 447-453.

ZHU, J. & MARCHANT, R. E. 2011. Design properties of hydrogel tissue-engineering scaffolds. Expert review of medical devices, 8, 607-626.

ZHU, M., WANG, Y., FERRACCI, G., ZHENG, J., CHO, N.-J. & LEE, B. H. 2019. Gelatin methacryloyl and its hydrogels with an exceptional degree of controllability and batch-to-batch consistency. Scientific Reports, 9, 6863.

ZHU, Z., WANG, Y., YANG, J., LUO, X. 2017. Hyaluronic acid: a versatile biomaterial in tissue engineering. Plastic and Aesthetic Research, 4, 219-227.